Eur. Phys. J. C (2026) 86:433
https://doi.org/10.1140/epjc/s10052-025-15217-3

THE EUROPEAN PHYSICAL JOURNAL C

Regular Article - Experimental Physics

Electroweak diboson production in association with a high-mass dijet system in semileptonic final states from pp collisions at $\sqrt{s} = 13$ TeV with the ATLAS detector

ATLAS Collaboration[⋆]

CERN, 1211 Geneva 23, Switzerland

Received: 25 March 2025 / Accepted: 17 December 2025

Abstract This paper reports the observation of electroweak diboson ($WW/WZ/ZZ$) production in association with a high-mass dijet system, in which final states with one boson decaying leptonically and the other boson decaying hadronically are studied. The hadronically decaying W/Z boson is reconstructed as either two small-radius jets or one large-radius jet with jet substructure requirements. The data analyzed correspond to an integrated luminosity of 140 fb^{-1} of proton–proton collisions at a center-of-mass energy of $\sqrt{s} = 13$ TeV collected with the ATLAS detector during the 2015-2018 data taking at the Large Hadron Collider. The electroweak production of $WW/WZ/ZZ$ in association with two jets is observed in a phase space dominated by vector-boson scattering with a significance of 7.4σ (expected 6.1σ) and the signal strength is determined to be $1.28^{+0.23}_{-0.21}$. The corresponding production cross section in a fiducial phase space is measured in addition. The signal strengths of both electroweak and QCD associated diboson productions are furthermore measured in a two-dimensional fit, the result of which agrees with the Standard Model prediction. The data are interpreted in the context of a dimension-8 effective field theory to probe anomalous quartic gauge couplings resulting in the first set of exclusion limits on the Wilson coefficients in the semileptonic channel reported by the ATLAS Collaboration. The observed limits for the S02, T0 and M0 operators are $(-3.96 < f_{S02}/\Lambda^4 < 3.96)$ TeV^{-4}, $(-0.25 < f_{T0}/\Lambda^4 < 0.22)$ TeV^{-4}, $(-1.26 < f_{M0}/\Lambda^4 < 1.25)$ TeV^{-4}.

Contents

1 Introduction

Vector Boson Scattering (VBS) involves both the self-couplings of the gauge bosons and their coupling to the Higgs boson. It is therefore crucial for probing the non-Abelian gauge structure of the electroweak (EWK) sector of the Standard Model (SM). In the absence of the SM Higgs boson, the amplitudes for VBS would increase as a function of partonic center-of-mass energy and ultimately violate unitarity [1,2]. The discovery of a Higgs boson in 2012 at the Large Hadron Collider (LHC) [3,4], with measured properties [5–8] consistent with those of the SM Higgs boson, represents a major milestone in understanding the EWK symmetry breaking. The investigation of the VBS component of EWK diboson production offers a crucial test of the SM and of the Higgs mechanism, and helps to validate the current understanding of the EWK symmetry breaking. The interest has now shifted to probing the EWK diboson scattering at higher energies. In this regard, the semileptonic channel offers a unique possibil-

⋆ e-mail: atlas.publications@cern.ch

Published online: 30 April 2026

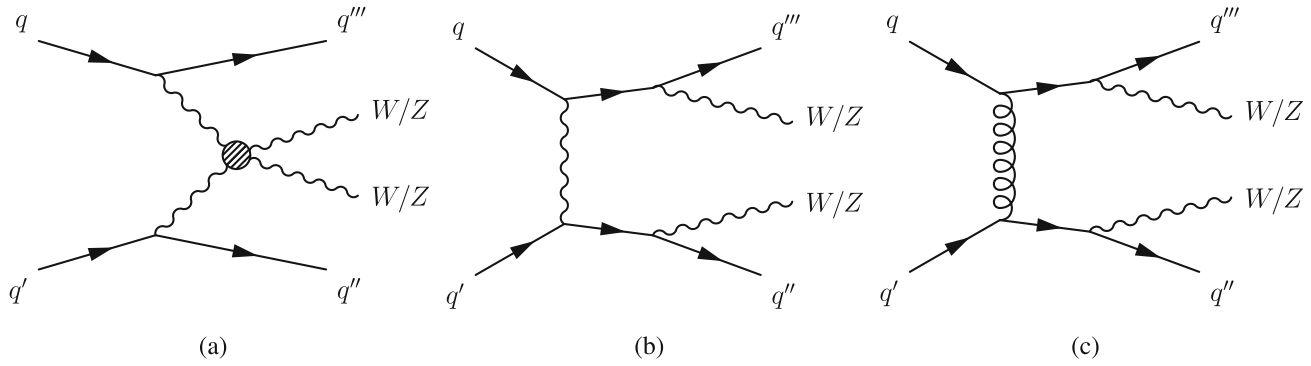

Fig. 1 Representative Feynman diagrams for **a** EWK $VVjj$ production via VBS, **b** EWK $VVjj$ production via a non-VBS contribution, and **c** QCD $VVjj$ production

ity to access EWK diboson events at a higher boson transverse momentum (p_{T}) than in other final states.

Theories of new phenomena beyond the SM (BSM) that foresee anomalous quartic gauge couplings (aQGC) [9,10] or include the presence of additional resonances [11,12] predict enhancements of VBS at high p_{T} of the vector bosons and at high invariant mass of the diboson system. The sensitivity of such BSM scenarios is closely tied to the energy growth of the longitudinal vector boson scattering amplitudes, which is governed over many orders of magnitude by the Goldstone Boson Equivalence Theorem. This energy-dependent behavior amplifies potential deviations from the Standard Model, making VBS a particularly powerful probe of electroweak symmetry breaking and new physics. The aQGC can be studied in EWK diboson production by comparing measured cross sections to SM predictions. The effects of these anomalous couplings can be parameterized in the SM effective field theory (EFT) framework. In addition to VBS diboson signatures, aQGC can also be constrained with triboson final states [13,14]. To model possible BSM contributions to the EWK VBS process in an EFT framework, the Eboli model [10] is used. This model introduces 21 new dimension-8 operators which satisfy the SM $SU(2) \times U(1)_Y$ symmetry. Among these operators, 19 affect the semileptonic final state.

The experimental signature of VBS is characterized by a pair of SM vector bosons ($V = W$ or Z) and two forward jets with a large rapidity separation and a large invariant mass. The SM predicts several processes with the same final state of two bosons and two jets. At tree level, the production of $VVjj$ has both an EWK contribution involving only EWK-interaction vertices, and a strong contribution (QCD-induced) involving two strong-interaction vertices. The EWK production can be further characterized into two components. The first component is EWK VBS production with actual scattering of the two EWK bosons. The scattering occurs via quartic gauge vertices, or triple gauge vertices involving the s- or t-channel exchange of a Higgs boson or a W/Z boson. The second component is an EWK non-VBS production that also has only EWK vertices, but without the scattering of the two bosons. The EWK VBS component cannot be separated from the other components in a gauge invariant way [15]. Despite the analysis being designed to enhance the VBS component, all the components introduced are included in the signal generation and all of them contribute to the total cross section. Representative Feynman diagrams at tree level are shown in Fig. 1.

The amount of diboson events in the semileptonic decay channel is higher than the one expected in fully leptonic final states; indeed, the branching fraction of a V decaying into quarks is more than a factor two larger than the one of the V decaying into charged leptons or neutrinos. On the other side, this decay channel is characterised by a larger contamination from other SM processes. Nevertheless, this final state offers a larger set of data in the high momentum phase space that can be analyzed to probe further the EWK interactions foreseen by the SM (by measuring the EWK VBS process) and to look further for deviations from the SM predictions (search for aQGC).

The effect of new physics introduced by aQGC can be estimated using an EFT [16] and parameterized linearly by an effective Lagrangian as:

$$\mathcal{L} = \mathcal{L}_{sm} + \sum_i \frac{c_i}{\Lambda^2}\mathcal{L}_i + \sum_n \frac{f_n}{\Lambda^4}\mathcal{L}_n,$$

where $\mathcal{L}_{sm}$ represents the SM term and $\mathcal{L}_i$ and $\mathcal{L}_n$ represent possible dimension-6 and dimension-8 operators; c_i and f_n are their corresponding Wilson coefficients, and Λ represents the energy scale at which the new degrees of freedom are integrated out. Both dimension-6 and dimension-8 operators contribute to the EWK VBS process, but due to the tight constraints on dimension-6 operators from inclusive diboson and Higgs measurements [17], only dimension-8 operators are discussed in this article.

Both the ATLAS and CMS Collaborations have searched for experimental evidence of EWK diboson production in

a VBS-enhanced phase space. So far, evidence or observation of EWK $VVjj$ production has been reported in the same-sign $W^{\pm}W^{\pm}jj$ [18,19], opposite-sign $W^{\pm}W^{\mp}jj$ [20,21], $WZjj$ [22,23], $ZZjj$ [24,25], $W\gamma jj$ [26,27], $Z(\to \nu\nu)\gamma jj$ [28], and $Z(\to ll)\gamma jj$ [29,30] channels with the weak bosons decaying in the fully leptonic final states using data collected at a center-of-mass energy of $\sqrt{s} = 13$ TeV. The ATLAS Collaboration reported observation of EWK $VVjj$ production in all these channels. This paper presents a measurement of EWK diboson production with two jets in a semileptonic final state. The CMS Collaboration reported an evidence in the semileptonic final state $W(\to l\nu)V \pm jj$ [31].

Several of the diboson channels referenced above are sensitive and constrain the production of aQGC; the same-sign $W^{\pm}W^{\pm}jj$, $WZjj$, $W\gamma jj$ and $Z(\to \nu\nu)\gamma jj$ channels provide constraints on EFT operators. The CMS Collaboration performed a search for aQGC in semileptonic final states using a partial dataset of 35.9 fb^{-1}, reporting EFT limits [32]. The ATLAS Collaboration had never reported EFT results in this final state, so this analysis allows EFT operators to be constrained at higher momentum than previous ATLAS results.

The ATLAS Collaboration reported a search for the EWK diboson production in the semileptonic final states [33], but using only a partial dataset of 35.5 fb^{-1}. This paper represents an improvement with respect to the cited result insofar it benefits from a larger dataset and improved reconstruction and calibration of the objects used, and it extends the scope of the analysis strategy and data interpretation.

Three $VVjj$ semileptonic decay channels are explored: a Z boson decaying into a pair of neutrinos, $Z \to \nu\nu$[1]; a W boson decaying into a charged lepton (an electron or muon, denoted by ℓ) and a neutrino, $W \to \ell\nu$; and a Z boson decaying into a pair of light charged leptons (electrons or muons, each denoted by ℓ), $Z \to \ell\ell$. In all cases, the other vector boson V is required to decay into a pair of quarks, $V \to qq$, leading to three reconstructed diboson final states: $ZV \to \nu\nu qq$, $WV \to \ell\nu qq$ and $ZV \to \ell\ell qq$. The reconstructed events are split according to the number of charged leptons in three categories: 0-, 1- and 2-lepton channels. A fiducial region of the measurement is defined to account for the geometrical, reconstruction and analysis acceptance of leptons and jets.

The $V \to qq$ decay is considered over a large p_{T} range of the vector boson; as p_{T} increases, the hadronic activity from the decay is bound in an increasingly narrower solid angle with a large overlap of the two jets. In this case, hadrons from the two quarks overlap in the detector and are more efficiently reconstructed as a single large-R jet. Therefore, two different reconstruction techniques for the $V \to qq$ decay are considered: resolved and merged. The resolved reconstruction attempts to identify two separate small-radius jets (small-R jets denoted by j) of hadrons from the $V \to qq$ decay, and the merged reconstruction uses a large-radius jet (large-R jet denoted by J) in conjunction with jet substructure techniques to identify the decay. Although the introduction of a merged category appears to be more challenging, it is a crucial category for semileptonic final states that allows the exploration of a kinematic regime defined by a boson $p_{\mathrm{T}} > 200$ GeV that would otherwise remain inaccessible with the resolved regime alone. In terms of sensitivity, the merged regime significantly contributes to the EWK VBS measurement while it is the dominant regime for the EFT interpretation. In total, six final states are included in this study: 0-, 1- and 2-lepton final states, each using resolved or merged $V \to qq$ reconstruction techniques; the merged final state is further divided in two regions as described in Sect. 5.

To probe the EWK production mechanism, the diboson semileptonic events are selected by requiring two additional energetic jets in the forward region of the detector. Dedicated kinematic requirements allow a further enhancement of the VBS component in the selected events.

To extract the signal and to measure the cross section for the EWK production of $VVjj$, a machine learning (ML) discriminant, which exploits the kinematics and the track multiplicity of the reconstructed jets, is used to separate the EWK-induced $VVjj$ production from other processes in the SM. Candidate signal events are used to measure the cross section of EWK $VVjj$ production in a region of kinematic phase space close to the detector and analysis acceptance. Both the EWK and QCD associated diboson production are measured in a two dimensional fit. Fiducial cross sections are measured in the 0-, 1- and 2-lepton channels. The diboson system invariant mass is combined with the ML discriminant to derive limits on the Wilson coefficients of the dimension-8 EFT Lagrangian.

2 ATLAS detector

The ATLAS experiment [34] at the LHC is a multipurpose particle detector with a forward–backward symmetric cylindrical geometry and a near 4π coverage in solid angle.[2] It consists of an inner tracking detector surrounded by a

[1] To simplify the notation, antiparticles are not explicitly labeled in this paper.

[2] ATLAS uses a right-handed coordinate system with its origin at the nominal interaction point (IP) in the centre of the detector and the z-axis along the beam pipe. The x-axis points from the IP to the centre of the LHC ring, and the y-axis points upwards. Cylindrical coordinates (r, ϕ) are used in the transverse plane, ϕ being the azimuthal angle around the z-axis. The pseudorapidity is defined in terms of the polar angle θ as $\eta = -\ln\tan(\theta/2)$. Angular distance is measured in units of $\Delta R \equiv \sqrt{(\Delta y)^2 + (\Delta\phi)^2}$.

thin superconducting solenoid providing a 2 T axial magnetic field, electromagnetic and hadronic calorimeters, and a muon spectrometer. The inner tracking detector (ID) covers the pseudorapidity range $|\eta| < 2.5$. It consists of silicon pixel, silicon microstrip, and transition radiation tracking detectors. Lead/liquid-argon (LAr) sampling calorimeters provide electromagnetic (EM) energy measurements with high granularity within the region $|\eta| < 3.2$. A steel/scintillator-tile hadronic calorimeter covers the central pseudorapidity range ($|\eta| < 1.7$). The endcap and forward regions are instrumented with LAr calorimeters for EM and hadronic energy measurements up to $|\eta| = 4.9$. The muon spectrometer (MS) surrounds the calorimeters and is based on three large superconducting air-core toroidal magnets with eight coils each. The field integral of the toroids ranges between 2.0 and 6.0 T m across most of the detector. The muon spectrometer includes a system of precision tracking chambers up to $|\eta| = 2.7$ and fast detectors for triggering up to $|\eta| = 2.4$. The luminosity is measured mainly by the LUCID–2 detector which is located close to the beampipe. A two-level trigger system is used to select events. The first-level trigger is implemented in hardware and uses a subset of the detector information to accept events at a rate close to 100 kHz. This is followed by a software-based trigger that reduces the accepted rate of complete events to 1.25 kHz on average, depending on the data-taking conditions. A software suite [35] is used in data simulation, in the reconstruction and analysis of real and simulated data, in detector operations, and in the trigger and data acquisition systems of the experiment.

3 Data and simulated event samples

3.1 Data

This analysis uses the 2015-2018 proton–proton (pp) collision data at $\sqrt{s} = 13$ TeV recorded with the ATLAS detector at the LHC for a total integrated luminosity of 140 fb^{-1} [36]. Events used for the analysis were recorded with all detector systems operating normally and passing data-quality requirements [37].

To optimize the trigger efficiency for the signal process, a combination of unprescaled single-lepton with tight isolation requirements and missing transverse momentum ($E_{\mathrm{T}}^{\mathrm{miss}}$) triggers were used [38–41]. During data-taking, the thresholds of the single-lepton triggers with tight isolation requirements were increased in stages alongside the increase in instantaneous luminosity. The lepton triggers with tight isolation were also complemented by triggers with looser isolation but higher E_{T} or p_{T} thresholds. In the 0-lepton channel, $E_{\mathrm{T}}^{\mathrm{miss}}$ triggers were used with the lowest threshold varying from 70 to 110 GeV. The single-muon (single-electron) triggers were used in the 2-lepton channel with lowest thresholds of 20 (24) to 26 (26) GeV. For the 1-lepton channel, the same single-lepton triggers were also used, but the single-muon triggers were complemented with $E_{\mathrm{T}}^{\mathrm{miss}}$ triggers. Since at the trigger level, the $E_{\mathrm{T}}^{\mathrm{miss}}$ calculation does not account for the presence of muons, the inclusion of $E_{\mathrm{T}}^{\mathrm{miss}}$ triggers reduces the efficiency loss from the difference in trigger and reconstructed muon tracking. The trigger efficiency for signal events in the 0 and 2-lepton channels is above 90%, and above 80% in the 1-lepton channel.

3.2 Signal and background simulation

EWK signal samples, $W(\to l\nu)V$, $Z(\to \nu\nu)V$, $Z(\to ll)V$, with one boson decaying leptonically and the other hadronically, were generated using MadGraph5_aMC@NLO 2.6.6 [42] at the order $O(\alpha_{\mathrm{EWK}}^6)$, where α_{EWK} is the EWK coupling constant. Both the VBS and non-VBS amplitudes of the $VVjj$ process were included. The latter contains also diagrams with a W boson and a top quark (Wtb) resulting into a $VVjj$ final state. This contribution is suppressed by an event selection requirement, but it cannot be completely removed to preserve the gauge invariance. Therefore, the signal process is represented by the EWK production and its vector-boson-scattering (EWK VBS) contribution will be enhanced by the analysis selection. The NNPDF3.0nlo [43] parton distribution functions (PDF) set was used and the parton shower and hadronization were modelled with Pythia 8.186 [44] using the A14 set of tuned parameters (tune) for the underlying event [45].

Potential modifications to the SM processes introduced by the Eboli model operators are implemented in the BSM signal samples. For each operator two terms were considered, the one including the Lagrangian term of the BSM effect only (pure-BSM) and the one including the SM-BSM interference. Both terms were modelled using MadGraph5_aMC@NLO v2.7.2 [42] at leading order (LO) with the boson decays simulated using MadSpin [46]. The NNPDF3.0lo [43] PDF set was used with Pythia 8.244 [47] for parton shower and hadronization. The total EWK VBS process for a certain operator and coupling value was then modelled by summing the SM EWK VBS process with the pure-BSM and the SM-BSM interference terms.

The background processes include the production of and Z bosons in association with jets (V+jets), top-quark pair production ($t\bar{t}$) and single-top quark production (single$-t$). The QCD-induced diboson production at order $O(\alpha_{EWK}^4\alpha_{QCD}^2)$ was also treated as a background process (QCD VV). The QCD and EWK diboson processes were generated separately and therefore the effect of the interference between the two was not included in the simulated samples; nevertheless this effect was estimated with a simplified procedure based on samples generated at the truth level without the full detector simulation. The interference

contribution was found to be 5% to 10% of the EWK process for the $Z(\to \nu\nu/ll)V$ samples and 10% to 20% for the $W(\to l\nu)V$ samples; the contribution is included in the analysis as a systematic effect.

The dominant V+jets background process was simulated with the SHERPA 2.2.1 [48] generator using next-to-leading-order (NLO) matrix elements (ME) for up to two partons, and LO matrix elements for up to four partons calculated with the COMIX [49] and OPENLOOPS [50–52] libraries. The QCD VV processes with one of the bosons decaying hadronically and the other one leptonically were simulated using SHERPA 2.2.1 with up to one additional parton at NLO and up to three additional partons at LO using the COMIX and OPENLOOPS programs. For both V+jets and QCD VV processes, the NNPDF3.0NNLO set of PDFs was used, and each sample matched with the SHERPA parton shower [53] using the MEPS@NLO prescription [54–57] and the set of tuned parameters developed by the SHERPA authors.

The $t\bar{t}$ and single-top quark processes were modelled using the POWHEG BOX v2 [58–62] generator at NLO with the NNPDF3.0NLO PDF set. The h_{damp} parameter, which regulates the high-p_{T} radiation against which the $t\bar{t}$ system recoils, was set to $1.5\,m_t$ [63]. The events were interfaced to PYTHIA 8.230 to model the parton shower, hadronization, and underlying event, with parameters set according to the A14 tune and using the NNPDF2.3LO set of PDFs [64]. For the single$-t$ channel, the top-quark decay was simulated using MADSPIN, while the remaining samples with top quarks have the top quark spin correlations preserved. The decays of bottom and charm hadrons were performed by EVTGEN 1.6.0 [65].

All simulated processes were normalized using the best currently available theoretical predictions for their cross sections. The V+jets cross sections were calculated at next-to-next-to-leading-order (NNLO) in QCD [66] and the QCD VV at NLO including LO contributions with two additional partons [57,67]. The $t\bar{t}$ production cross section was calculated at NNLO in QCD, including resummation of next-to-next-to-leading logarithmic (NNLL) soft-gluon terms [68,69]. The single$-t$ production cross sections were calculated to NLO in QCD [70], including the soft-gluon resummation at NNLL [71] for the Wt process. The normalization of the V+jets and $t\bar{t}$ processes in the relevant phase space were further improved by using data driven estimations in control regions as detailed in Sect. 5.

Simulated events were processed with a detailed detector simulation [72] based on Geant4 [73]. The generation of the simulated event samples includes the effect of multiple pp interactions per bunch crossing, as well as the effect on the detector response due to interactions from bunch crossings before or after the one containing the hard interaction (pile-up). The MC samples were reweighted to match the pile-up conditions in the data.

4 Object reconstruction

Collision vertices are formed from tracks with $p_T > 500$ MeV. The vertex candidate with the highest Σp_T^2 of its associated tracks is selected as the primary vertex. All selected events are required to contain a primary vertex with at least two associated tracks.

Electrons are identified as isolated energy clusters in the electromagnetic calorimeter matched to ID tracks, and are required to have $E_T > 7$ GeV and $|\eta| < 2.47$, excluding the electromagnetic calorimeter barrel–endcap transition region $1.37 < |\eta| < 1.52$. A likelihood-based requirement [74] is imposed to reduce the background from non-prompt electrons or hadrons misidentified as electrons. Electrons are classified as either 'loose', 'medium' or 'tight' according to the likelihood-based identification criteria described in Ref. [75].

Muons are reconstructed by a combined fit to the ID and MS tracks and are required to have $p_{\text{T}} > 7$ GeV and $|\eta| < 2.5$. Muons must pass identification requirements based on the number of hits in the ID and MS subsystems, and on the significance of the difference $|q/p_{\text{MS}} - q/p_{\text{ID}}|$ [76] , where q is the charge and p_{MS} (p_{ID}) is the momentum of the muon measured in the MS (ID). Similarly to electrons, muons are classified as either 'loose', 'medium' or 'tight', following the criteria in Ref. [77].

In this analysis, only 'loose' or 'tight' electrons and muons are selected. All electrons and muons are required to be isolated by using selections based on the sum in small cones around the lepton direction of the p_{T} of tracks, of calorimeter E_T, or both, to further reduce backgrounds from non-isolated sources. Leptons of loose quality with $p_{\text{T}} < 100$ GeV are required to pass a 'FixedCutLoose' isolation requirement ([74,76]) and no isolation requirement is applied for $p_{\text{T}} > 100$ GeV so as not to remove the leptons from $Z \to \ell\ell$ decays which are near one another; the same strategy was used in Ref. [78]. Furthermore, leptons are required to have associated tracks satisfying $|d_0/\sigma_{d_0}| < 5$ (3) and $|z_0 \times \sin\theta| < 0.5$ mm for electrons (muons), where d_0 is the transverse impact parameter relative to the beam line, σ_{d_0} is its uncertainty, and z_0 is the distance between the longitudinal position of the track along the beam line at the point where d_0 is measured and the longitudinal position of the primary vertex.

Two types of jets are employed in the analysis. Both of them are reconstructed using the anti-k_t algorithm [79,80] but different values of the radius parameter R. Small-R jets are reconstructed by clustering particle-flow objects [81] with a radius parameter of $R = 0.4$ and are required to have $p_{\text{T}} > 20$ GeV for $|\eta| < 2.5$ and $p_{\text{T}} > 30$ GeV for $2.5 < |\eta| < 4.5$. A jet vertex tagger (JVT) [82] is applied to jets with 20 GeV $< p_{\text{T}} < 60$ GeV and $|\eta| < 2.4$ to suppress jets from pile-up interactions. This tagger uses information on tracks associated with the primary vertex and pile-up ver-

tices. The forward-JVT (fJVT) [83] with the loose working point is also applied to jets with 20 GeV $< p_{\mathrm{T}} <$ 120 GeV and $2.5 < |\eta| < 4.5$. Energy- and η-dependent correction factors derived from MC simulations are applied to correct jets to the particle level [84]. Several in situ techniques are employed to correct for differences between data and simulation and to measure the resolution of jets [85]. Small-R jets containing b-hadrons are identified using a multivariate algorithm (b-tagging) based on a deep feed-forward neural network (DL1 b-tagging) [86]. The chosen b-tagging algorithm has an efficiency of 70% for b-quark jets in simulated $t\bar{t}$ events, with a light-flavor jet rejection factor of about 390 and a c-jet rejection factor of about 9.4 [86].

Large-R jets are reconstructed with a radius parameter of $R = 1.0$ and they are built from topological clusters, which are calibrated to the hadronic scale using the local hadronic cell weighting scheme [87]. To mitigate the effects of pile-up and soft radiation, the large-R jets are groomed following the trimming algorithm [88]. Trimming takes the original constituents of the jet and reclusters them using the k_t algorithm [89] with a smaller radius parameter, R_{subjet}, to produce a collection of subjets. These subjets are discarded if they carry less than a specific fraction (f_{cut}) of the original jet p_{T}. The trimming parameters were optimized for W/Z boson tagging and are $R_{\mathrm{subjet}} = 0.2$ and $f_{\mathrm{cut}} = 5\%$. The large-R jet four-momenta are recomputed from the remaining subjets, and the jet energies are calibrated to particle level using correction factors derived from MC simulations [90]. The jet energy scale and resolution are measured using SM events relying on other and well calibrated objects as reference; the jet mass response is measured using the masses of high-p_T W bosons and top quarks, and by comparing the jet mass measured using the energy deposited in the calorimeter with that using the momenta of charged-particle tracks [91]. Large-R jets are required to have $p_{\mathrm{T}} > 200$ GeV, $|\eta| < 2.0$ and a mass $m_J > 50$ GeV. Moreover, the jet substructure variable, D_2, reconstructed from energy correlation functions based on energies and pair-wise angles of the sub-constituents [92,93] is used. The D_2 variable is sensitive to the 2-prong sub-structure expected from the W/Z bosons decay. Furthermore, the multiplicity of tracks associated to the large-R jet before the grooming algorithm and passing standard reconstruction criteria with $p_{\mathrm{T}} > 500$ MeV ($n_{\mathrm{Tracks}}^{\mathrm{ungroomed}}$) is used to further improve the background rejection.

Boson tagging is applied to large-R jets to select those consistent with $V \to qq$ decays. The tagger is based on three variables, namely the sub-structure variables, D_2 and $n_{\mathrm{Tracks}}^{\mathrm{ungroomed}}$, and the jet mass. Large-R jets from a $V \to qq$ decay are expected to have values for the D_2 and the $n_{\mathrm{Tracks}}^{\mathrm{ungroomed}}$ variables smaller than the ones of jets initiated by quarks or gluons, while the mass is expected to peak around the W or Z boson mass. The algorithm operating points are based on simultaneous requirements on the three variables; they are designed to provide a constant efficiency independent of the large-R jet p_{T} for the signals studied and they are labelled according to their efficiency. The requirement thresholds applied to the three variables therefore depend on the p_{T} of the jet and are shown in Fig. 2. A similar tagging scheme was used in previous diboson searches [78,94]. In this analysis, two working points, one with 50% efficiency and the other one with 80% efficiency, are used to define two analysis regions with different purities.

The missing transverse energy, $E_{\mathrm{T}}^{\mathrm{miss}}$ is reconstructed by taking the negative vectorial sum of all the reconstructed and calibrated electrons, muons, and small-R jets. An additional term is used to account for soft radiation that leaves tracks in the inner detector that are not used in any reconstructed physics object [95]. Large-R jets are not included in this definition to avoid double counting with small-R jets. The track-based missing transverse momentum, p_T^{miss}, is the vectorial sum of the transverse momenta reconstructed from particle tracks. Both $E_{\mathrm{T}}^{\mathrm{miss}}$ and p_T^{miss} are utilized in the event selection.

An overlap-removal procedure is applied to the selected leptons and jets to remove ambiguities in the identification of the objects mentioned above and to assign a unique hypothesis to each object. If an electron and a small-R jet are separated by $\Delta R < 0.2$, the jet is removed. The electron is removed if the separation satisfies $0.2 < \Delta R < 0.4$. If a muon and a small-R jet are separated by $\Delta R < 0.2$ and if the jet has less than three tracks or the energy and momentum differences between the muon and the jet are small, the jet is removed. Otherwise the muon is removed if the separation satisfies $\Delta R < 0.4$. To prevent double-counting of energy from an electron inside a large-R jet, the large-R jet is removed if an electron and a large-R jet are separated by $\Delta R < 1.0$. Small-R jets and large-R jets are reconstructed independently from the same energy depositions for a given event. No overlap removal is applied between large-R jets and small-R jets.

5 Event selection and background estimation

According to the number of selected electrons and muons, each event is classified as belonging to the 0-, 1- or 2-lepton channel. After requiring a candidate boson decaying into leptons (V_{lep}), the events in all three channels are required to contain two forward small-R jets (called tagging jets) with a high invariant mass. The V candidate decaying into hadrons (V_{had}) is reconstructed as either two small-R jets in the resolved selection, or one large-R jet in the merged selection. The event selection is designed to guarantee the statistical independence of the channels and to maximize the combined

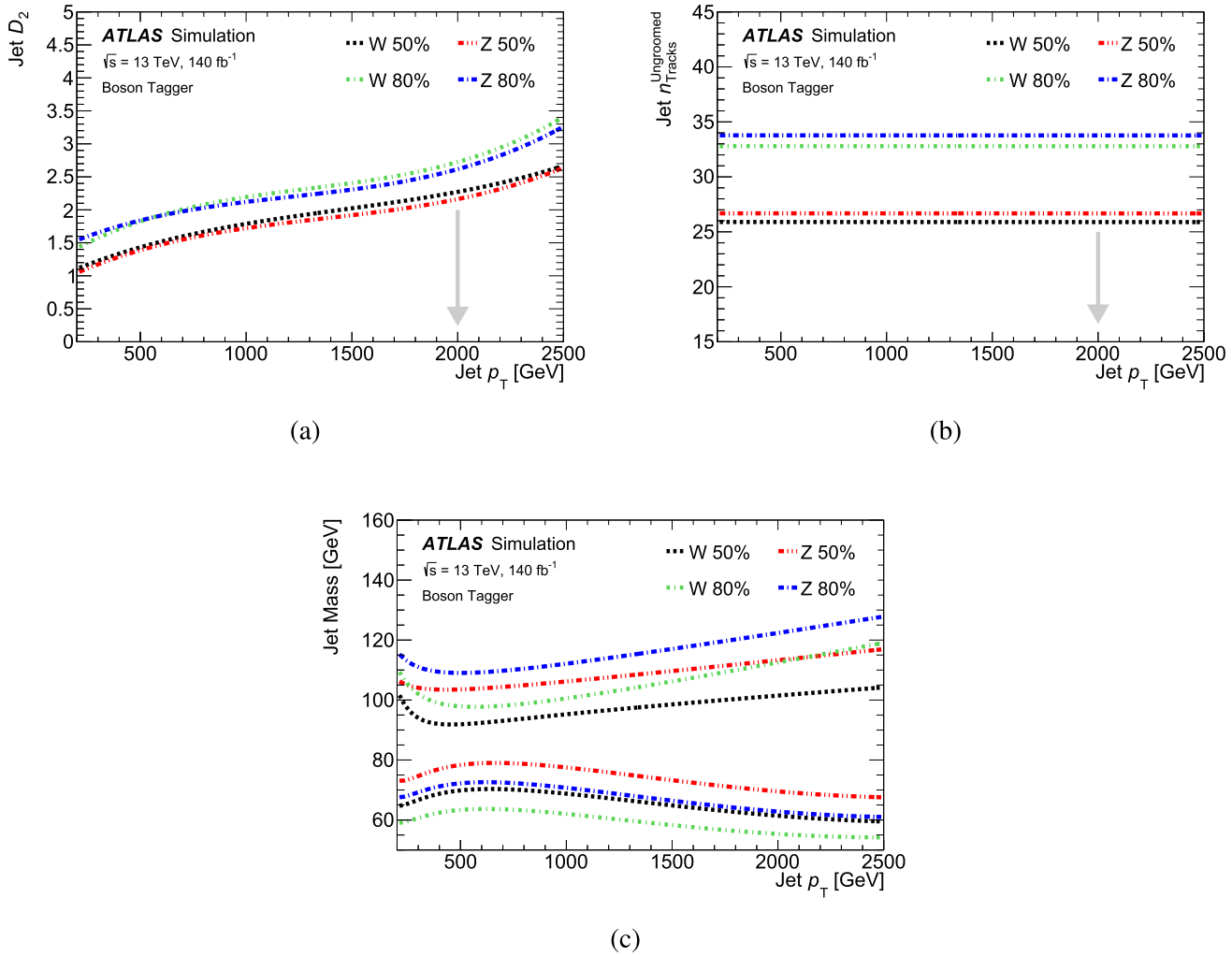

Fig. 2 The requirement thresholds applied by the boson tagging algorithm on **a** D_2, **b** $n_{\text{Tracks}}^{\text{ungroomed}}$, and **c** jet-mass for different boson hypothesis and working points corresponding to 50% and 80% signal efficiency as a function of jet p_{T}. All three requirements are applied to derive the efficiency of the working point. The grey arrow shows the direction of the requirement applied for the D_2 and $n_{\text{Tracks}}^{\text{ungroomed}}$ variables, while for the mass, jets within the window are selected

sensitivity of the analysis. The selection results in nine non-overlapping distinct signal regions (SR): for each of the three lepton channels, there are three categories based on the choice and selections on the V_{had} candidate, one for the resolved and two (one for each boson tagger working point) for merged V_{had} candidate.

The event selection for the entire analysis is summarized in Table 1. More details are given in the following Sections.

5.1 Event selection

Signal events in the 0-lepton channel are typically characterized by a hadronically decaying V boson recoiling against a large amount of $E_{\text{T}}^{\text{miss}}$ stemming from either a $Z \to \nu\nu$ decay or a $W \to \ell\nu$ decay with the lepton outside of the acceptance of the detector. An initial selection is made by requiring $E_{\text{T}}^{\text{miss}} > 200$ GeV, and rejecting events with electrons or muons passing the loose quality requirements. Further selections are applied to reduce the amount of multijet background. This background originates primarily from the presence of misidentified jets and non-collision phenomena. It is suppressed by requiring a $p_{\text{T}}^{\text{miss}}$ of at least 50 GeV and an $E_{\text{T}}^{\text{miss}}$ of at least 200 GeV. Further angular selection criteria are applied, $\Delta\phi(\mathbf{E}_{\text{T}}^{\text{miss}}, \mathbf{p}_{\text{T}}^{\text{miss}}) < \pi/2$, $\min[\Delta\phi(\mathbf{E}_{\text{T}}^{\text{miss}}, \text{small-}R \text{ jet})] > \pi/6$, $\Delta\phi(\mathbf{E}_{\text{T}}^{\text{miss}}, V_{\text{had}}) > \pi/9$. The multijet background is found to be negligible after this set of selections.

The 1-lepton channel targets events with a leptonically decaying W boson. The $W \to \ell\nu$ candidates are selected by requiring one isolated lepton (electron or muon) satisfying

Table 1 Summary of the event selection in the 0-, 1- and 2-lepton channels

Selection	0-lepton	1-lepton	2-lepton
Trigger	$E_{\mathrm{T}}^{\mathrm{miss}}$ triggers	Single-electron triggers Single-muon or $E_{\mathrm{T}}^{\mathrm{miss}}$ triggers	Single-lepton triggers
$V \to \nu\nu/\ell\nu/\ell\ell$	0 'Loose' leptons $p_{\mathrm{T}} > 7\,\mathrm{GeV}$	1 'Tight' lepton $p_{\mathrm{T}} > 27\,\mathrm{GeV}$	2 'Loose' leptons $p_{\mathrm{T}} > 27\,\mathrm{GeV}$
	$E_{\mathrm{T}}^{\mathrm{miss}} > 200\,\mathrm{GeV}$	0 other 'Loose' leptons with $p_{\mathrm{T}} > 7\,\mathrm{GeV}$	
	$p_{\mathrm{T}}^{\mathrm{miss}} > 50\,\mathrm{GeV}$	$E_{\mathrm{T}}^{\mathrm{miss}} > 80\,\mathrm{GeV}$	$83 < m_{ee} < 99\,\mathrm{GeV}$
	$\Delta\phi(\mathbf{E}_{\mathrm{T}}^{\mathrm{miss}}, \mathbf{p}_{\mathrm{T}}^{\mathrm{miss}}) < \pi/2$		$-0.0117 \times p_{\mathrm{T}}^{\mu\mu} + 85.63\,\mathrm{GeV} < m_{\mu\mu}$
	$\min[\Delta\phi(\mathbf{E}_{\mathrm{T}}^{\mathrm{miss}}, \text{small-}R \text{ jet})] > \pi/6$		$0.0185 \times p_{\mathrm{T}}^{\mu\mu} + 94\,\mathrm{GeV} > m_{\mu\mu}$
	$\Delta\phi(\mathbf{E}_{\mathrm{T}}^{\mathrm{miss}}, V_{\mathrm{had}}) > \pi/9$		
VBS topology tagging jets	Largest m_{jj} pair with $\eta_{\mathrm{tag}\ j_1} \cdot \eta_{\mathrm{tag}\ j_2} < 0$		
	$m_{jj}^{\mathrm{tag}} > 400\,\mathrm{GeV}$, $p_{\mathrm{T}}^{tag\ j_{1,2}} > 30\,\mathrm{GeV}$		
$V \to J$	Leading p_{T} large-R jet		
	$p_{\mathrm{T}} > 200$ GeV, $\lvert\eta\rvert < 2$		
	V boson tagger requirements on m_J, D_2, and $n_{\mathrm{Tracks}}^{\mathrm{ungroomed}}$		
$V \to jj$	Two leading p_{T} small-R jets		
	$p_{\mathrm{T}} > 20\,\mathrm{GeV}$ if $\lvert\eta\rvert < 2.5$, and $p_{\mathrm{T}} > 30\,\mathrm{GeV}$ if $2.5 < \lvert\eta\rvert < 4.5$		
	$p_{\mathrm{T}}^{j_1} > 40\,\mathrm{GeV}$		
	$64 < m_{jj} < 106\,\mathrm{GeV}$		
Top veto	$m_{jjj} > 220\,\mathrm{GeV}$ (resolved only)		
Additional b-jet veto	No	Yes	No

the tight criteria with $p_{\mathrm{T}} > 27$ GeV. Events are required to have $E_{\mathrm{T}}^{\mathrm{miss}} > 80$ GeV, and must not have any additional loose lepton. In order to reconstruct the invariant mass of the WV system, the neutrino momentum four-vector is reconstructed by imposing a W boson mass constraint on the lepton-neutrino system. The neutrino p_{T} components are set equal to the $E_{\mathrm{T}}^{\mathrm{miss}}$, and the unknown z-component of the momentum (p_z) is obtained from the resulting quadratic equation. The p_z is chosen either as the smaller, in absolute value, of the two real solutions or, if the solution is complex, as its real part.

In the 2-lepton channel, the $Z \to \ell\ell$ candidates are identified by requiring two isolated same-flavor leptons satisfying the loose criteria. Both the leading- and subleading-p_{T} leptons must satisfy $p_{\mathrm{T}} > 27$ GeV. The trigger efficiency is stable as a function of the lepton p_{T} when the lepton matching the trigger decision has a p_{T} above that threshold. The same p_{T} requirement is applied on both leptons to ensure an optimal signal-to-background ratio. Opposite charges are required for the muon pairs but not for the electron pairs, since electrons are more susceptible to charge mis-identification due to the conversion of photons from bremsstrahlung, especially at high p_{T}. The dilepton invariant mass is required to be consistent with that of the Z boson: $83 < m_{ee} < 99$ GeV in the case of electrons and $(-0.0117 \times p_{\mathrm{T}}^{\mu\mu} + 85.63\ \mathrm{GeV}) < m_{\mu\mu} < (0.0185 \times p_{\mathrm{T}}^{\mu\mu} + 94\ \mathrm{GeV})$ in the case of muons. The p_{T}-dependent requirement on $m_{\mu\mu}$ recovers the selection efficiency at high $p_{\mathrm{T}}^{\mu\mu}$, which would otherwise fall due to the degraded dimuon invariant mass resolution [96].

Tagging jets are selected from the entire small-R jets collection. Candidate jets are required to pass the basic kinematic selections introduced in Sect. 4. The candidate jets are then required to be in opposite hemispheres, $\eta_{\mathrm{tag},j_1} \cdot \eta_{\mathrm{tag},j_2} < 0$, and the candidate jet pair is selected as the one with the highest invariant mass. Once the candidate pair is identified, the invariant mass of the two tagging jets is further required to satisfy $m_{jj}^{\mathrm{tag}} > 400$ GeV and both tagging jets are required to have $p_{\mathrm{T}} > 30$ GeV.

Once the tagging jets are identified, the merged selection is applied as the first step in identifying a V_{had} candidate. If an event is not selected as merged, then the resolved selection is used. The merged regime contributes less than the resolved one to the overall signal efficiency of the EWK process, roughly 30% of signal events have a boson with a p_{T} greater than 200 GeV, but the lower background contamination results in a contribution to the sensitivity to the EWK process that is competitive with the one of the resolved regime. The merged regime sensitivity is instead the leading one for the aQGC samples. The V_{had} candidates are selected in each of the three lepton channels. According to the merged regime selection, events are required to have at least one large-R jet; large-R jets overlapping with one of the selected tagging jets are discarded, if there is more than one, the one with the leading p_{T} is selected as signal jet. In the 2-lepton channel, events

with the signal large-R jet overlapping with one of the two selected leptons, within $\Delta R < 0.4$, are rejected as $Z \to ee$ candidates can potentially be reconstructed as large-R jets.

Two SRs are defined in the merged regime by requirements on the boson tagging, as discussed in Sect. 4. The high-purity (HP) SR comprises events which pass the 50% boson tagger working point requirement. An orthogonal low-purity (LP) SR is defined with events which fail the high-purity requirement but still pass the 80% boson tagger working point. Both regions are defined without distinguishing between the W and Z hypotheses, requiring that the large-R jet satisfies either W or Z boson tagging.

In the resolved selection, the tagging jets are excluded from the pool of jets used to identify the signal jets candidates; the remaining two leading p_{T} small-R jets are labelled as signal jets. Events are required to have the dijet invariant mass falling in the $m_{W/Z}$ window: $64 < m_{jj} < 106$ GeV. Out of the jets forming the selected V_{had} candidate, the leading-p_{T} one must have $p_{\mathrm{T}} > 40$ GeV.

Finally, in the 1-lepton channel, the event is rejected if it contains any b-tagged small-R jet that is not a tagging jet or a jet forming a V_{had} candidate (resolved) or a jet that overlaps the V_{had} candidate jet (merged), in order to reduce the contribution from top-quark processes.

The tagging jets selection is designed to enhance the VBS contribution over the other EWK contributions. Despite this selection, a significant contribution from the top-quark associated production, i.e. from diagrams with the Wtb vertex, is found in the resolved regime. Therefore, a further selection is applied to improve the purity of the VBS contribution. A triple-jet system is reconstructed selecting the jets coming from the V_{had} and an additional jet (without any requirement on the b-tagging) such that the three-jet mass is the closest to the top-quark mass. Events with a three-jet mass below 220 GeV are rejected, allowing a reduction of the top-quark associated production to 10% in $WZjj$ and to 30% in $WWjj$ samples in the resolved regime; the corresponding efficiency for the VBS events if of around 65%. The contribution of the top-quark associated production is already suppressed in the boosted regime after the other selection requirements; a further requirement based on the reconstructed top mass similar to the one used in the resolved regime does not reduce it further and is therefore not applied.

The regions as defined above are not completely orthogonal, and so to simplify the statistical procedure, a region prioritization scheme is used to maximize the signal sensitivity while removing overlapping events. Merged regions are prioritized over resolved regions and all events are sorted into only one possible analysis region. The flow is summarized schematically in Fig. 3.

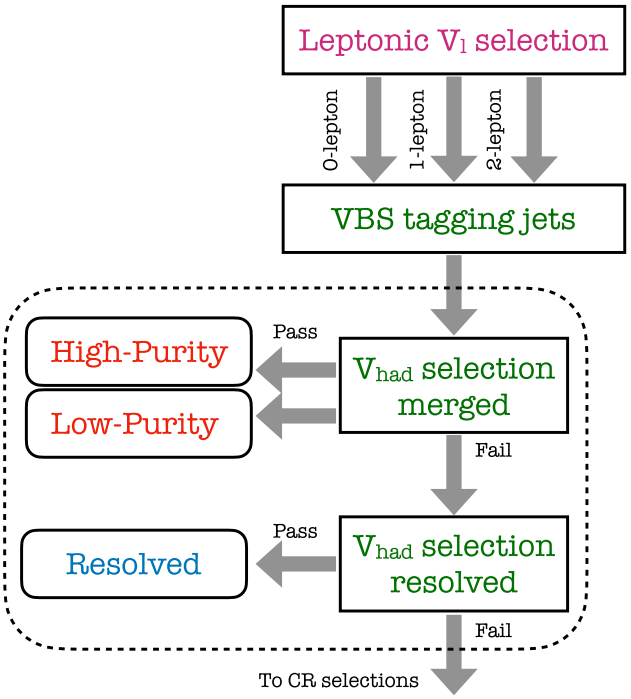

Fig. 3 Schematic of the analysis categorisation flow

5.2 Background estimation

The dominant backgrounds in the 1-lepton channel are W+jets and $t\bar{t}$ production; in the 2-lepton channel it is Z+jets production; while in the 0-lepton channel, they all contribute significantly. Single-top and QCD-induced diboson production are small backgrounds for all channels. The background contributions are estimated using a combination of MC and data-driven techniques; indeed, the shapes of kinematic variable distributions are taken from MC simulations in all cases and the normalisation of the main backgrounds are constrained using dedicated control regions (CRs).

A V+jets CR is defined for each of the three SRs in all the three lepton channels; specifically, these CRs are named ZCR in the 2-lepton channel, WCR in the 1-lepton channel and VCR in the 0-lepton channel since the first two channels are mainly populated by Z+jets and W+jets processes, respectively, while the 0-lepton channel is populated by a mixture of both processes. These CRs are defined using exactly the same requirements as in the SRs but reverting the mass requirement, m_J or m_{jj}, of the V_{had} candidate. The ZCRs are dominated by the Z+jets contribution, with a purity higher than 90% in all regions. They are therefore used to constrain its contribution in SRs through simultaneous fits, as discussed in Sect. 9. The WCRs are enriched in the W+jets process, with purities of 47% and 64% in the merged and resolved categories of the 1-lepton channel, respectively; the remaining events are primarily from $t\bar{t}$ production.

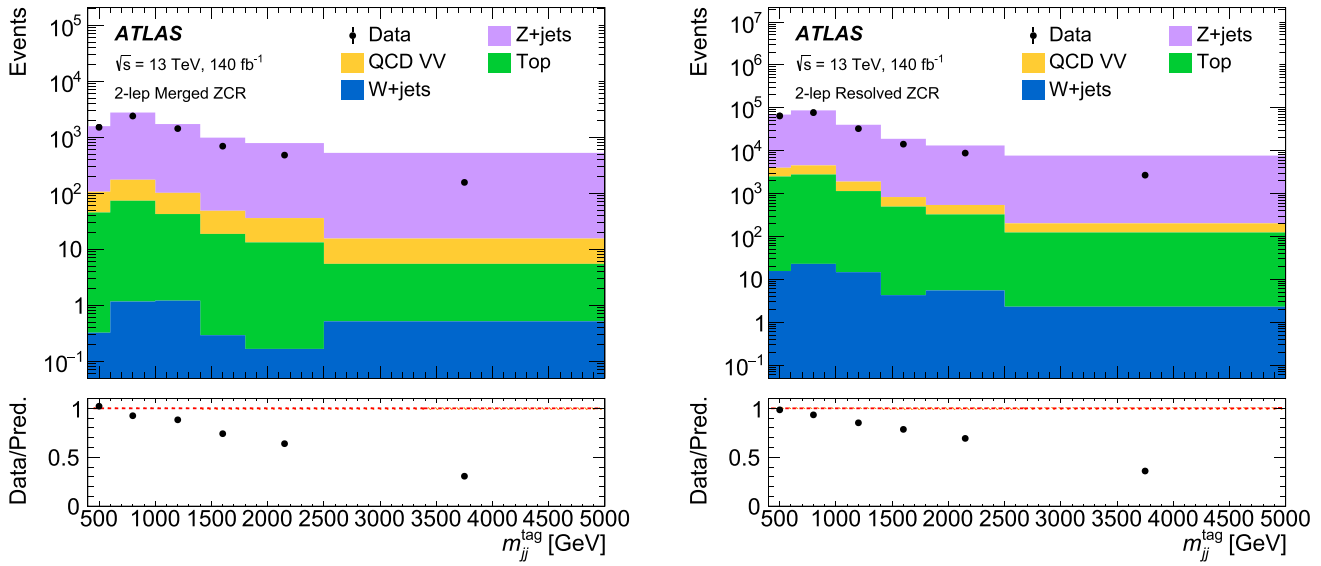

Fig. 4 The measured (dots) distribution as a function of m_{jj}^{tag} in the 2-lepton ZCR in the merged (**a**) and resolved (**b**) regions. The last bin contains overflow events. The different simulated processes are shown as stacked histograms. The predictions are normalised to the generator cross section including the pile-up reweighting and other trigger and leptons related scale factors. The bottom panel shows the ratio of data to prediction, without systematic uncertainties

The three $t\bar{t}$ CRs, TCRs, are defined to contain events satisfying the SRs selection of the 1-lepton channel and requiring a b-jet instead of vetoing it. These CRs are dominated by $t\bar{t}$ production, with a purity of 90% and 75% for the merged and resolved categories respectively, with remaining background contributions from single-top, V+jets or diboson production, for both the merged and the resolved event topologies.

The m_{jj}^{tag} distributions are not well modelled by the SHERPA simulated W+jets (Z+jets) events, as reported in Ref. [33]. A similar effect in the SHERPA modelling was also reported for diboson events [97]. The modelling is studied in the WCRs (ZCRs); an example of the effect in the merged and resolved ZCRs is shown in Fig. 4.

A data-driven procedure, similar to that described in [33], is applied to the simulated W+jets and Z+jets events to correct for this shape mis-modelling. Reweighting factors are derived from WCRs and ZCRs as functions of m_{jj}^{tag}, and applied in all SRs and CRs (for the 0-, 1-, and 2-lepton regions) to the MC simulation of W+jets and Z+jets events. The non-W+jets (Z+jets) contributions, as predicted by MC, are subtracted from data and the resulting distribution is normalized to unity; the resulting shape is compared with the one from the MC simulation of W+jets (Z+jets) processes and the reweighting factors are estimated by performing a linear fit as a function of m_{jj}^{tag}. Reweighting factors are applied to events provided that the computed values are positive; if a computed value is negative, a factor of zero is assigned instead. Given the observed mismodeling, a linear model was found to be sufficient to describe and correct it; more complex models, although capable of incorporating additional event information, did not lead to significant improvements.

The procedure is done separately for the merged and resolved analyses. For the W+jets process, the reweighting factor derived in the WCRs ranges from 1.04 (1.16) at $m_{jj}^{\text{tag}} = 400$ GeV to 0.58 (0.51) at $m_{jj}^{\text{tag}} = 3000$ GeV in the resolved (merged) analysis. For the Z+jets process, the reweighting factor derived in the ZCRs ranges from 1.10 (1.20) at $m_{jj}^{\text{tag}} = 400$ GeV in the resolved (merged) analysis to 0.56 (0.55) at $m_{jj}^{\text{tag}} = 3000$ GeV. A demonstration of the procedure for the Z+jets is shown in Fig. 5.

Dedicated reweighting factors are needed for the MC simulation of W+jets and Z+jets events in the 0-lepton channel because the phase space is different between the 0-lepton selection and the 1- and 2-lepton selections so that the reweightings described above are not applicable. A similar linear fit procedure is applied to the sum of the W+jets and Z+jets events in VCR as function of m_{jj}^{tag}; the reweighting factor derived in the VCR ranges from 1.03 (0.96) at $m_{jj}^{\text{tag}} = 400$ GeV to 0.74 (0.62) at $m_{jj}^{\text{tag}} = 3000$ GeV in the resolved (merged) analysis.

Good agreement between the prediction from MC simulation and the data in the VCR is achieved after the reweighting procedure is applied. The systematic uncertainty associated with this reweighting procedure is described in Sect. 8. Conservative 100% uncertainties in the fitted parameters are con-

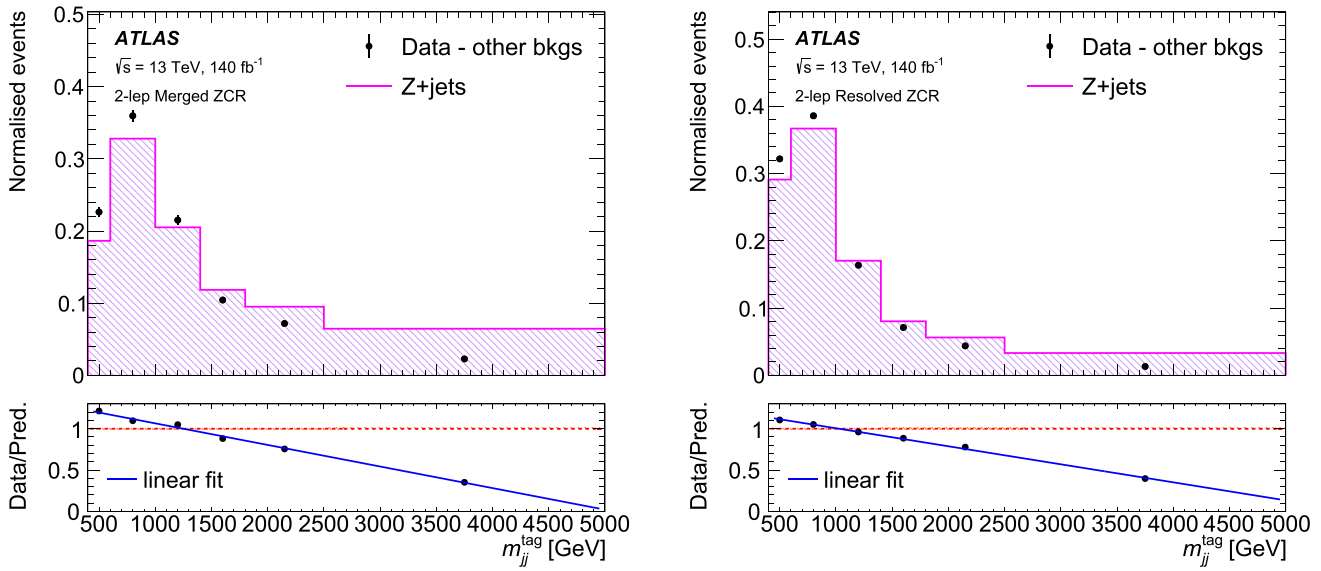

Fig. 5 The measured distribution after background subtraction and linear fit as a function of m_{jj}^{tag} in the **a** merged and **b** resolved 2-lepton ZCR. The simulated Z+jets process is shown as a histogram while the dots show the data after the subtraction of the other background processes; the distributions are normalised to unity. The bottom panel shows the ratio of the data to the prediction, together with the linear fit (solid line)

sidered, which will be constrained by the fit as discussed in Sect. 8.

6 Machine learning approach for final discriminant

The target signal in this analysis is the EWK $VVjj$ production and specifically its VBS contribution. The VBS signal topology is characterized by two extra hard jets that are produced in the two opposite forward regions of the detector. Both of them usually have high $|\eta|$ and energy values and the dijet pair is characterized by a high invariant mass and a large angular separation. Furthermore, the invariant mass of the reconstructed diboson system is also higher for VBS signal events. These represent some key discriminating variables.

To improve the separation from the background processes, a ML approach based on a recurrent neural network (RNN) architecture [78,98] is developed for this analysis. The architecture of the network is based on a RNN in the resolved regime SRs. In the merged regime, the architecture of the network is extended to also include a branch based on a deep neural network (DNN), with a few hidden flat layers, taking into account the large-R jet information.

The RNN architecture has already been exploited for a few applications by the ATLAS Collaboration; it was first used in the context of heavy-flavour identification [99] and then deployed for a vector-boson-fusion classification task in diboson resonant searches [78]. Since it is an architecture designed to handle input features organized in sequences of variable length, it is a good architecture to deal with final states with a variable number of jets, such as the one probed here.

The RNN model is trained to separate the signal from the SM background processes and the output scores are used as final discriminants in the analysis. To fully benefit from the deep learning regime, low-level input variables, i.e. the four-momentum of the jets and the track multiplicity (p_{T}, η, ϕ, E and n_{Tracks}) are used. Specifically, the RNN implementation available in Keras [100] is used and the Tensorflow package [101] is used as backend for the mathematical computation. A maximum of five jets is considered for each event; this upper value is optimized by checking the final sensitivity of the analysis; including less jets would mean missing some hard-scatter jets when some pile-up jets have a higher p_{T} than one of the forward VBS jets, while including more jets would introduce further systematic uncertainties in the result. A dedicated training is needed in each lepton channel due to the different background composition. Moreover, for the merged regime, one global training without the HP/LP separation is applied to maximize the statistics for the training.

To construct the RNN discriminant, the architecture is designed to leverage recurrent features through two hidden

RNN layers and an output layer with a single node. The training process is set for a maximum of 200 epochs but terminates if there are 10 consecutive iterations without improvement. A dropout rate of 0.3 is applied, and the Adam [102] optimizer is utilized. The two long short-term memory (LSTM) [98] layers use the hyperbolic tangent activation function, while the output layer employs a sigmoid activation function [103]. The MC sample is divided into three parts: 56% for training, 30% for testing, and 14% for validation. During training, the signal and background events are weighted according to their physical cross sections and MC weights. For the V + jets process, the additional reweighting derived to correct the m_{jj} distribution, as discussed in Sect. 5, is applied; this ensures a more accurate description of the background events during training, and therefore leads to a more optimal model. Finally, a global normalization factor is applied to ensure that the signal and background samples contain the same total number of events, providing a balanced representation of both classes during training.

For the merged regime, the large-R jet candidate information is added to further enhance the VBS signal-to-background separation completing the set of information related to the V_{had} decay; specifically, the four-momentum components (p_{T}, η, ϕ, E) of the large-R jet candidate are used as additional input variables. The architecture in this case is extended with an additional branch, based on a set of dense layers, that processes the information of the large-R jet and combine it with the information of the small-R jets sequences processed through the RNN layers. The use of an extended architecture allows the exploitation of the correlation across the tagging jets and the V_{had}; for simplicity, this extended architecture will also be referenced to as RNN in the following.

Figure 6 shows the RNN scores for the signal and background samples, including the training and test MC samples for the 0-, 1- and 2-lepton merged and resolved SRs. The score distributions show how well the RNN distinguishes between signal and background; the ratio of RNN scores for the test and training samples indicates a good agreement between them and demonstrates the absence of overtraining. Moreover, a k-Fold cross-validation test is performed; the input samples are split into training and test events sliding the test sample $k = 5$ times, each time training and testing on independent samples. The performance is found to be consistent within the statistical uncertainty of the sample, confirming that no overtraining is caused from the input sample.

7 Fiducial phase-space definition

To minimize the extrapolation uncertainty, the cross section is measured with respect to a truth fiducial region which closely mimics the reconstructed region. The fiducial phase space of the measurement is defined using stable final-state particles [104]. The full fiducial selection is summarized in Table 2.

Truth charged leptons (electrons or muons) are required not to originate from hadron decays and to have $p_{\text{T}} > 27$ GeV and $|\eta| < 2.5$. The lepton four-vector is adjusted to include photon radiation within $\Delta R < 0.1$. The truth-level $E_{\text{T}}^{\text{miss}}$ is calculated from the four-vector sum of all neutrinos in the event. Small-R and large-R jets at the truth level are clustered using the same algorithms as the reconstruction level jets using all particles except for prompt charged leptons, neutrinos, and photons from $W/Z/H/\tau$ decays. Truth large-R jets are required to have $p_{\text{T}} > 200$ GeV and $|\eta| < 2.0$. Similarly, truth small-R jets are required to have $p_{\text{T}} > 20$ GeV if $|\eta| < 2.5$, and $p_{\text{T}} > 30$ GeV for $2.5 < |\eta| < 4.5$. Jets containing b-hadrons are labeled as truth b-jets.

The VBS topology is identified by the requirement of two truth small-R jets with $p_{\text{T}} > 30$ GeV, $\eta_{\text{tag } j_1} \cdot \eta_{\text{tag } j_2} < 0$ and dijet mass $m_{jj}^{tag} > 400$ GeV. If more than one dijet pair satisfies these conditions, the pair with highest mass is retained. The V_{had} candidate jets are selected in the merged and resolved regions as either the leading large-R jet or the two remaining highest-p_{T} small-R jets, respectively.

The truth fiducial region is further subdivided into categories which align with the corresponding signal regions. The 0-, 1-, 2-lepton regions are defined by requiring the corresponding number of truth charged leptons. Additionally, the 0-lepton (1-lepton) region requires truth $E_{\text{T}}^{\text{miss}} > 200$ (80) GeV. The truth merged regions are required to contain a truth large-R jet passing the above requirements with $\Delta R(J, j) > 1.4$ with respect to the VBS topology jets and the jet mass passing the $64 < m_J < 106$ GeV requirement. No W/Z-tagging is employed at the truth level so the merged regions are not separated into HP/LP regions as the reconstruction level is. The acceptance effect due to different jet substructure requirements between the truth fiducial region, which is substructure-inclusive, and the reconstruction level W/Z-tagging is evaluated to be negligible. Resolved events are selected from the remaining events failing the merged selection if the leading (subleading) p_{T} of the V_{had} small-R jet has $p_{\text{T}} > 40\,(20)$ GeV, and the mass of the pair satisfies $64 < m_{jj} < 106$ GeV. The resolved regions also require the three-jet mass closest to the top-quark mass to have $m_{jjj} > 220$ GeV, following the selection at the reconstruction level to suppress EWK $t\bar{t}$ production in the fiducial phase space. Additionally, in the 1-lepton region, the V_{had} candidate jets are required not to be truth b-jets.

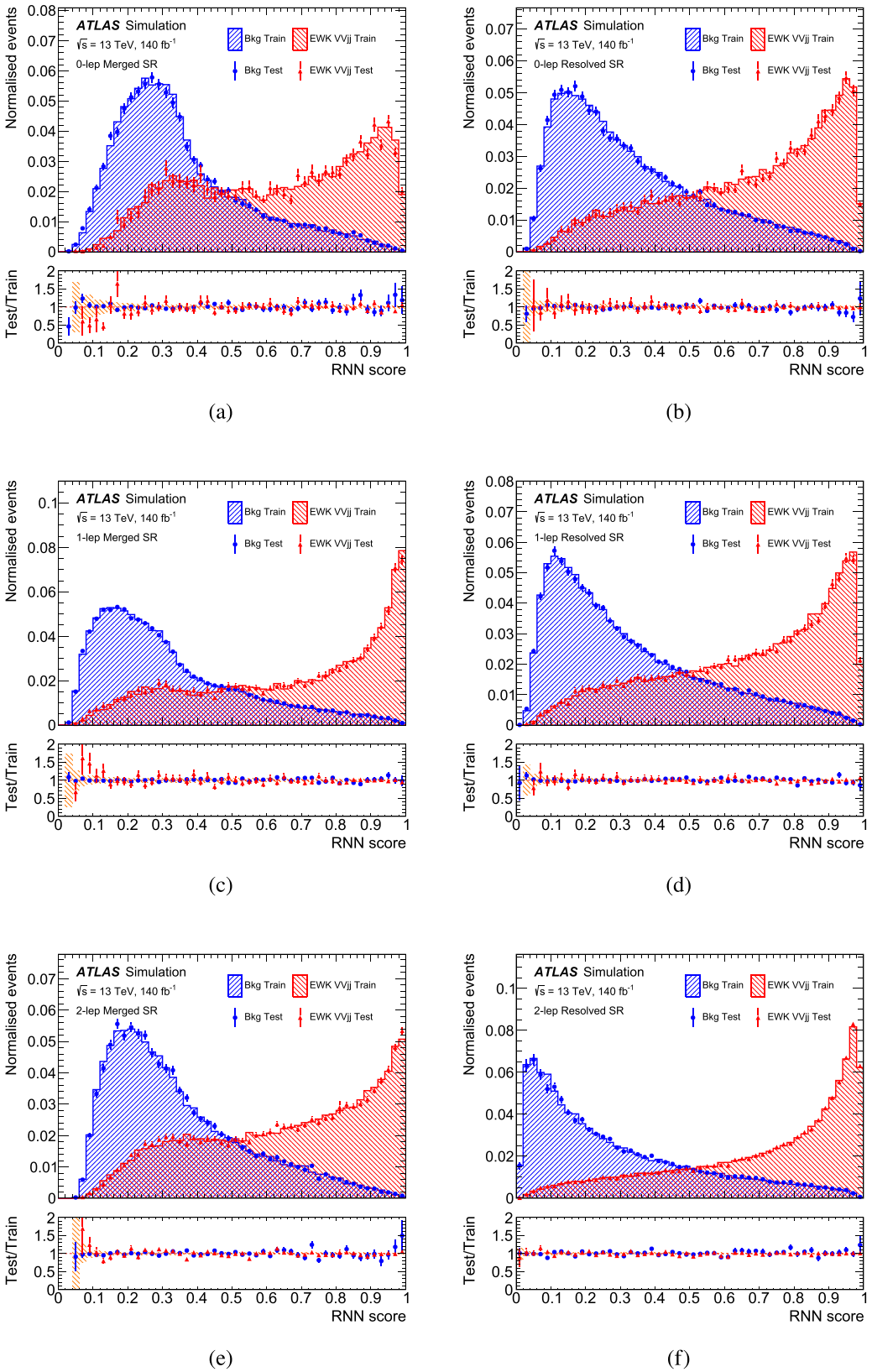

Fig. 6 RNN score distributions for signal and background samples showing the training (histograms) and test (markers) datasets for the **a**, **b** 0-, **c**, **d** 1- and **e**, **f** 2-lepton, **a**, **c**, **e** merged and **b**, **d**, **f** resolved SRs. The ratio of the test and training RNN scores in the signal and background samples is shown in the bottom panel

Table 2 Summary of the object and event selection performed at the truth level to define the fiducial regions

Object selection			
Leptons	$p_{\mathrm{T}} > 27$ GeV, $\lvert\eta\rvert < 2.5$		
Small-R jets	$p_{\mathrm{T}} > 20$ GeV if $\lvert\eta\rvert < 2.5$ and $p_{\mathrm{T}} > 30$ GeV if $2.5 < \lvert\eta\rvert < 4.5$		
Large-R jets	$p_{\mathrm{T}} > 200$ GeV, $\lvert\eta\rvert < 2.0$		
Event selection			
Selection	0-lepton	1-lepton	2-lepton
$V \to \nu\nu/\ell\nu/\ell\ell$	$E_{\mathrm{T}}^{\mathrm{miss}} > 200$ GeV	1 lepton	2 leptons
		$E_{\mathrm{T}}^{\mathrm{miss}} > 80$ GeV	
VBS topology tagging jets	Largest m_{jj} pair with $\eta_{\mathrm{tag}\ j_1} \cdot \eta_{\mathrm{tag}\ j_2} < 0$,		
	$p_{\mathrm{T}}^{tag\ j_{1,2}} > 30$ GeV, m_{jj}^{tag}>400 GeV		
$V \to J$	Leading p_{T} large-R jet		
	$64 < m_J < 106$ GeV		
$V \to jj$	Two leading p_{T} small-R jets		
	$p_{\mathrm{T}}^{j_1}$ >40 GeV, $p_{\mathrm{T}}^{j_2}$ >20 GeV		
	$64 < m_{jj} < 106$ GeV		
	$m_{jjj} > 220$ GeV		
Additional b-jet veto	No	Yes	No

8 Systematic uncertainties

Systematic uncertainties result in both changes to the overall predicted yields of processes, as well as shape effects on the kinematic observables. Broadly, the systematic uncertainties can be categorized as either experimental uncertainties arising from the detector and reconstruction performance, and theory modelling uncertainties in the background and signal simulation. The uncertainties quoted in this section are the relative uncertainties on the specified quantity, and not the propagated uncertainty in the analysis sensitivity.

8.1 Experimental uncertainties

The uncertainty in the combined 2015–2018 integrated luminosity is 0.83% [36], obtained using the LUCID-2 detector [105] for the primary luminosity measurements. An additional uncertainty in the re-weighting procedure for the pile-up simulation is included to cover the uncertainty in the ratio of the predicted and measured inelastic cross section [106].

The uncertainties associated to the lepton triggers are found to be negligible as the efficiency for the selected signal events is high. The modelling of the electron and muon reconstruction, identification, and isolation efficiencies is evaluated using tag-and-probe methods with $Z \to \ell\ell$ events in both data and simulation [75–77]. Corrections of the order of 1% are applied to the simulation to better model the performance seen in data. Uncertainties in the electron (muon) energy (momentum) scale and resolution are also considered [107,108].

Uncertainties in the small-R jet energy scale and resolution are determined using MC simulation and data-driven techniques [85]. For central jets, the total relative uncertainty in the jet energy scale varies in the range 1–5% for $p_{\mathrm{T}} > 20$ GeV. The uncertainty in the small-R jet energy resolution ranges from 25% for jets with a p_{T} of 20 GeV to less than 5% for jets with $p_{\mathrm{T}} > 300$ GeV. Since the EWK VBS topology is enriched in quark-like jets, the q/g fraction is estimated in MC in the signal regions as functions of the jet p_{T} and η and is propagated to the relevant components of the uncertainties to accommodate for potential different responses of quark and gluon initiated jets. Uncertainties in the efficiencies for successfully tagging b-jets and for mis-tagging light-flavour jets are determined from studies in $t\bar{t}$ enriched samples [86,109]. Uncertainties in the tracks associated to jets are measured in pile-up events using random triggers [110] and the uncertainty in their multiplicity is evaluated from dijet events [111].

The uncertainties in the large-R jet energy scale and resolution are determined using a similar methodology as for the small-R jets and are found to be of the order of 1% and 15%, respectively, in the region of interest [91]. In addition, the uncertainty in the jet mass scale and resolution is also measured and found to be 1-5% and 10-20%, respectively, for jets near the W/Z mass [91,112]. A dedicated calibration for the boson tagger is included. The strategy foresees to calibrate the efficiency working points for W/Z-initiated signal jets and for quark/gluon-initiated background jets that are used in the simulation of the various processes considered. Calibrations and uncertainties in MC are evaluated in data CRs

[113]. Signal-like jets are selected in a $t\bar{t}$ enriched region for $p_{\mathrm{T}} < 600$ GeV, and extrapolated to higher p_{T} via alternative MC modelling samples, while background-like jets are evaluated from dijet and γ+jet events. The uncertainty in the signal efficiency is approximately 20% for the 50% efficiency working point, and the uncertainty in the background efficiency can vary from 3 to 10% as a function of p_{T}.

Similarly to the lepton triggers, the $E_{\mathrm{T}}^{\mathrm{miss}}$ trigger uncertainties are evaluated to be negligible. Uncertainties in the lepton and jet resolution are directly propagated to the $E_{\mathrm{T}}^{\mathrm{miss}}$ uncertainty. An additional uncertainty [95] in the soft radiation term, defined in Sect. 4, is also considered.

8.2 Modelling uncertainties

Theoretical uncertainties for $VVjj$ signal processes include the choice of PDF and QCD scale, as well as the parton-shower modelling. They are accounted for as acceptance effects in bins of the final RNN distribution. The PDF uncertainties are estimated using the NNPDF3.0NLO prescription [43], and the QCD scale uncertainties are estimated by varying the nominal choices of the renormalisation, μ_{R}, and factorisation, μ_{F}, scales independently by factors of two and one-half and considering their envelope. The resulting signal modelling acceptance uncertainty due to QCD scale and PDF choices is at maximum 10% and 5%, respectively, across all signal regions. An additional uncertainty in the parton-showering modelling of the signal process is also assessed by comparing the nominal MC generator prediction to an alternative sample showered with Herwig 7 [114,115]. This uncertainty can be as large as 20% in the high RNN region.

Due to the fact that the EWK and QCD $VVjj$ processes are generated separately, the interference term is not included. The impact of the missing term is estimated at the fiducial level by comparing an inclusive $VVjj$ calculation with the separate QCD and EWK calculations, using the same configuration as the nominal EWK generation. The ensuing difference is used to evaluate the size of the interference term, which is included as an uncertainty in the nominal EWK $VVjj$ MC prediction, parameterized as a function of the m_{jj}^{tag} variable defined at truth level. At reconstructed level, this results in a 5% (20%) uncertainty in the RNN distribution in the resolved (merged) SRs. This uncertainty is found to be small compared to other theory uncertainties.

The normalizations of the dominant W+jets, Z+jets, and $t\bar{t}$ background processes are evaluated directly in the final simultaneous fit to the SRs and CRs, as detailed in Sect. 9.1. A modelling uncertainty on the RNN shape for the W+jets and Z+jets processes is estimated from a comparison to an alternative MC generator choice, MadGraph5_aMC@NLO +Pythia. An additional modelling uncertainty on the V+jets processes to account for the m_{jj}^{tag} reweighting procedure discussed in Sect. 5 is also evaluated conservatively as the difference between the shapes before and after the reweighting. This reweighting uncertainty is evaluated bin-by-bin in the final RNN observable, and is found to vary with respect to the nominal prediction from a few percent to up to 50% in the 1- and 2-lepton channels, and up to 20% in the 0-lepton channel. Similarly, the shape uncertainty for the $t\bar{t}$ process is obtained by a comparison to an alternative Herwig 7.04 sample using the H7UE set of tuned parameters [115] and the MMHT2014LO PDF set [116].

The cross section for the QCD VV and single$-t$ contributions are estimated from the best theoretical cross section available as detailed in Sect. 3.2. An uncertainty in the modelling of the QCD VV process in this phase space is estimated by comparing to an alternative MC generator choice, Powheg Box +Pythia. A normalization uncertainty of 20% in single$-t$ is assumed with no further shape variation [117]. Similarly to the signal process, the uncertainties from PDF and QCD scale choices for all background processes are calculated separately, and found to be smaller than the other sources of background modelling uncertainty.

9 Results

9.1 Statistical analysis

The statistical analysis is based on the RooFit [118] and RooStats [119] frameworks to define a binned likelihood function, and the profile-likelihood ratio [120] is used as test statistic to classify the level of agreement between a model and the observed data. The analysis performs a fit across all SRs and CRs detailed in Sect. 5 simultaneously. In the CRs, the m_{jj}^{tag} observable is used over several bins to help constrain the uncertainties associated to the background modelling and the m_{jj}^{tag} reweighting procedure. The observable in the SRs is the RNN distribution, binned using a dedicated procedure detailed in Refs. [121,122] to ensure a fine binning in the signal sensitive regions while maintaining a low statistical uncertainty in the expected background prediction. Sources of uncertainty are treated as additional nuisance parameters in the likelihood function. In particular, the W+jets, Z+jets, and $t\bar{t}$ normalizations in each of the merged and resolved regions are unconstrained floating parameters, and allowed to converge to the values which provide optimal agreement with the data. All experimental systematic uncertainties are correlated amongst all regions and constrained by additional Gaussian terms in the likelihood as parametrized by external measurements. Modelling uncertainties are treated similarly except for the fact that they are uncorrelated across the lepton channels; the m_{jj}^{tag} reweighting uncertainties are decorrelated across the lepton channels and between the merged and resolved regions. Each component of the signal uncertainties

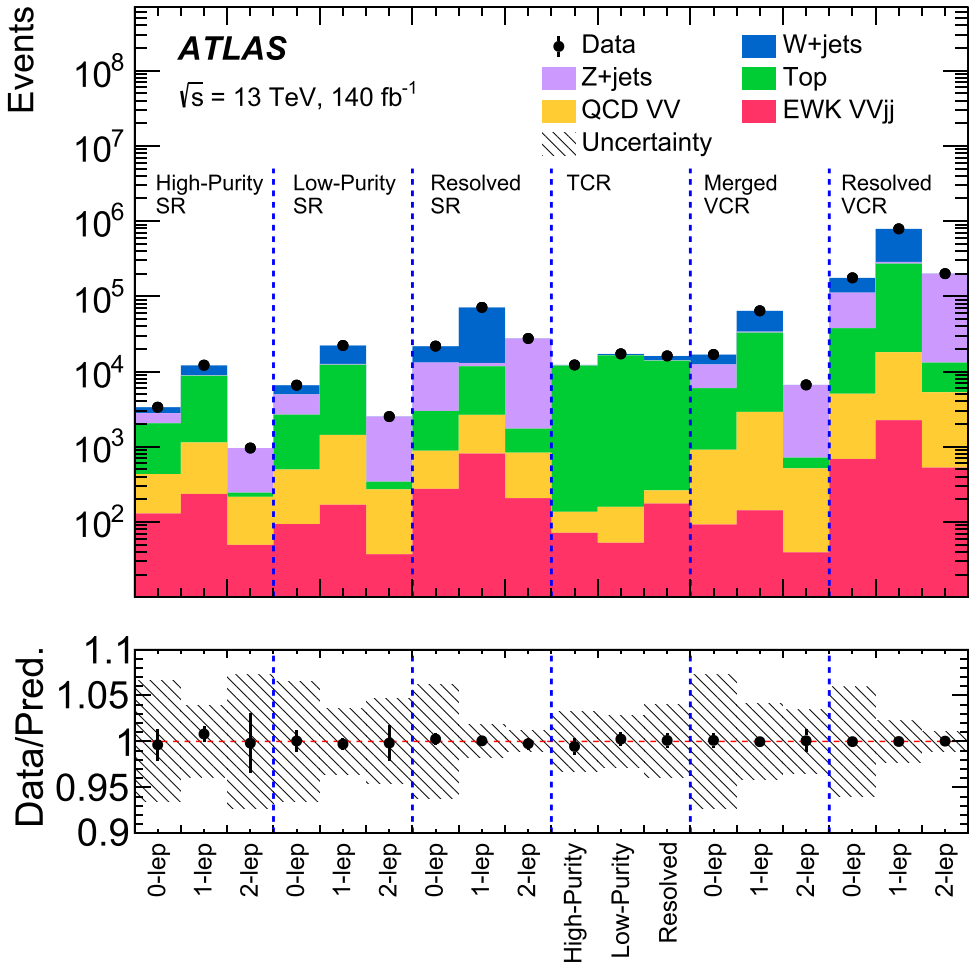

Fig. 7 Data and stacked post-fit predicted yields in the various regions. The systematic uncertainty in the prediction is shown as a hatched band

is individually included in the fit and it is correlated across all the analysis regions.

9.2 Inclusive measurement

To measure the EWK $VVjj$ cross section, the parameter of interest is the normalization of the $VVjj$ process cross section relative to to the SM prediction $\mu = \frac{\sigma_{\text{obs}}}{\sigma_{\text{exp}}}$, which is allowed to float to its optimal value in the fit. The extracted yields in each region of each of the processes considered are shown in Fig. 7. The post-fit RNN score distributions of the signal-plus-background fit are shown in Fig. 8. In general, good agreement of the model with data is found when including the EWK $VVjj$ contribution. The description of the background model in the analysis regions is checked on other variables not used directly in the fit model, such as the invariant mass of the reconstructed diboson system m_{VV} and m_{jj}^{tag}, finding a similarly good description.

The measured EWK $VVjj$ signal strength μ_{EWK}^{obs} is found to be

$$\mu_{EWK}^{\text{obs}} = 1.28^{+0.23}_{-0.21} = 1.28 \pm 0.09(\text{stat})^{+0.20}_{-0.19}(\text{syst}).$$

This is within 1.5σ agreement of the predicted value, with a p-value of 0.16. The measured signal strength is comparable to those also measured by the ATLAS Collaboration in leptonic $VVjj$ analyses [20,22,24,97]. The background-only hypothesis is excluded with a significance of 7.4σ, while the expected significance is 6.1σ.

The μ_{EWK}^{obs} value for each of the individual lepton channels and for the resolved and merged regimes is measured by performing a fit with, respectively, three and two parameters to extract; the results are shown in Fig. 9. It can be seen that the 1 and 2-lepton channels are in good agreement with the SM prediction while the 0-lepton channel measures a higher EWK VV j j contribution, with a 2.3σ compatibility with the inclusive measurement. The measured signal strength for the 1-lepton channel is $1.02^{+0.26}_{-0.24}$ and this result is compatible with the value measured by the CMS Collaboration [31].

Table 3 shows the contributions of all experimental and theory uncertainties to the fitted signal strength. The analysis is primarily dominated by systematic uncertainties, mainly arising from the theory and modelling factors, while experimental uncertainties related to the reconstructed jets also play a significant role. The background modelling and m_{jj}^{tag}

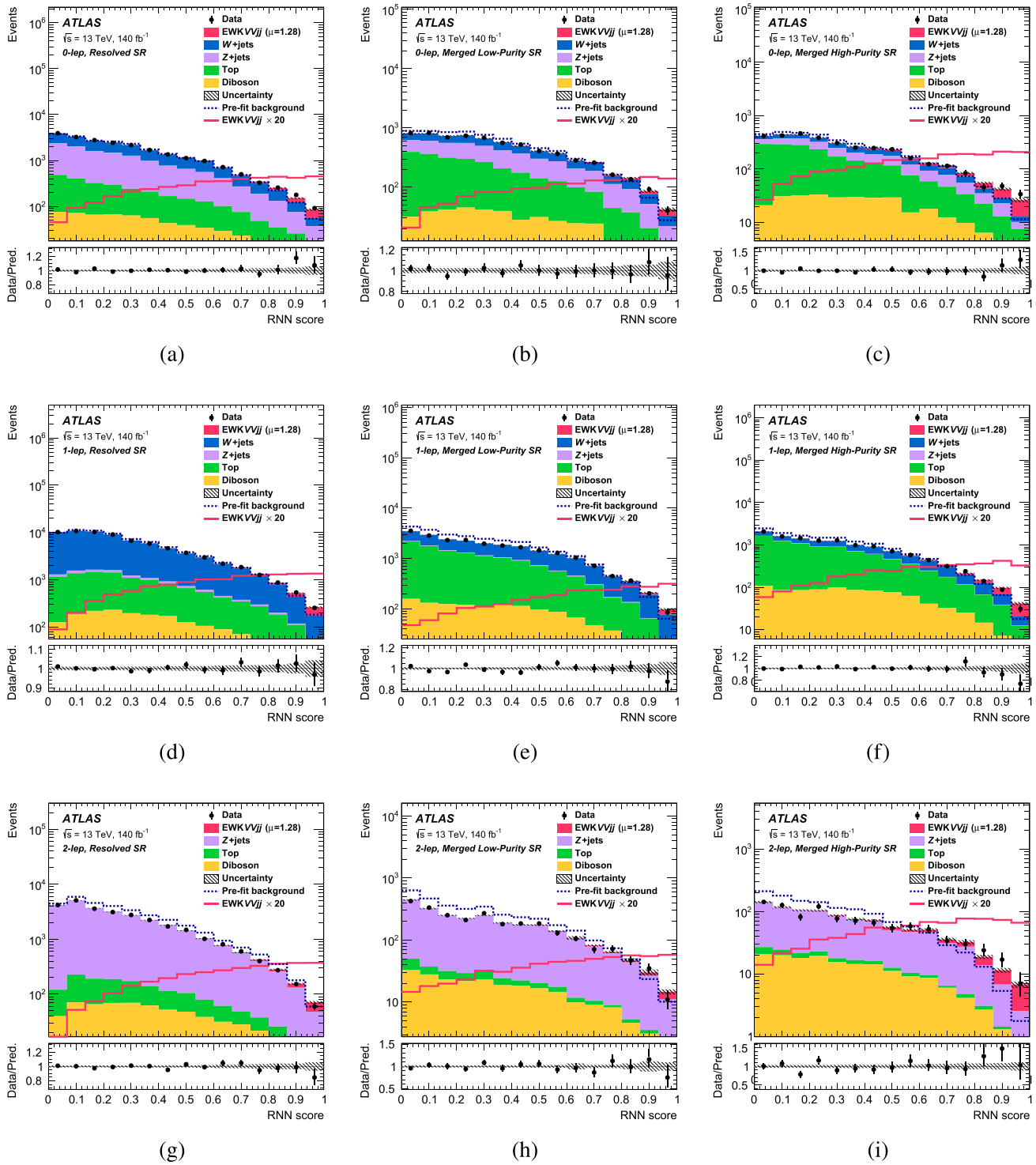

Fig. 8 Distribution of the RNN score for data (dots) and post-fit prediction separated by process (stacked histograms). The EWK $VVjj$ signal is also shown separately scaled for visibility by a factor of 20. For comparison, the pre-fit background distribution is overlayed as a dotted histogram. The total uncertainty including all statistical, experimental, and modelling uncertainties is overlayed as a hatched area. The bottom panel shows the ratio of data to the fitted signal-plus-background model

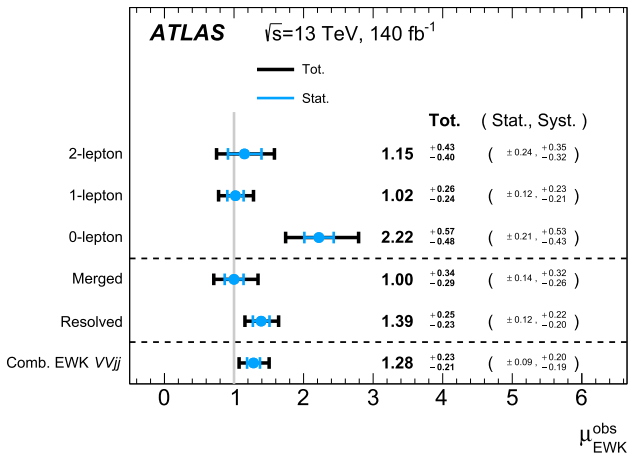

Fig. 9 Extracted signal strength μ^{obs}_{EWK} from the combined fit, as well as from the fits which allow various signal regions to be uncorrelated. The total, statistical and systematic uncertainties in these values are displayed

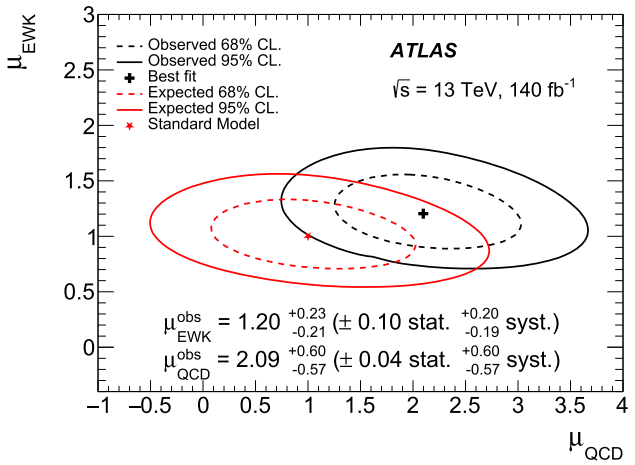

Fig. 10 The two dimensional 68% and 95% negative log-likelihood contours for the simultaneous fit to μ_{EWK} and μ_{QCD}. The SM prediction from the generator is highlighted as a star

Table 3 The symmetrized uncertainty in the extracted signal-strength parameter μ from different sources. The systematic sources of uncertainty are separated into theory modelling uncertainties and experimental uncertainties, which are further sub-divided into different groups according to their origin

Uncertainty source	σ_μ
Total	0.22
Statistical	0.09
Systematic	0.20
Theory and modelling uncertainties	
Floating normalizations	0.04
Z+jets	0.06
W+jets	0.07
$t\bar{t}$	0.02
QCD $VVjj$	0.05
Single-top	0.01
m^{tag}_{jj} reweighting	0.07
Signal modelling	0.13
MC statistics	0.07
Experimental uncertainties	
Jets and $E^{\text{miss}}_{\text{T}}$	0.09
Tracking	0.03
Leptons	< 0.01
b-tagging	< 0.01
Luminosity	0.01

uncertainties represent the leading sources constrained by the fit, primarily due to the constraining power of the CRs.

An additional fit is also performed allowing both the EWK and QCD $VVjj$ contributions to be simultaneously extracted. The negative log-likelihood contours of this fit are shown in Fig. 10. The measured value of the EWK $VVjj$ signal strength in this fit is found to be consistent with the result obtained when the QCD $VVjj$ normalization is constrained to the generator prediction, indicating low correlation between these observables. A slight tension with respect to the MC generator predictions is found in these fits, which is similarly seen in other EWK VBS-enhanced EWK $VVjj$ topologies [22,31], and may be indicative of a poor generator modelling of the QCD VV spectrum at high jet multiplicity.

9.3 Fiducial measurement

The cross sections in the fiducial regions described in Sect. 7 are extracted from a fit in which the normalization effects from the theory modelling uncertainty in the signal are removed. All other experimental, statistical, and theory modelling uncertainties are retained. The fiducial cross section is then obtained from the fitted signal strength multiplied by the predicted generator cross section in the fiducial region and the fiducial-to-reconstructed region acceptance. A combined measurement is performed using a single signal strength. Measurements for the individual lepton channels and for the resolved and merged regimes are also performed with separate fits to extract, respectively, three and two parameters. The effects of migrations between the various fiducial regions into the same fully-reconstructed region are taken into account by a linear transformation of the individual channel signal strengths by the estimated migration effects in simulations. The prediction of the cross section includes only LO calcu-

Table 4 Expected and observed fiducial cross section of the EWK $VVjj$ process. The combined measurement refers to the case in which one signal strength is measured using all the analysis SRs. The cross sections are also presented in fiducial bins across lepton multiplicity and in the merged and resolved fiducial regions

	Combined	0-lepton	1-lepton	2-lepton	Resolved	Merged
$\sigma_{EWK}^{\text{fid,exp}}$	20.4 ± 3.5 fb	7.3 ± 2.5 fb	10.3 ± 2.5 fb	2.8 ± 1.1 fb	11.7 ± 3.4 fb	8.7 ± 2.5 fb
$\sigma_{EWK}^{\text{fid,obs}}$	29.2 ± 4.9 fb	15.7 ± 2.8 fb	10.7 ± 2.8 fb	3.1 ± 1.1 fb	17.9 ± 4.3 fb	11.4 ± 3.4 fb

lations since the EWK NLO corrections are not available for the semileptonic final state.

The total fiducial cross section for the EWK $VVjj$ production summed across all fiducial regions is found to be $\sigma_{EWK}^{\text{fid,obs}} = 29.2 \pm 4.9$ fb. The measured signal strength is $\mu_{EWK}^{\text{obs}} = 1.43 \pm 0.24$; it differs with respect to the inclusive signal strength due to the different fit approaches. The impact of the parton-shower and QCD scale systematic uncertainties is lower in the fiducial measurement fit since only the impact on the shape is evaluated, and not the impact on the expected normalization. These uncertainties are larger in the 0-lepton channel due to a tighter analysis selection with respect to the other two channels. This results in a higher relative importance for the SRs of the 0-lepton channel, in which an upward fluctuation is observed. The results of the fiducial cross-section measurements in different sub-regions are shown in Table 4; in each region, a separate normalization is used in the extraction. The measured cross sections are in agreement with the SM expectations. In the fits to extract the signal strength for each lepton channel, only the 0-lepton channel measures a higher cross section, with a compatibility of 2.1σ with the combined measurement. This measurement complements the one conducted by the CMS Collaboration [31] as this result also includes the 0- and 2-lepton channels that were not considered in that measurement and it considers a fiducial phase space that is tighter with respect to the one defined in the CMS analysis.

9.4 EFT interpretation

The distribution of events in the SRs are also used to constrain higher-order operators in an EFT framework. In particular, new operators of mass-dimension 8 contribute to aQGCs, which would enhance EWK $VVjj$ production at high diboson invariant mass, m_{VV}.

The Eboli model [10] is employed to describe the signal, which introduces 21 new dimension-8 operators satisfying the SM $SU(2) \times U(1)_Y$ symmetry. These operators can be categorized by the types of coupling; scalar types that only contain covariant derivatives of the Higgs field: f_{S0}, f_{S1}, f_{S2}, tensor types that only contain field strengths: $f_{T0}, \ldots, f_{T9}$, and mixed operators that exhibit two covariant derivatives of the Higgs field and two field strengths: $f_{M0}, \ldots, f_{M7}$. As a convention, the whole Lagrangian term for an operator is denoted by its Wilson coefficient i.e. $\mathcal{L}_n = \frac{f_n}{\Lambda^4} O_n$ will be denoted as f_n. Due to the fact that the operators O_{S0} and O_{S2} are Hermitian conjugates, they are varied simultaneously with equal coefficient values f_{S02}.

The EFT contributions are modelled with MC samples, as described in Sect. 3.2, using a decomposition of the process amplitude. The total matrix element with the addition of new dimension-8 operators can be written as

$$|A_{SM} + \frac{f_i}{\Lambda^4} A_i|^2 = |A_{SM}^2| + \sum_i \frac{f_i^2}{\Lambda^8} |A_i^2| + \sum_i 2\frac{f_i}{\Lambda^4} \text{Re}(A_{SM}^\star A_i) + \sum_{i \neq j} \frac{f_i}{\Lambda^4} \frac{f_j}{\Lambda^4} \text{Re}(A_i^\star A_j),$$

where $|A_{SM}|^2$ is the SM matrix element, $|A_i^2|$ represents the pure-EFT matrix elements for the f_i operator, and $2\text{Re}(A_{SM}^\star A_i)$ is its corresponding interference term with the SM. The term $\text{Re}(A_i^\star A_j)$ includes the possible interference term between EFT operators f_i and f_j, and will not be considered here. Individual simulation samples for the pure-EFT and interference terms are generated; to obtain predictions at a specific coupling point, these samples are scaled quadratically and linearly by f_i, respectively.

The EFT results are extracted in a similar fit setup as described in Sect. 9.1, where now the EFT coefficients f_i, are set as the parameters of interest. Since the EFT is expected to contribute more at high m_{VV}, each of the SRs is further split into two (high and low) m_{VV} bins to improve the sensitivity and the RNN score is used as final discriminant. The high- and low-m_{VV} regions are split at $m_{VV} = 1500$ GeV in the 1- and 2-lepton channels; in the 0-lepton channel, the transverse mass (m_{T}), defined as the invariant mass of the V_{had} candidate and the $E_{\text{T}}^{\text{miss}}$ vector in the transverse plane, is used instead with the splitting occurring at 1050 GeV (1200 GeV) in the merged (resolved) region. The CRs in this fit are the same as those in the inclusive measurement. The post-fit RNN score distributions in the more aQGC-sensitive high m_{VV} bin are shown in Fig. 11; the binning of the distributions was reduced to account for the lower number of events expected in the high m_{VV} bin. The distributions agree reasonably well with the SM predictions.

For the EFT interpretations, the EWK $VVjj$ normalization and the signal strength of the EFT process are left free in

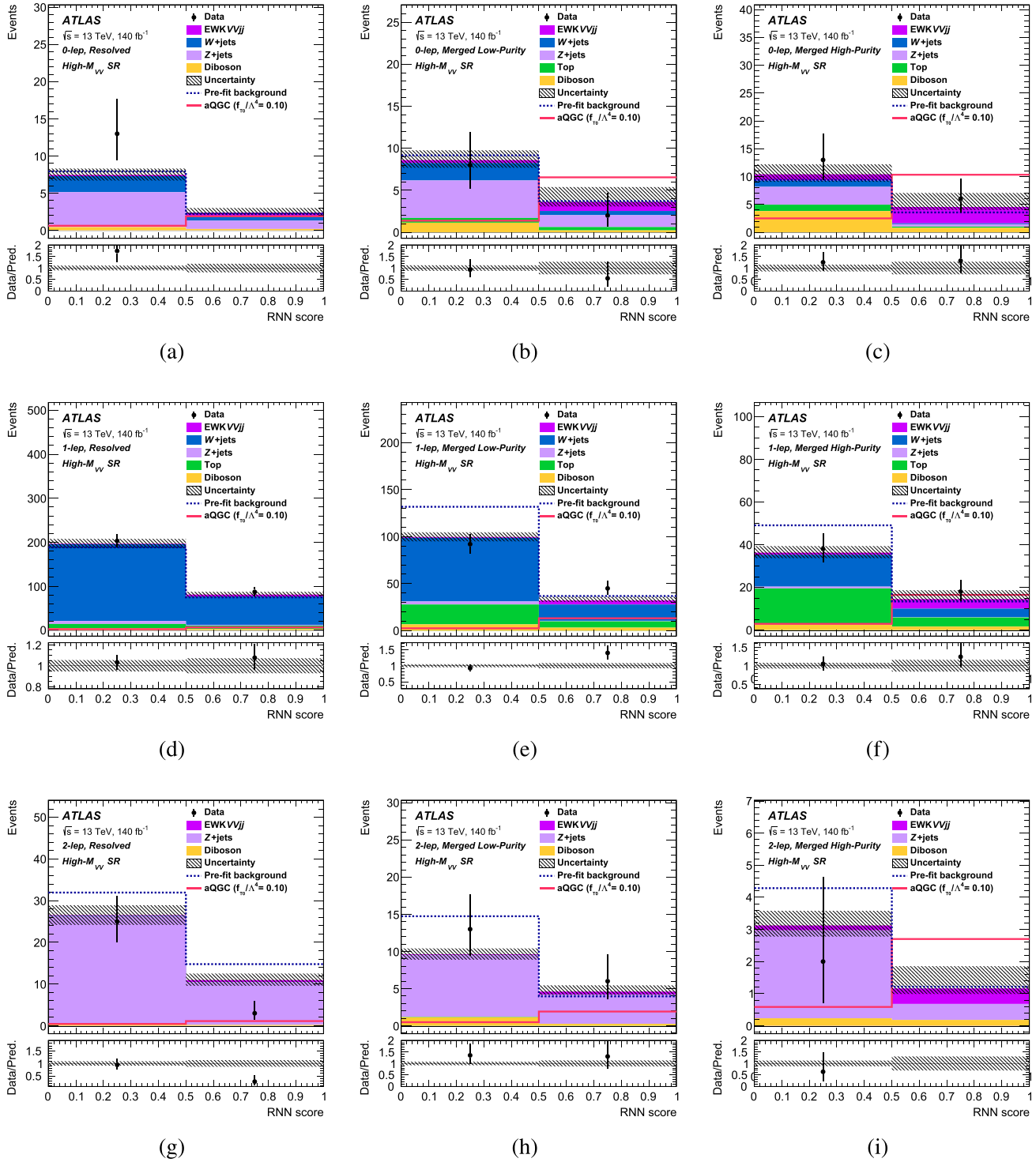

Fig. 11 Distribution of the RNN score for data (dots) and post-fit prediction separated by process (stacked histograms) for the high-m_{VV} aQGC signal regions. The f_{T0} operator is shown separately with a normalisation corresponding to $f/\Lambda^4 = 0.10\,\text{TeV}^{-4}$. For comparison, the pre-fit background distribution is overlayed as a dotted histogram. The total uncertainty including all statistical, experimental, and modelling uncertainties is overlayed as a hatched area. The bottom panel shows the ratio of data to the fitted signal-plus-background model

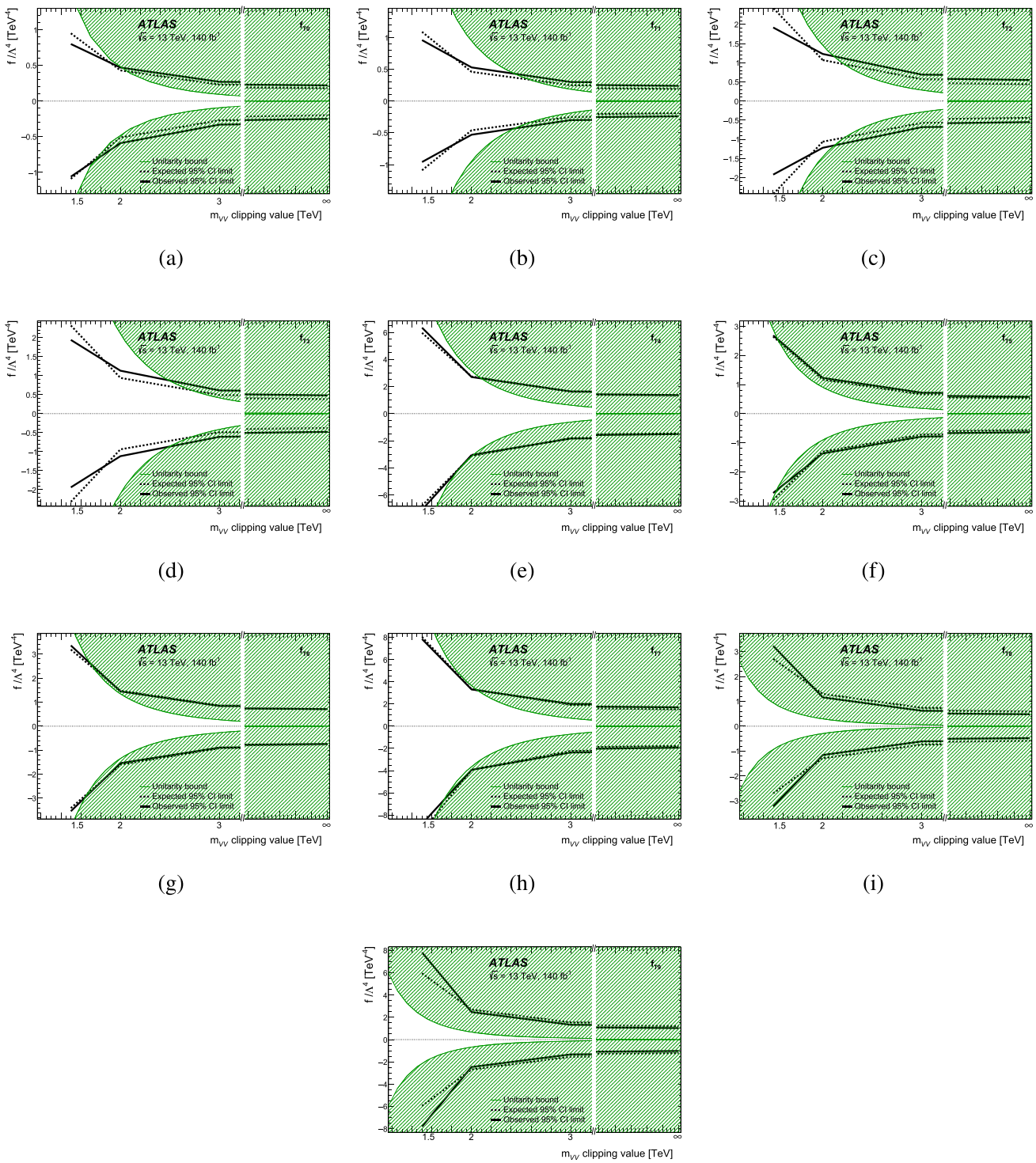

Fig. 12 Expected and observed 95% confidence limits for the dimension-8 f_T operators as a function of the clipping scale. Regions excluded by unitarity constraints are shown as a hatched area

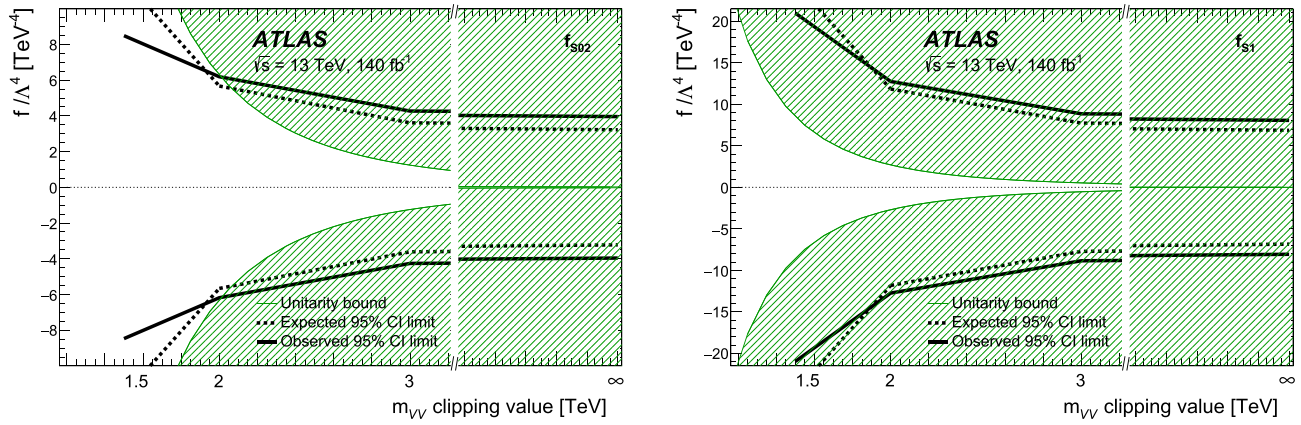

Fig. 13 Expected and observed 95% confidence limits for the dimension-8 f_S operators as a function of the clipping scale. Regions excluded by unitarity constraints are shown as a hatched area

the fit. The EWK $VVjj$ normalization is constrained by the low m_{VV} bins; the post-fit value is compatible with the one obtained in the inclusive measurement. Confidence intervals are set at the 95% confidence level assuming that the Wald approximation holds [120,123].

To provide interpretable limits which avoid the unitarity violation at high center of mass energy, the clipping method, described in Ref. [124], is used. In this method, a clipping scale E_{clip} is chosen and signal events with truth m_{VV} greater than this clipping scale are removed. The expected and observed 95% confidence level limits on the different aQGC operators as functions of the clipping scale are shown in Figs. 12, 13 and 14. The theory unitary bounds for each operator are taken from Ref. [125] considering partial-wave unitarity for a single operator at a time. A summary of the expected and observed limits on the different dimension-8 EFT operators is shown in Table 5.

This result improves upon the constraints from other ATLAS searches for aQGC [13,20,22,26,28,97,126,126] for all f_S and f_M type operators. Improvements are found for both the first clipping point that, in most cases, is within the unitarity bound and for the limits without any clipping scale. The latter improvement can be as large as a factor 3.3 for f_{M0}, 1.8 for f_{M1}, 1.5 for f_{M7}, 1.5 for f_{S02} and 2.9 for f_{S1} compared to the best limits reported by the ATLAS Collaboration in other diboson channels. The f_T operators are instead found to be more tightly constrained by the measurement of $Z(\to \nu\nu)\gamma$ in association with two jets [28].

10 Conclusion

A measurement of EWK $VVjj$ production in proton–proton collisions is performed in the semileptonic final states, using 140 fb^{-1} of data collected at $\sqrt{s} = 13$ TeV by the ATLAS experiment at the LHC. The analysis is performed in three decay topologies based on the lepton multiplicity and in two boson p_{T} regimes. The measured phase space is designed to be enriched in the EWK VBS component. The total process is observed with a significance of 7.4σ, while 6.1σ was expected. The EWK $VVjj$ production cross section is measured to be 29.2 ± 4.9 fb (expected 20.4 ± 3.5) in a fiducial phase space close to the detector and analysis acceptance. The signal strengths of both electroweak and QCD associated diboson productions are measured in a two-dimensional fit, in agreement with the SM prediction.

Additionally, a search is conducted on possible anomalous quartic gauge couplings, and dimension-8 EFT operator contributions to EWK VBS production were tested. No significant deviation from the SM prediction is observed, and constraints on the Wilson coefficients of 19 operators are presented for the first time in this final state by the ATLAS Collaboration. Some of these constraints are competitive with or better than previous results from other EWK VBS and triboson measurements. The observed limits for the S02, T0 and M0 operators are $(-3.96 < f_{S02}/\Lambda^4 < 3.96)$ TeV^{-4}, $(-0.25 < f_{T0}/\Lambda^4 < 0.22)$ TeV^{-4}, $(-1.26 < f_{M0}/\Lambda^4 < 1.25)$ TeV^{-4}.

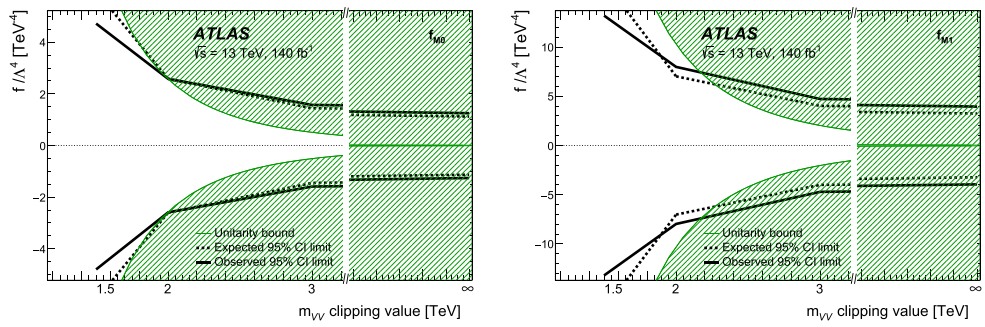

(a)

(b)

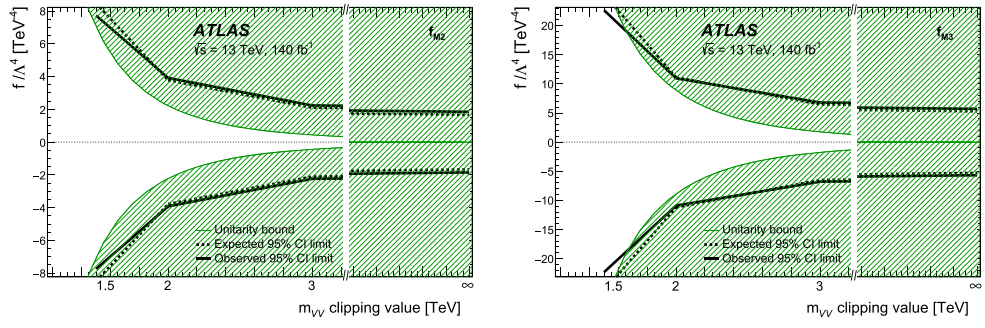

(c)

(d)

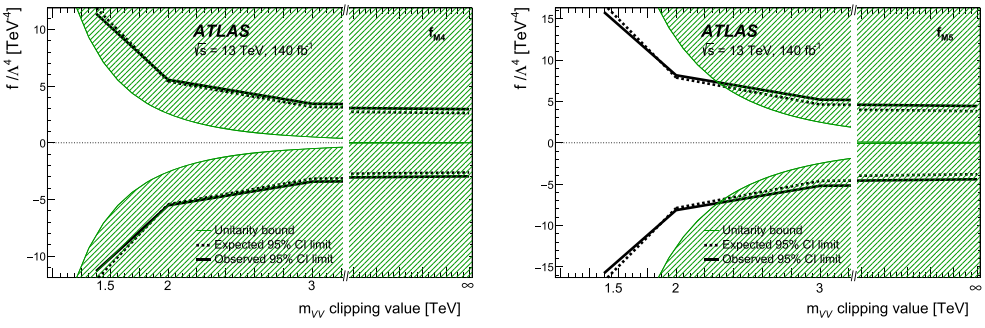

(e)

(f)

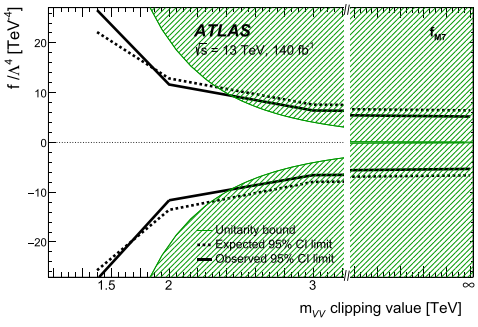

(g)

Fig. 14 Expected and observed 95% confidence limits for the dimension-8 f_M operators as a function of the clipping scale. Regions excluded by unitarity constraints are shown as a hatched area

Table 5 Expected and observed 95% confidence interval limits on the Wilson coefficients f_N/Λ^4 of various dimension-8 operators. Limits are obtained considering a single Wilson coefficient to be non-zero at a time. First, the limit obtained without any clipping scale is shown, followed by the limit at the clipping scale where the operator crosses the unitarity bounds, along with the value of the clipping scale itself

Wilson coefficient	Expected limit [TeV^{-4}]	Observed limit [TeV^{-4}]	Expected limit unitarized [TeV^{-4}]	Observed limit unitarized [TeV^{-4}]
f_{T0}/Λ^4	[−0.20, 0.18]	[−0.25, 0.22]	[−0.79, 0.47] at [1.76, 1.96] TeV	[−0.85, 0.47] at [1.73, 2.00] TeV
f_{T1}/Λ^4	[−0.19, 0.19]	[−0.24, 0.24]	[−0.34, 0.34] at [2.59, 2.59] TeV	[−0.43, 0.43] at [2.43, 2.43] TeV
f_{T2}/Λ^4	[−0.44, 0.44]	[−0.55, 0.55]	[−0.95, 0.96] at [2.22, 2.22] TeV	[−1.16, 1.17] at [2.12, 2.11] TeV
f_{T3}/Λ^4	[− −0.38, 0.38]	[−0.48, 0.48]	[−0.62, 0.62] at [2.71, 2.71] TeV	[−0.88, 0.88] at [2.49, 2.48] TeV
f_{T4}/Λ^4	[−1.46, 1.32]	[−1.51, 1.37]	[−3.03, 2.60] at [2.02, 2.09] TeV	[−3.03, 2.60] at [2.02, 2.10] TeV
f_{T5}/Λ^4	[−0.57, 0.53]	[−0.64, 0.58]	–	[−2.65, 2.57] at [1.53, 1.54] TeV
f_{T6}/Λ^4	[−0.76, 0.72]	[−0.74, 0.71]	[−2.82, 2.01] at [1.66, 1.73] TeV	[−2.98, 2.62] at [1.64, 1.69] TeV
f_{T7}/Λ^4	[−1.78, 1.52]	[−1.94, 1.70]	[−7.88, 4.29] at [1.65, 1.90] TeV	[−6.70, 4.11] at [1.72, 1.91] TeV
f_{T8}/Λ^4	[−0.59, 0.59]	[−0.48, 0.48]	–	–
f_{T9}/Λ^4	[−1.22, 1.22]	[−1.02, 1.03]	–	–
f_{S02}/Λ^4	[−3.22, 3.22]	[−3.96, 3.96]	[−5.53, 5.54] at [2.07, 2.67] TeV	[−6.16, 6.17] at [2.01, 2.01] TeV
f_{S1}/Λ^4	[−6.84, 6.86]	[−8.06, 8.06]	–	-
f_{M0}/Λ^4	[−1.13, 1.12]	[−1.26, 1.25]	[−2.61, 2.58] at [2.00, 2.00] TeV	[−2.71, 2.65] at [1.97, 1.98] TeV
f_{M1}/Λ^4	[−3.23, 3.24]	[−3.95, 3.95]	[−6.22, 6.22] at [2.27, 2.27] TeV	[−7.42, 7.43] at [2.17, 2.17] TeV
f_{M2}/Λ^4	[−1.66, 1.67]	[−1.85, 1.85]	–	–
f_{M3}/Λ^4	[−5.29, 5.29]	[−5.68, 5.71]	[−23.69, 23.39] at [1.57, 1.57] TeV	[−18.62, 19.10] at [1.66, 1.65] TeV
f_{M4}/Λ^4	[−2.62, 2.62]	[−2.96, 2.97]	–	–
f_{M5}/Λ^4	[−3.81, 3.82]	[−4.41, 4.44]	[−6.80, 6.80] at [2.33, 2.33] TeV	[−7.28, 7.30] at [2.29, 2.29] TeV
f_{M7}/Λ^4	[−5.32, 5.20]	[−6.60, 6.43]	[−9.47, 9.38] at [2.43, 2.43] TeV	[−11.91, 11.11] at [2.29, 2.33] TeV

Acknowledgements We thank CERN for the very successful operation of the LHC and its injectors, as well as the support staff at CERN and at our institutions worldwide without whom ATLAS could not be operated efficiently. The crucial computing support from all WLCG partners is acknowledged gratefully, in particular from CERN, the ATLAS Tier-1 facilities at TRIUMF/SFU (Canada), NDGF (Denmark, Norway, Sweden), CC-IN2P3 (France), KIT/GridKA (Germany), INFN-CNAF (Italy), NL-T1 (Netherlands), PIC (Spain), RAL (UK) and BNL (USA), the Tier-2 facilities worldwide and large non-WLCG resource providers. Major contributors of computing resources are listed in Ref. [127]. We gratefully acknowledge the support of ANPCyT, Argentina; YerPhI, Armenia; ARC, Australia; BMWFW and FWF, Austria; ANAS, Azerbaijan; CNPq and FAPESP, Brazil; NSERC, NRC and CFI, Canada; CERN; ANID, Chile; CAS, MOST and NSFC, China; Minciencias, Colombia; MEYS CR, Czech Republic; DNRF and DNSRC, Denmark; IN2P3-CNRS and CEA-DRF/IRFU, France; SRNSFG, Georgia; BMFTR, HGF and MPG, Germany; GSRI, Greece; RGC and Hong Kong SAR, China; ICHEP and Academy of Sciences and Humanities, Israel; INFN, Italy; MEXT and JSPS, Japan; CNRST, Morocco; NWO, Netherlands; RCN, Norway; MNiSW, Poland; FCT, Portugal; MNE/IFA, Romania; MSTDI, Serbia; MSSR, Slovakia; ARIS and MVZI, Slovenia; DSI/NRF, South Africa; MICIU/AEI, Spain; SRC and Wallenberg Foundation, Sweden; SERI, SNSF and Cantons of Bern and Geneva, Switzerland; NSTC, Taipei; TENMAK, Türkiye; STFC/UKRI, United Kingdom; DOE and NSF, United States of America. Individual groups and members have received support from BCKDF, CANARIE, CRC and DRAC, Canada; CERN-CZ, FORTE and PRIMUS, Czech Republic; COST, ERC, ERDF, Horizon 2020, ICSC-NextGenerationEU and Marie Skłodowska-Curie Actions, European Union; Investissements d'Avenir Labex, Investissements d'Avenir Idex and ANR, France; DFG and AvH Foundation, Germany; Herakleitos, Thales and Aristeia programmes co-financed by EU-ESF and the Greek NSRF, Greece; BSF-NSF and MINERVA, Israel; NCN and NAWA, Poland; La Caixa Banking Foundation, CERCA Programme Generalitat de Catalunya and PROMETEO and GenT Programmes Generalitat Valenciana, Spain; Göran Gustafssons Stiftelse, Sweden; The Royal Society and Leverhulme Trust, United Kingdom. In addition, individual members wish to acknowledge support from Armenia: Yerevan Physics Institute (FAPERJ); CERN: European Organization for Nuclear Research (CERN DOCT); Chile: Agencia Nacional de Investigación y Desarrollo (FONDECYT 1230812, FONDECYT 1240864, Fondecyt 3240661, Fondecyt Regular 1240721); China: Chinese Ministry of Science and Technology (MOST-2023YFA1605700, MOST-2023YFA1609300), National Natural Science Foundation of China (NSFC-12175119, NSFC 12275265); Czech Republic: Czech Science Foundation (GACR-24-11373S), Ministry of Education Youth and Sports (ERC-CZ-LL2327, FORTE CZ.02.01.01/00/22_008/0004632), PRIMUS Research Programme (PRIMUS/21/SCI/017); EU: H2020 European Research Council (ERC-101002463); European Union: European Research Council (BARD No. 101116429, ERC-948254, ERC 101089007), European Regional Development Fund (SMASH COFUND 101081355, SLO ERDF), Horizon 2020 Framework Programme (MUCCA-CHIST-ERA-19-XAI-00), European Union, Future Artificial Intelligence Research (FAIR-NextGenerationEU PE000 00013), Horizon 2020 (EuroHPC-EHPC-DEV-2024D11-051), Italian Center for High Performance Computing, Big Data and Quantum Computing (ICSC, NextGenerationEU); France: Agence Nationale de la Recherche (ANR-21-CE31-0022, ANR-22-EDIR-0002, ANR-24-CE31-0504-01); Germany: Baden-Württemberg Stiftung (BW Stiftung-Postdoc Eliteprogramme), Deutsche Forschungsgemeinschaft (DFG-469666862, DFG-CR 312/5-2); China: Research Grants Council (GRF); Italy: Istituto Nazionale di Fisica Nucleare (ICSC, NextGenerationEU), Ministero dell'Università e della Ricerca (NextGenEU 153D23001490006 M4C2.1.1, NextGenEU I53D23000820006 M4C2.1.1, NextGenEU I53D23001490006 M4C2.1.1); Japan: Japan Society for the Promotion of Science (JSPS KAKENHI JP22H01227, JSPS KAKENHI JP22H04944, JSPS KAKENHI JP22KK0227, JSPS KAKENHI JP23KK0245, JSPS KAKENHI JP24K23939); Norway: Research Council of Norway (RCN-314472); Poland: Ministry of Science and Higher Education (IDUB AGH, POB8, D4 no 9722), Polish National Science Centre (NCN 2021/42/E/ST2/00350, NCN OPUS 2023/51/B/ST2/02507, NCN OPUS nr 2022/47/B/ST2/03059, NCN UMO-2019/34/E/ST2/00393, UMO-2022/47/O/ST2/00148, UMO-2023/49/B/ST2/04085, UMO-2023/51/B/ST2/00920, UMO-2024/53/N/ST2/00869); Portugal: Foundation for Science and Technology (FCT); Spain: Generalitat Valenciana (Artemisa, FEDER, IDIFEDER/2018/048), Ministry of Science and Innovation (MCIN & NextGenEU PCI2022-135018-2, MICIN & FEDER PID2021-125273NB, RYC 2019-028510-I, RYC2020-030254-I, RYC2021-031273-I, RYC2022-038164-I); Sweden: Carl Trygger Foundation (Carl Trygger Foundation CTS 22:2312), Swedish Research Council (Swedish Research Council 2023-04654, VR 2021-03651, VR 2022-03845, VR 2022-04683, VR 2023-03403, VR 2024-05451), Knut and Alice Wallenberg Foundation (KAW 2018.0458, KAW 2022.0358, KAW 2023.0366); Switzerland: Swiss National Science Foundation (SNSF - PCEFP2_194658); United Kingdom: Leverhulme Trust (Leverhulme Trust RPG-2020-004), Royal Society (NIF-R1-231091); United States of America: U.S. Department of Energy (ECA DE-AC02-76SF00515), Neubauer Family Foundation.

Data Availability Statement This manuscript has associated data in a data repository. [Author's comment: The public release of data supporting the findings of this article will follow the CERN Open Data Policy [128]. The values of relevant plots and tables associated with this article are stored in HEPData https://www.hepdata.net/record/157860.]

Code Availability Statement This manuscript has associated code/software in a data repository. [Author's comment: The ATLAS Collaboration's Athena software, including the configuration of the event generators, is open source (http://gitlab.cern.ch/atlas/athena).]

Funded by SCOAP[3].

References

1. B.W. Lee, C. Quigg, H.B. Thacker, Strength of weak interactions at very high energies and the Higgs boson mass. Phys. Rev. Lett. **38**, 883 (1977). https://doi.org/10.1103/PhysRevLett.38.883
2. B.W. Lee, C. Quigg, H.B. Thacker, Weak interactions at very high energies: the role of the Higgs-boson mass. Phys. Rev. D **16**, 1519 (1977). https://doi.org/10.1103/PhysRevD.16.1519
3. ATLAS Collaboration, Observation of a new particle in the search for the Standard Model Higgs boson with the ATLAS detector at the LHC. Phys. Lett. B **716**, 1 (2012). https://doi.org/10.1016/j.physletb.2012.08.020. arXiv:1207.7214 [hep-ex]
4. CMS Collaboration, Observation of a new boson at a mass of 125 GeV with the CMS experiment at the LHC. Phys. Lett. B

716, 30 (2012). https://doi.org/10.1016/j.physletb.2012.08.021. arXiv:1207.7235 [hep-ex]
5. ATLAS Collaboration, Measurements of the Higgs boson production and decay rates and coupling strengths using pp collision data at $\sqrt{s} = 7$ and 8 TeV in the ATLAS experiment. Eur. Phys. J. C **76**, 6 (2016). https://doi.org/10.1140/epjc/s10052-015-3769-y. arXiv:1507.04548 [hep-ex]
6. ATLAS Collaboration, Study of the spin and parity of the Higgs boson in diboson decays with the ATLAS detector. Eur. Phys. J. C **75**, 476 (2015). https://doi.org/10.1140/epjc/s10052-015-3685-1. arXiv:1506.05669 [hep-ex] [Erratum: Eur. Phys. J. C 76 152, (2016). https://doi.org/10.1140/epjc/s10052-016-3934-y]
7. CMS Collaboration, Precise determination of the mass of the Higgs boson and tests of compatibility of its couplings with the standard model predictions using proton collisions at 7 and 8 TeV. Eur. Phys. J. C **75**, 212 (2015). https://doi.org/10.1140/epjc/s10052-015-3351-7. arXiv:1412.8662 [hep-ex]
8. CMS Collaboration, Constraints on the spin-parity and anomalous HVV couplings of the Higgs boson in proton collisions at 7 and 8 TeV. Phys. Rev. D **92**, 012004 (2015). https://doi.org/10.1103/PhysRevD.92.012004. arXiv:1411.3441 [hep-ex]
9. O.J.P. Éboli, M.C. Gonzalez-Garcia, S.M. Lietti, Bosonic quartic couplings at CERN LHC. Phys. Rev. D **69**, 095005 (2004). https://doi.org/10.1103/PhysRevD.69.095005. arXiv:hep-ph/0310141
10. O.J.P. Éboli, M.C. Gonzalez-Garcia, J.K. Mizukoshi, $pp \to jje^{\pm}\mu^{\pm}\nu\nu$ and $jje^{\pm}\mu^{\mp}\nu\nu$ at $O(\alpha_{em}^6)$ and $O(\alpha_{em}^4\alpha_s^2)$ for the study of the quartic electroweak gauge boson vertex at CERN LHC. Phys. Rev. D **74**, 073005 (2006). https://doi.org/10.1103/PhysRevD.74.073005. arXiv:hep-ph/0606118
11. J. Chang, K. Cheung, C.-T. Lu, T.-C. Yuan, WW scattering in the era of post-Higgs-boson discovery. Phys. Rev. D **87**, 093005 (2013). https://doi.org/10.1103/PhysRevD.87.093005. arXiv:1303.6335 [hep-ph]
12. D. Espriu, B. Yencho, Longitudinal WW scattering in light of the "Higgs boson" discovery. Phys. Rev. D **87**, 055017 (2013). https://doi.org/10.1103/PhysRevD.87.055017. arXiv:1212.4158 [hep-ph]
13. ATLAS Collaboration, Measurement of $Z\gamma\gamma$ production in pp collisions at $\sqrt{s} = 13$ TeV with the ATLAS detector. Eur. Phys. J. C **83**, 539 (2023). https://doi.org/10.1140/epjc/s10052-023-11579-8. arXiv:2211.14171 [hep-ex]
14. CMS Collaboration, Measurements of the $pp \to W\gamma\gamma$ and $pp \to Z\gamma\gamma$ cross sections and limits on anomalous quartic gauge couplings at $\sqrt{s} = 8$ TeV. JHEP **10**, 072 (2017). https://doi.org/10.1007/JHEP10(2017)072. arXiv:1704.00366 [hep-ex]
15. V. Barger, K. Cheung, T. Han, R.J.N. Phillips, Strong W^+W^+ scattering signals at pp supercolliders. Phys. Rev. D **42**, 3052 (1990). https://doi.org/10.1103/PhysRevD.42.3052
16. C. Degrande et al., Effective field theory: a modern approach to anomalous couplings. Ann. Phys. **335**, 21 (2013). https://doi.org/10.1016/j.aop.2013.04.016. arXiv:hep-ph/1205.4231
17. ATLAS Collaboration, Combined effective field theory interpretation of Higgs boson and weak boson production and decay with ATLAS data and electroweak precision observables, ATL-PHYS-PUB-2022-037 (2022). https://cds.cern.ch/record/2816369
18. ATLAS Collaboration, Observation of electroweak production of a same-sign W boson pair in association with two jets in pp collisions at $\sqrt{s} = 13$ TeV with the ATLAS detector. Phys. Rev. Lett. **123**, 161801 (2019). https://doi.org/10.1103/PhysRevLett.123.161801. arXiv:1906.03203 [hep-ex]
19. CMS Collaboration, Observation of electroweak production of same-sign W boson pairs in the two jet and two same-sign lepton final state in proton–proton collisions at $\sqrt{s} = 13$ TeV. Phys. Rev. Lett. **120**, 081801 (2018). https://doi.org/10.1103/PhysRevLett.120.081801. arXiv:1709.05822 [hep-ex]
20. ATLAS Collaboration, Observation of electroweak production of W^+W^- in association with jets in proton–proton collisions at $\sqrt{s} = 13$ TeV with the ATLAS detector. JHEP **07**, 254. (2024). https://doi.org/10.1007/JHEP07(2024)254. arXiv:2403.04869 [hep-ex]
21. CMS Collaboration, Observation of electroweak W^+W^- pair production in association with two jets in proton–proton collisions at $\sqrt{s} = 13$ TeV. Phys. Lett. B **841**, 137495 (2023). https://doi.org/10.1016/j.physletb.2022.137495. arXiv:2205.05711 [hep-ex]
22. ATLAS Collaboration, Measurements of electroweak $W^{\pm}Z$ boson pair production in association with two jets in pp collisions at $\sqrt{s} = 13$ TeV with the ATLAS detector. JHEP **06**, 192 (2024). https://doi.org/10.1007/JHEP06(2024)192. arXiv:2403.15296 [hep-ex]
23. CMS Collaboration, Measurement of electroweak WZ boson production and search for new physics in $WZ+$ two jets events in pp collisions at $\sqrt{s} = 13$ TeV. Phys. Lett. B **795**, 281 (2019). https://doi.org/10.1016/j.physletb.2019.05.042. arXiv:1901.04060 [hep-ex]
24. ATLAS Collaboration, Observation of electroweak production of two jets and a Z-boson pair. Nat. Phys. **19**, 237 (2023). https://doi.org/10.1038/s41567-022-01757-y. arXiv:2004.10612 [hep-ex]
25. CMS Collaboration, Evidence for electroweak production of four charged leptons and two jets in proton-proton collisions at $\sqrt{s} = 13$ TeV. Phys. Lett. B **812**, 135992 (2021). https://doi.org/10.1016/j.physletb.2020.135992. arXiv:2008.07013 [hep-ex]
26. ATLAS Collaboration, Fiducial and differential cross-section measurements of electroweak $W\gamma jj$ production in pp collisions at $\sqrt{s} = 13$ TeV with the ATLAS detector. Eur. Phys. J. C **84**, 1064 (2024). https://doi.org/10.1140/epjc/s10052-024-13311-6. arXiv:2403.02809 [hep-ex]
27. CMS Collaboration, Measurement of the electroweak production of $W\gamma$ in association with two jets in proton-proton collisions at $\sqrt{s} = 13$ TeV. Phys. Rev. D **108**, 032017 (2023). https://doi.org/10.1103/PhysRevD.108.032017. arXiv:2212.12592 [hep-ex]
28. ATLAS Collaboration, Measurement of electroweak $Z(\nu\bar{\nu})\gamma jj$ production and limits on anomalous quartic gauge couplings in pp collisions at $\sqrt{s} = 13$ TeV with the ATLAS detector. JHEP **06**, 082 (2023). https://doi.org/10.1007/JHEP06(2023)082. arXiv:2208.12741 [hep-ex]
29. ATLAS Collaboration, Measurement of the cross-sections of the electroweak and total production of a $Z\gamma$ pair in association with two jets in pp collisions at $\sqrt{s} = 13$ TeV with the ATLAS detector. Phys. Lett. B **846**, 138222 (2023). https://doi.org/10.1016/j.physletb.2023.138222. arXiv:2305.19142 [hep-ex]
30. CMS Collaboration, Measurement of the electroweak production of $Z\gamma$ and two jets in proton–proton collisions at $\sqrt{s} = 13$ TeV and constraints on anomalous quartic gauge couplings. Phys. Rev. D **104**, 072001 (2021). https://doi.org/10.1103/PhysRevD.104.072001. arXiv:2106.11082 [hep-ex]
31. CMS Collaboration, Evidence for WW/WZ vector boson scattering in the decay channel $\ell\nu qq$ produced in association with two jets in proton–proton collisions at $\sqrt{s} = 13$ TeV. Phys. Lett. B **834**, 137438 (2022). https://doi.org/10.1016/j.physletb.2022.137438. arXiv:2112.05259 [hep-ex]
32. CMS Collaboration, Search for anomalous electroweak production of vector boson pairs in association with two jets in proton–proton collisions at 13 TeV. Phys. Lett. B **798**, 134985 (2019). https://doi.org/10.1016/j.physletb.2019.134985. arXiv:1905.07445 [hep-ex]
33. ATLAS Collaboration, Search for electroweak diboson production in association with a high-mass dijet system in semileptonic final states in pp collisions at $\sqrt{s} = 13$ TeV with the ATLAS detector. Phys. Rev. D **100**, 032007 (2019). https://doi.org/10.1103/PhysRevD.100.032007. arXiv:1905.07714 [hep-ex]

34. ATLAS Collaboration, The ATLAS Experiment at the CERN large hadron collider. JINST **3**, S08003 (2008). https://doi.org/10.1088/1748-0221/3/08/S08003
35. ATLAS Collaboration, Software and computing for Run 3 of the ATLAS experiment at the LHC. Eur. Phys. J. C **85**, 234 (2025). https://doi.org/10.1140/epjc/s10052-024-13701-w. arXiv:2404.06335 [hep-ex]
36. ATLAS Collaboration, Luminosity determination in pp collisions at $\sqrt{s} = 13$ TeV using the ATLAS detector at the LHC. Eur. Phys. J. C **83**, 982 (2023). https://doi.org/10.1140/epjc/s10052-023-11747-w. arXiv:2212.09379 [hep-ex]
37. ATLAS Collaboration, Selection of jets produced in 13 TeV proton–proton collisions with the ATLAS detector, ATLAS-CONF-2015-029 (2015). https://cds.cern.ch/record/2037702
38. ATLAS Collaboration, Performance of the ATLAS trigger system in. Eur. Phys. J. C **77**(2017), 317 (2015). https://doi.org/10.1140/epjc/s10052-017-4852-3. arXiv:1611.09661 [hep-ex]
39. ATLAS Collaboration, Performance of electron and photon triggers in ATLAS during LHC Run 2. Eur. Phys. J. C **80**, 47 (2020). https://doi.org/10.1140/epjc/s10052-019-7500-2. arXiv:1909.00761 [hep-ex]
40. ATLAS Collaboration, Performance of the ATLAS muon triggers in Run 2. JINST **15**, P09015 (2020). https://doi.org/10.1088/1748-0221/15/09/p09015. arXiv:2004.13447 [physics.ins-det]
41. ATLAS Collaboration, Performance of the missing transverse momentum triggers for the ATLAS detector during Run-2 data taking. JHEP **08**, 080 (2020). https://doi.org/10.1007/JHEP08(2020)080. arXiv:2005.09554 [hep-ex]
42. J. Alwall et al., The automated computation of tree-level and next-to-leading order differential cross sections, and their matching to parton shower simulations. JHEP **07**, 079 (2014). https://doi.org/10.1007/JHEP07(2014)079. arXiv:1405.0301 [hep-ph]
43. NNPDF Collaboration, R.D. Ball et al., Parton distributions for the LHC run II. JHEP **04**, 040 (2015). https://doi.org/10.1007/JHEP04(2015)040. arXiv:1410.8849 [hep-ph]
44. T. Sjöstrand, S. Mrenna, P. Skands, A brief introduction to PYTHIA 8.1. Comput. Phys. Commun. **178**, 852 (2008). https://doi.org/10.1016/j.cpc.2008.01.036. arXiv:0710.3820 [hep-ph]
45. ATLAS Collaboration, ATLAS Pythia 8 tunes to 7 TeV data, ATL-PHYS-PUB-2014-021 (2014). https://cds.cern.ch/record/1966419
46. P. Artoisenet, R. Frederix, O. Mattelaer, R. Rietkerk, Automatic spin-entangled decays of heavy resonances in Monte Carlo simulations. JHEP **03**, 015 (2013). https://doi.org/10.1007/JHEP03(2013)015. arXiv:1212.3460 [hep-ph]
47. T. Sjöstrand et al., An introduction to PYTHIA 8.2. Comput. Phys. Commun. **191**, 159 (2015). https://doi.org/10.1016/j.cpc.2015.01.024. arXiv:1410.3012 [hep-ph]
48. E. Bothmann et al., Event generation with Sherpa 2.2. SciPost Phys. **7**, 034 (2019). https://doi.org/10.21468/SciPostPhys.7.3.034. arXiv:1905.09127 [hep-ph]
49. T. Gleisberg, S. Höche, Comix, a new matrix element generator. JHEP **12**, 039 (2008). https://doi.org/10.1088/1126-6708/2008/12/039. arXiv:0808.3674 [hep-ph]
50. F. Buccioni et al., OpenLoops 2. Eur. Phys. J. C **79**, 866 (2019). https://doi.org/10.1140/epjc/s10052-019-7306-2. arXiv:1907.13071 [hep-ph]
51. F. Cascioli, P. Maierhöfer, S. Pozzorini, Scattering amplitudes with open loops. Phys. Rev. Lett. **108**, 111601 (2012). https://doi.org/10.1103/PhysRevLett.108.111601. arXiv:1111.5206 [hep-ph]
52. A. Denner, S. Dittmaier, L. Hofer, Collier: a fortran-based complex one-loop library in extended regularizations. Comput. Phys. Commun. **212**, 220 (2017). https://doi.org/10.1016/j.cpc.2016.10.013. arXiv:1604.06792 [hep-ph]
53. S. Schumann, F. Krauss, A parton shower algorithm based on Catani–Seymour dipole factorisation. JHEP **03**, 038 (2008). https://doi.org/10.1088/1126-6708/2008/03/038. arXiv:0709.1027 [hep-ph]
54. S. Höche, F. Krauss, M. Schönherr, F. Siegert, A critical appraisal of NLO+PS matching methods. JHEP **09**, 049 (2012). https://doi.org/10.1007/JHEP09(2012)049. arXiv:1111.1220 [hep-ph]
55. S. Höche, F. Krauss, M. Schönherr, F. Siegert, QCD matrix elements + parton showers. The NLO case. JHEP **04**, 027 (2013). https://doi.org/10.1007/JHEP04(2013)027. arXiv:1207.5030 [hep-ph]
56. S. Catani, F. Krauss, B.R. Webber, R. Kuhn, QCD matrix elements + parton showers. JHEP **11**, 063 (2001). https://doi.org/10.1088/1126-6708/2001/11/063. arXiv:hep-ph/0109231
57. S. Höche, F. Krauss, S. Schumann, F. Siegert, QCD matrix elements and truncated showers. JHEP **05**, 053 (2009). https://doi.org/10.1088/1126-6708/2009/05/053. arXiv:0903.1219 [hep-ph]
58. E. Re, Single-top Wt-channel production matched with parton showers using the POWHEG method. Eur. Phys. J. C **71**, 1547 (2011). https://doi.org/10.1140/epjc/s10052-011-1547-z. arXiv:1009.2450 [hep-ph]
59. S. Frixione, G. Ridolfi, P. Nason, A positive-weight next-to-leading-order Monte Carlo for heavy flavour hadroproduction. JHEP **09**, 126 (2007). https://doi.org/10.1088/1126-6708/2007/09/126. arXiv:0707.3088 [hep-ph]
60. P. Nason, A new method for combining NLO QCD with shower Monte Carlo algorithms. JHEP **11**, 040 (2004). https://doi.org/10.1088/1126-6708/2004/11/040. arXiv:hep-ph/0409146
61. S. Frixione, P. Nason, C. Oleari, Matching NLO QCD computations with parton shower simulations: the POWHEG method. JHEP **11**, 070 (2007). https://doi.org/10.1088/1126-6708/2007/11/070. arXiv:0709.2092 [hep-ph]
62. S. Alioli, P. Nason, C. Oleari, E. Re, A general framework for implementing NLO calculations in shower Monte Carlo programs: the POWHEG BOX. JHEP **06**, 043 (2010). https://doi.org/10.1007/JHEP06(2010)043. arXiv:1002.2581 [hep-ph]
63. ATLAS Collaboration, Studies on top-quark Monte Carlo modelling for Top2016, ATL-PHYS-PUB-2016-020 (2016). https://cds.cern.ch/record/2216168
64. NNPDF Collaboration, R.D. Ball, et al., Parton distributions with LHC data. Nucl. Phys. B **867**, 244 (2013). https://doi.org/10.1016/j.nuclphysb.2012.10.003. arXiv:1207.1303 [hep-ph]
65. D.J. Lange, The EvtGen particle decay simulation package. Nucl. Instrum. Methods A **462**, 152 (2001). https://doi.org/10.1016/S0168-9002(01)00089-4
66. C. Anastasiou, L. Dixon, K. Melnikov, F. Petriello, High-precision QCD at hadron colliders: electroweak gauge boson rapidity distributions at next-to-next-to leading order. Phys. Rev. D **69**, 094008 (2004). https://doi.org/10.1103/PhysRevD.69.094008. arXiv:hep-ph/0312266
67. T. Gleisberg et al., Event generation with SHERPA 1.1. JHEP **02**, 007 (2009). https://doi.org/10.1088/1126-6708/2009/02/007. arXiv:0811.4622 [hep-ph]
68. M. Czakon, P. Fiedler, A. Mitov, Total Top-quark pair-production cross section at hadron colliders through $\mathcal{O}(\alpha\_S^4)$. Phys. Rev. Lett. **110**, 252004 (2013). https://doi.org/10.1103/PhysRevLett.110.252004. arXiv:1303.6254 [hep-ph]
69. M. Czakon, A. Mitov, Top++: a program for the calculation of the top-pair cross-section at hadron colliders. Comput. Phys. Commun. **185**, 2930 (2014). https://doi.org/10.1016/j.cpc.2014.06.021. arXiv:1112.5675 [hep-ph]
70. N. Kidonakis, Next-to-next-to-leading logarithm resummation for s-channel single top quark production. Phys. Rev. D **81**, 054028 (2010). https://doi.org/10.1103/PhysRevD.81.054028. arXiv:hep-ph/1001.5034

71. N. Kidonakis, Two-loop soft anomalous dimensions for single top quark associated production with a W^- or H^-. Phys. Rev. D **82**, 054018 (2010). https://doi.org/10.1103/PhysRevD.82.054018. arXiv:1005.4451 [hep-ph]
72. ATLAS Collaboration, The ATLAS simulation infrastructure. Eur. Phys. J. C **70**, 823. (2010). https://doi.org/10.1140/epjc/s10052-010-1429-9. arXiv:1005.4568 [physics.ins-det]
73. S. Agostinelli et al., Geant4—a simulation toolkit. Nucl. Instrum. Methods A **506**, 250 (2003). https://doi.org/10.1016/S0168-9002(03)01368-8
74. ATLAS Collaboration, Electron and photon efficiencies in LHC Run 2 with the ATLAS experiment. JHEP **05**, 162 (2024). https://doi.org/10.1007/JHEP05(2024)162. arXiv:2308.13362 [hep-ex]
75. ATLAS Collaboration, Electron and photon performance measurements with the ATLAS detector using the 2015–2017 LHC proton–proton collision data. JINST **14**, P12006 (2019). https://doi.org/10.1088/1748-0221/14/12/P12006. arXiv:1908.00005 [hep-ex]
76. ATLAS Collaboration, Muon reconstruction and identification efficiency in ATLAS using the full Run 2 pp collision data set at $\sqrt{s} = 13$ TeV. Eur. Phys. J. C **81**, 578 (2021). https://doi.org/10.1140/epjc/s10052-021-09233-2. arXiv:2012.00578 [hep-ex]
77. ATLAS Collaboration, Muon reconstruction performance of the ATLAS detector in proton–proton collision data at $\sqrt{s} = 13$ TeV. Eur. Phys. J. C **76**, 292 (2016). https://doi.org/10.1140/epjc/s10052-016-4120-y. arXiv:1603.05598 [hep-ex]
78. ATLAS Collaboration, Search for heavy diboson resonances in semileptonic final states in pp collisions at $\sqrt{s} = 13$ TeV with the ATLAS detector. Eur. Phys. J. C **80**, 1165 (2020). https://doi.org/10.1140/epjc/s10052-020-08554-y. arXiv:2004.14636 [hep-ex]
79. M. Cacciari, G.P. Salam, G. Soyez, The anti-k_t jet clustering algorithm. JHEP **04**, 063 (2008). https://doi.org/10.1088/1126-6708/2008/04/063. arXiv:0802.1189 [hep-ph]
80. M. Cacciari, G.P. Salam, G. Soyez, FastJet user manual. Eur. Phys. J. C **72**, 1896 (2012). https://doi.org/10.1140/epjc/s10052-012-1896-2. arXiv:1111.6097 [hep-ph]
81. ATLAS Collaboration, Jet reconstruction and performance using particle flow with the ATLAS detector. Eur. Phys. J. C **77**, 466 (2017). https://doi.org/10.1140/epjc/s10052-017-5031-2. arXiv:1703.10485 [hep-ex]
82. ATLAS Collaboration, Performance of pile-up mitigation techniques for jets in pp collisions at $\sqrt{s} = 8$ TeV using the ATLAS detector. Eur. Phys. J. C **76**, 581 (2016). https://doi.org/10.1140/epjc/s10052-016-4395-z. arXiv:1510.03823 [hep-ex]
83. ATLAS Collaboration, Identification and rejection of pile-up jets at high pseudorapidity with the ATLAS detector. Eur. Phys. J. C **77**, 580 (2017). https://doi.org/10.1140/epjc/s10052-017-5081-5. arXiv:1705.02211 [hep-ex] [Erratum: Eur. Phys. J. C 77 (2017) 712.DOI: https://doi.org/10.1140/epjc/s10052-017-5245-3]
84. ATLAS Collaboration, Jet energy scale measurements and their systematic uncertainties in proton–proton collisions at $\sqrt{s} = 13$ TeV with the ATLAS detector. Phys. Rev. D **96**, 072002 (2017). https://doi.org/10.1103/PhysRevD.96.072002. arXiv:1703.09665 [hep-ex]
85. ATLAS Collaboration, Jet energy scale and resolution measured in proton–proton collisions at $\sqrt{s} = 13$ TeV with the ATLAS detector. Eur. Phys. J. C **81**, 689 (2021). https://doi.org/10.1140/epjc/s10052-021-09402-3. arXiv:2007.02645 [hep-ex]
86. ATLAS Collaboration, ATLAS b-jet identification performance and efficiency measurement with $t\bar{t}$ events in pp collisions at $\sqrt{s} = 13$ TeV. Eur. Phys. J. C **79**, 970 (2019). https://doi.org/10.1140/epjc/s10052-019-7450-8. arXiv:1907.05120 [hep-ex]
87. ATLAS Collaboration, Topological cell clustering in the ATLAS calorimeters and its performance in LHC Run 1. Eur. Phys. J. C **77**, 490 (2017). https://doi.org/10.1140/epjc/s10052-017-5004-5. arXiv:1603.02934 [hep-ex]
88. D. Krohn, J. Thaler, L.-T. Wang, Jet trimming. JHEP **02**, 084 (2010). https://doi.org/10.1007/JHEP02(2010)084. arXiv:0912.1342 [hep-ph]
89. S.D. Ellis, D.E. Soper, Successive combination jet algorithm for hadron collisions. Phys. Rev. D **48**, 3160 (1993). https://doi.org/10.1103/PhysRevD.48.3160. arXiv:hep-ph/9305266
90. ATLAS Collaboration, Performance of jet substructure techniques for large-R jets in proton–proton collisions at $\sqrt{s} = 7$ TeV using the ATLAS detector. JHEP **09**, 076 (2013). https://doi.org/10.1007/JHEP09(2013)076. arXiv:1306.4945 [hep-ex]
91. ATLAS Collaboration, In situ calibration of large-radius jet energy and mass in 13 TeV proton–proton collisions with the ATLAS detector. Eur. Phys. J. C **79**, 135 (2019). https://doi.org/10.1140/epjc/s10052-019-6632-8. arXiv:1807.09477 [hep-ex]
92. A.J. Larkoski, I. Moult, D. Neill, Power counting to better jet observables. JHEP **12**, 009 (2014). https://doi.org/10.1007/JHEP12(2014)009. arXiv:1409.6298 [hep-ph]
93. A.J. Larkoski, I. Moult, D. Neill, Analytic boosted boson discrimination. JHEP **05**, 117 (2016). https://doi.org/10.1007/JHEP05(2016)117. arXiv:1507.03018 [hep-ph]
94. ATLAS Collaboration, Search for diboson resonances in hadronic final states in 139 fb^{-1} of pp collisions at $\sqrt{s} = 13$ TeV with the ATLAS detector. JHEP **09**, 091 (2019). https://doi.org/10.1007/JHEP09(2019)091. arXiv:1906.08589 [hep-ex]
95. ATLAS Collaboration, The performance of missing transverse momentum reconstruction and its significance with the ATLAS detector using 140 fb^{-1} of $\sqrt{s} = 13$ TeV pp collisions. Eur. Phys. J. C **85**, 606 (2025). https://doi.org/10.1140/epjc/s10052-025-14062-8. arXiv:2402.05858 [hep-ex]
96. ATLAS Collaboration, Searches for heavy ZZ and ZW resonances in the $\ell\ell qq$ and $\nu\nu qq$ final states in pp collisions at $\sqrt{s} = 13$ TeV with the ATLAS detector, https://doi.org/10.1007/JHEP03(2018)009 JHEP 03 009, (2018). arXiv:1708.09638 [hep-ex]
97. ATLAS Collaboration, Measurement and interpretation of same-sign W boson pair production in association with two jets in pp collisions at $\sqrt{s} = 13$ TeV with the ATLAS detector. JHEP **04**, 026 (2024). https://doi.org/10.1007/JHEP04(2024)026. arXiv:2312.00420 [hep-ex]
98. A. Sherstinsky, Fundamentals of recurrent neural network (RNN) and long short-term memory (LSTM) network. Phys. D Nonlinear Phenom. **404**, 132306 (2020). https://doi.org/10.1016/j.physd.2019.132306. arXiv:1808.03314 [cs.LG]
99. ATLAS Collaboration, Identification of jets containing b-hadrons with recurrent neural networks at the ATLAS Experiment, ATL-PHYS-PUB-2017-003 (2017). https://cds.cern.ch/record/2255226
100. F. Chollet et al., Keras (2015). https://keras.io
101. M. Abadi, et al., TensorFlow: large-scale machine learning on heterogeneous distributed systems (2016). arXiv:1603.04467 [cs.DC]
102. D.P. Kingma, J. Ba, Adam: a method for stochastic optimization (2017). arXiv:1412.6980 [cs.LG]
103. S.R. Dubey, S.K. Singh, B.B. Chaudhuri, Activation functions in deep learning: a comprehensive survey and benchmark (2022). arXiv:2109.14545 [cs.LG]
104. ATLAS Collaboration, Proposal for particle-level object and observable definitions for use in physics measurements at the LHC, ATL-PHYS-PUB-2015-013 (2015). https://cds.cern.ch/record/2022743
105. G. Avoni et al., The new LUCID-2 detector for luminosity measurement and monitoring in ATLAS. JINST **13**, P07017 (2018). https://doi.org/10.1088/1748-0221/13/07/P07017

106. ATLAS Collaboration, Measurement of the inelastic proton–proton cross section at $\sqrt{s} = 13$ TeV with the ATLAS detector at the LHC. Phys. Rev. Lett. **117**, 182002 (2016). https://doi.org/10.1103/PhysRevLett.117.182002. arXiv:1606.02625 [hep-ex]
107. ATLAS Collaboration, Electron and photon energy calibration with the ATLAS detector using LHC Run 2 data. JINST **19**, P02009 (2024). https://doi.org/10.1088/1748-0221/19/02/P02009. arXiv:2309.05471 [hep-ex]
108. ATLAS Collaboration, Studies of the muon momentum calibration and performance of the ATLAS detector with pp collisions at $\sqrt{s} = 13$ TeV. Eur. Phys. J. C **83**, 686 (2023). https://doi.org/10.1140/epjc/s10052-023-11584-x. arXiv:2212.07338 [hep-ex]
109. ATLAS Collaboration, Calibration of the light-flavour jet mistagging efficiency of the b-tagging algorithms with Z+jets events using 139 fb^{-1} of ATLAS proton–proton collision data at $\sqrt{s} = 13$ TeV. Eur. Phys. J. C **83**, 728 (2023). https://doi.org/10.1140/epjc/s10052-023-11736-z. arXiv:2301.06319 [hep-ex]
110. ATLAS Collaboration, Early inner detector tracking performance in the 2015 data at $\sqrt{s} = 13$ TeV, ATL-PHYS-PUB-2015-051 (2015). https://cds.cern.ch/record/2110140
111. ATLAS Collaboration, Measurement of the charged-particle multiplicity inside jets from $\sqrt{s} = 8$ TeV pp collisions with the ATLAS detector. Eur. Phys. J. C **76**, 322 (2016). https://doi.org/10.1140/epjc/s10052-016-4126-5. arXiv:1602.00988 [hep-ex]
112. ATLAS Collaboration, Measurement of the ATLAS detector jet mass response using forward folding with 80 fb^{-1} of $\sqrt{s} = 13$ TeV pp data, ATLAS-CONF-2020-022 (2020). https://cds.cern.ch/record/2724442
113. ATLAS Collaboration, Boosted hadronic vector boson and top quark tagging with ATLAS using Run 2 data, ATL-PHYS-PUB-2020-017 (2020). https://cds.cern.ch/record/2724149
114. M. Bähr et al., Herwig++ physics and manual. Eur. Phys. J. C **58**, 639 (2008). https://doi.org/10.1140/epjc/s10052-008-0798-9. arXiv:0803.0883 [hep-ph]
115. J. Bellm, et al., Herwig 7.0/Herwig++ 3.0 release note. Eur. Phys. J. C **76**, 196 (2016). https://doi.org/10.1140/epjc/s10052-016-4018-8. arXiv:1512.01178 [hep-ph]
116. L.A. Harland-Lang, A.D. Martin, P. Motylinski, R.S. Thorne, Parton distributions in the LHC era: MMHT 2014 PDFs. Eur. Phys. J. C **75**, 204 (2015). https://doi.org/10.1140/epjc/s10052-015-3397-6. arXiv:1412.3989 [hep-ph]
117. ATLAS Collaboration, Measurement of the cross-section for producing a W boson in association with a single top quark in pp collisions at $\sqrt{s} = 13$ TeV with ATLAS. JHEP **01**, 063 (2018). https://doi.org/10.1007/JHEP01(2018)063. arXiv:1612.07231 [hep-ex]
118. W. Verkerke, D. Kirkby, The RooFit toolkit for data modeling (2003). arXiv:physics/0306116 [physics.data-an]
119. L. Moneta, et al., The RooStats Project, PoS ACAT2010 057 (2010). https://doi.org/10.22323/1.093.0057. arXiv:1009.1003 [physics.data-an]
120. G. Cowan, K. Cranmer, E. Gross, O. Vitells, Asymptotic formulae for likelihood-based tests of new physics. Eur. Phys. J. C **71**, 1554 (2011). https://doi.org/10.1140/epjc/s10052-011-1554-0. arXiv:1007.1727 [physics.data-an] [Erratum: Eur. Phys. J. C 73 2501. (2013). DOI: https://doi.org/10.1140/epjc/s10052-013-2501-z]
121. ATLAS Collaboration, Search for the $b\bar{b}$ decay of the Standard Model Higgs boson in associated $(W/Z)H$ production with the ATLAS detector. JHEP **01**, 069 (2015). https://doi.org/10.1007/JHEP01(2015)069. arXiv:1409.6212 [hep-ex]
122. ATLAS Collaboration, Evidence for the $H \to b\bar{b}$ decay with the ATLAS detector. JHEP **12**, 024 (2017). https://doi.org/10.1007/JHEP12(2017)024. arXiv:1708.03299 [hep-ex]
123. S.S. Wilks, The large-sample distribution of the likelihood ratio for testing composite hypotheses. Ann. Math. Stat. **9**, 60 (1938). https://doi.org/10.1214/aoms/1177732360
124. CMS Collaboration, Measurements of production cross sections of WZ and same-sign WW boson pairs in association with two jets in proton–proton collisions at $\sqrt{s} = 13$ TeV. Phys. Lett. B **809**, 135710 (2020). https://doi.org/10.1016/j.physletb.2020.135710. arXiv:2005.01173 [hep-ex]
125. E.D.S. Almeida, O.J.P. Éboli, M.C. Gonzalez–Garcia, Unitarity constraints on anomalous quartic couplings. Phys. Rev. D **101**, 113003 (2020). https://doi.org/10.1103/physrevd.101.113003. arXiv:hep-ph/2004.05174
126. ATLAS Collaboration, Differential cross-section measurements of the production of four charged leptons in association with two jets using the ATLAS detector. JHEP **01**, 004 (2024). https://doi.org/10.1007/JHEP01(2024)004. arXiv:2308.12324 [hep-ex]
127. ATLAS Collaboration, ATLAS Computing Acknowledgements, ATL-SOFT-PUB-2025-001 (2025). https://cds.cern.ch/record/2922210
128. CERN, CERN Open Data Policy for the LHC Experiments. CERN-OPEN-2020-013 (2020). https://cds.cern.ch/record/2745133

ATLAS Collaboration

G. Aad[104], E. Aakvaag[17], B. Abbott[123], S. Abdelhameed[119a], K. Abeling[55], N. J. Abicht[49], S. H. Abidi[30], M. Aboelela[45], A. Aboulhorma[36e], H. Abramowicz[157], Y. Abulaiti[120], B. S. Acharya[69a,69b,n], A. Ackermann[63a], C. Adam Bourdarios[4], L. Adamczyk[87a], S. V. Addepalli[149], M. J. Addison[103], J. Adelman[118], A. Adiguzel[22c], T. Adye[137], A. A. Affolder[139], Y. Afik[40], M. N. Agaras[13], A. Aggarwal[102], C. Agheorghiesei[28c], F. Ahmadov[39,ae], S. Ahuja[97], X. Ai[143b], G. Aielli[76a,76b], A. Aikot[169], M. Ait Tamlihat[36e], B. Aitbenchikh[36a], M. Akbiyik[102], T. P. A. Åkesson[100], A. V. Akimov[151], D. Akiyama[174], N. N. Akolkar[25], S. Aktas[22a], G. L. Alberghi[24b], J. Albert[171], P. Albicocco[53], G. L. Albouy[60], S. Alderweireldt[52], Z. L. Alegria[124], M. Aleksa[37], I. N. Aleksandrov[39], C. Alexa[28b], T. Alexopoulos[10], F. Alfonsi[24b], M. Algren[56], M. Alhroob[173], B. Ali[135], H. M. J. Ali[93,x], S. Ali[32], S. W. Alibocus[94], M. Aliev[34c], G. Alimonti[71a], W. Alkakhi[55], C. Allaire[66], B. M. M. Allbrooke[152], J. S. Allen[103], J. F. Allen[52], P. P. Allport[21], A. Aloisio[72a,72b], F. Alonso[92], C. Alpigiani[142], Z. M. K. Alsolami[93], A. Alvarez Fernandez[102], M. Alves Cardoso[56], M. G. Alviggi[72a,72b], M. Aly[103], Y. Amaral Coutinho[83b], A. Ambler[106], C. Amelung[37], M. Amerl[103], C. G. Ames[111], T. Amezza[130], D. Amidei[108], B. Amini[54], K. Amirie[161], A. Amirkhanov[39], S. P. Amor Dos Santos[133a], K. R. Amos[169], D. Amperiadou[158], S. An[84], C. Anastopoulos[145], T. Andeen[11], J. K. Anders[94], A. C. Anderson[59], A. Andreazza[71a,71b], S. Angelidakis[9], A. Angerami[42], A. V. Anisenkov[39], A. Annovi[74a], C. Antel[56], E. Antipov[151], M. Antonelli[53], F. Anulli[75a], M. Aoki[84], T. Aoki[159], M. A. Aparo[152], L. Aperio Bella[48], M. Apicella[31], C. Appelt[157], A. Apyan[27], S. J. Arbiol Val[88], C. Arcangeletti[53], A. T. H. Arce[51], J- F. Arguin[110], S. Argyropoulos[158], J. -H. Arling[48], O. Arnaez[4], H. Arnold[151], G. Artoni[75a,75b], H. Asada[113], K. Asai[121], S. Asai[159], S. Asatryan[179], N. A. Asbah[37], R. A. Ashby Pickering[173], A. M. Aslam[97], K. Assamagan[30], R. Astalos[29a], K. S. V. Astrand[100], S. Atashi[165], R. J. Atkin[34a], H. Atmani[36f], P. A. Atmasiddha[131], K. Augsten[135], A. D. Auriol[41], V. A. Austrup[103], G. Avolio[37], K. Axiotis[56], G. Azuelos[110,ai], D. Babal[29b], H. Bachacou[138], K. Bachas[158,r], A. Bachiu[35], E. Bachmann[50], M. J. Backes[63a], A. Badea[40], T. M. Baer[108], P. Bagnaia[75a,75b], M. Bahmani[19], D. Bahner[54], K. Bai[126], J. T. Baines[137], L. Baines[96], O. K. Baker[178], E. Bakos[16], D. Bakshi Gupta[8], L. E. Balabram Filho[83b], V. Balakrishnan[123], R. Balasubramanian[4], E. M. Baldin[38], P. Balek[87a], E. Ballabene[24b,24a], F. Balli[138], L. M. Baltes[63a], W. K. Balunas[33], J. Balz[102], I. Bamwidhi[119b], E. Banas[88], M. Bandieramonte[132], A. Bandyopadhyay[25], S. Bansal[25], L. Barak[157], M. Barakat[48], E. L. Barberio[107], D. Barberis[18b], M. Barbero[104], M. Z. Barel[117], T. Barillari[112], M -S. Barisits[37], T. Barklow[149], P. Baron[136], D. A. Baron Moreno[103], A. Baroncelli[62], A. J. Barr[129], J. D. Barr[98], F. Barreiro[101], J. Barreiro Guimarães da Costa[14], M. G. Barros Teixeira[133a], S. Barsov[38], F. Bartels[63a], R. Bartoldus[149], A. E. Barton[93], P. Bartos[29a], A. Basan[102], M. Baselga[49], S. Bashiri[88], A. Bassalat[66,b], M. J. Basso[162a], S. Bataju[45], R. Bate[170], R. L. Bates[59], S. Batlamous[101], M. Battaglia[139], D. Battulga[19], M. Bauce[75a,75b], M. Bauer[79], P. Bauer[25], L. T. Bayer[48], L. T. Bazzano Hurrell[31], J. B. Beacham[112], T. Beau[130], J. Y. Beaucamp[92], P. H. Beauchemin[164], P. Bechtle[25], H. P. Beck[20,q], K. Becker[173], A. J. Beddall[82], V. A. Bednyakov[39], C. P. Bee[151], L. J. Beemster[16], M. Begalli[83d], M. Begel[30], J. K. Behr[48], J. F. Beirer[37], F. Beisiegel[25], M. Belfkir[119b], G. Bella[157], L. Bellagamba[24b], A. Bellerive[35], C. D. Bellgraph[68], P. Bellos[21], K. Beloborodov[38], D. Benchekroun[36a], F. Bendebba[36a], Y. Benhammou[157], K. C. Benkendorfer[61], L. Beresford[48], M. Beretta[53], E. Bergeaas Kuutmann[167], N. Berger[4], B. Bergmann[135], J. Beringer[18a], G. Bernardi[5], C. Bernius[149], F. U. Bernlochner[25], F. Bernon[37], A. Berrocal Guardia[13], T. Berry[97], P. Berta[136], A. Berthold[50], A. Berti[133a], R. Bertrand[104], S. Bethke[112], A. Betti[75a,75b], A. J. Bevan[96], L. Bezio[56], N. K. Bhalla[54], S. Bharthuar[112], S. Bhatta[151], P. Bhattarai[149], Z. M. Bhatti[120], K. D. Bhide[54], V. S. Bhopatkar[124], R. M. Bianchi[132], G. Bianco[24b,24a], O. Biebel[111], M. Biglietti[77a], C. S. Billingsley[45], Y. Bimgdi[36f], M. Bindi[55], A. Bingham[177], A. Bingul[22b], C. Bini[75a,75b], G. A. Bird[33], M. Birman[175], M. Biros[136], S. Biryukov[152], T. Bisanz[49], E. Bisceglie[24b,24a], J. P. Biswal[137], D. Biswas[147], I. Bloch[48], A. Blue[59], U. Blumenschein[96], J. Blumenthal[102], V. S. Bobrovnikov[39], M. Boehler[54], B. Boehm[172], D. Bogavac[13], A. G. Bogdanchikov[38], L. S. Boggia[130], V. Boisvert[97], P. Bokan[37], T. Bold[87a], M. Bomben[5], M. Bona[96], M. Boonekamp[138], A. G. Borbély[59], I. S. Bordulev[38], G. Borissov[93], D. Bortoletto[129], D. Boscherini[24b], M. Bosman[13], K. Bouaouda[36a], N. Bouchhar[169], L. Boudet[4], J. Boudreau[132], E. V. Bouhova-Thacker[93], D. Boumediene[41], R. Bouquet[57b,57a], A. Boveia[122], J. Boyd[37], D. Boye[30], I. R. Boyko[39], L. Bozianu[56], J. Bracinik[21], N. Brahimi[4], G. Brandt[177], O. Brandt[33], B. Brau[105], J. E. Brau[126], R. Brener[175], L. Brenner[117], R. Brenner[167], S. Bressler[175], G. Brianti[78a,78b],

D. Britton[59], D. Britzger[112], I. Brock[25], R. Brock[109], G. Brooijmans[42], A. J. Brooks[68], E. M. Brooks[162b], E. Brost[30], L. M. Brown[171,162a], L. E. Bruce[61], T. L. Bruckler[129], P. A. Bruckman de Renstrom[88], B. Brüers[48], A. Bruni[24b], G. Bruni[24b], D. Brunner[47a,47b], M. Bruschi[24b], N. Bruscino[75a,75b], T. Buanes[17], Q. Buat[142], D. Buchin[112], A. G. Buckley[59], O. Bulekov[82], B. A. Bullard[149], S. Burdin[94], C. D. Burgard[49], A. M. Burger[91], B. Burghgrave[8], O. Burlayenko[54], J. Burleson[168], J. T. P. Burr[33], J. C. Burzynski[148], E. L. Busch[42], V. Büscher[102], P. J. Bussey[59], J. M. Butler[26], C. M. Buttar[59], J. M. Butterworth[98], W. Buttinger[137], C. J. Buxo Vazquez[109], A. R. Buzykaev[39], S. Cabrera Urbán[169], L. Cadamuro[66], D. Caforio[58], H. Cai[132], Y. Cai[24b,114c,24a], Y. Cai[114a], V. M. M. Cairo[37], O. Cakir[3a], N. Calace[37], P. Calafiura[18a], G. Calderini[130], P. Calfayan[35], G. Callea[59], L. P. Caloba[83b], D. Calvet[41], S. Calvet[41], R. Camacho Toro[130], S. Camarda[37], D. Camarero Munoz[27], P. Camarri[76a,76b], C. Camincher[171], M. Campanelli[98], A. Camplani[43], V. Canale[72a,72b], A. C. Canbay[3a], E. Canonero[97], J. Cantero[169], Y. Cao[168], F. Capocasa[27], M. Capua[44b,44a], A. Carbone[71a,71b], R. Cardarelli[76a], J. C. J. Cardenas[8], M. P. Cardiff[27], G. Carducci[44b,44a], T. Carli[37], G. Carlino[72a], J. I. Carlotto[13], B. T. Carlson[132,s], E. M. Carlson[171], J. Carmignani[94], L. Carminati[71a,71b], A. Carnelli[4], M. Carnesale[37], S. Caron[116], E. Carquin[140f], I. B. Carr[107], S. Carrá[73a,73b], G. Carratta[24b,24a], A. M. Carroll[126], M. P. Casado[13,i], M. Caspar[48], F. L. Castillo[4], L. Castillo Garcia[13], V. Castillo Gimenez[169], N. F. Castro[133a,133e], A. Catinaccio[37], J. R. Catmore[128], T. Cavaliere[4], V. Cavaliere[30], L. J. Caviedes Betancourt[23b], Y. C. Cekmecelioglu[48], E. Celebi[82], S. Cella[37], V. Cepaitis[56], K. Cerny[125], A. S. Cerqueira[83a], A. Cerri[74a,74b,al], L. Cerrito[76a,76b], F. Cerutti[18a], B. Cervato[71a,71b], A. Cervelli[24b], G. Cesarini[53], S. A. Cetin[82], P. M. Chabrillat[130], S. Chakraborty[173], J. Chan[18a], W. Y. Chan[159], J. D. Chapman[33], E. Chapon[138], B. Chargeishvili[155b], D. G. Charlton[21], C. Chauhan[136], Y. Che[114a], S. Chekanov[6], S. V. Chekulaev[162a], G. A. Chelkov[39,a], B. Chen[157], B. Chen[171], H. Chen[114a], H. Chen[30], J. Chen[144a], J. Chen[148], M. Chen[129], S. Chen[89], S. J. Chen[114a], X. Chen[144a], X. Chen[15,ah], Z. Chen[62], C. L. Cheng[176], H. C. Cheng[64a], S. Cheong[149], A. Cheplakov[39], E. Cherepanova[117], R. Cherkaoui El Moursli[36e], E. Cheu[7], K. Cheung[65], L. Chevalier[138], V. Chiarella[53], G. Chiarelli[74a], G. Chiodini[70a], A. S. Chisholm[21], A. Chitan[28b], M. Chitishvili[169], M. V. Chizhov[39,t], K. Choi[11], Y. Chou[142], E. Y. S. Chow[116], K. L. Chu[175], M. C. Chu[64a], X. Chu[14,114c], Z. Chubinidze[53], J. Chudoba[134], J. J. Chwastowski[88], D. Cieri[112], K. M. Ciesla[87a], V. Cindro[95], A. Ciocio[18a], F. Cirotto[72a,72b], Z. H. Citron[175], M. Citterio[71a], D. A. Ciubotaru[28b], A. Clark[56], P. J. Clark[52], N. Clarke Hall[98], C. Clarry[161], S. E. Clawson[48], C. Clement[47a,47b], Y. Coadou[104], M. Cobal[69a,69c], A. Coccaro[57b], R. F. Coelho Barrue[133a], R. Coelho Lopes De Sa[105], S. Coelli[71a], L. S. Colangeli[161], B. Cole[42], P. Collado Soto[101], J. Collot[60], R. Coluccia[70a,70b], P. Conde Muiño[133a,133g], M. P. Connell[34c], S. H. Connell[34c], E. I. Conroy[129], M. Contreras Cossio[11], F. Conventi[72a,aj], H. G. Cooke[21], A. M. Cooper-Sarkar[129], L. Corazzina[75a,75b], F. A. Corchia[24b,24a], A. Cordeiro Oudot Choi[142], L. D. Corpe[41], M. Corradi[75a,75b], F. Corriveau[106,ac], A. Cortes-Gonzalez[159], M. J. Costa[169], F. Costanza[4], D. Costanzo[145], B. M. Cote[122], J. Couthures[4], G. Cowan[97], K. Cranmer[176], L. Cremer[49], D. Cremonini[24b,24a], S. Crépé-Renaudin[60], F. Crescioli[130], T. Cresta[73a,73b], M. Cristinziani[147], M. Cristoforetti[78a,78b], V. Croft[117], J. E. Crosby[124], G. Crosetti[44b,44a], A. Cueto[101], H. Cui[98], Z. Cui[7], W. R. Cunningham[59], F. Curcio[169], J. R. Curran[52], M. J. Da Cunha Sargedas De Sousa[57b,57a], J. V. Da Fonseca Pinto[83b], C. Da Via[103], W. Dabrowski[87a], T. Dado[37], S. Dahbi[154], T. Dai[108], D. Dal Santo[20], C. Dallapiccola[105], M. Dam[43], G. D'amen[30], V. D'Amico[111], J. Damp[102], J. R. Dandoy[35], D. Dannheim[37], G. D'anniballe[74a,74b], M. Danninger[148], V. Dao[151], G. Darbo[57b], S. J. Das[30], F. Dattola[48], S. D'Auria[71a,71b], A. D'Avanzo[72a,72b], T. Davidek[136], J. Davidson[173], I. Dawson[96], K. De[8], C. De Almeida Rossi[161], R. De Asmundis[72a], N. De Biase[48], S. De Castro[24b,24a], N. De Groot[116], P. de Jong[117], H. De la Torre[118], A. De Maria[114a], A. De Salvo[75a], U. De Sanctis[76a,76b], F. De Santis[70a,70b], A. De Santo[152], J. B. De Vivie De Regie[60], J. Debevc[95], D. V. Dedovich[39], J. Degens[94], A. M. Deiana[45], J. Del Peso[101], L. Delagrange[130], F. Deliot[138], C. M. Delitzsch[49], M. Della Pietra[72a,72b], D. Della Volpe[56], A. Dell'Acqua[37], L. Dell'Asta[71a,71b], M. Delmastro[4], C. C. Delogu[102], P. A. Delsart[60], S. Demers[178], M. Demichev[39], S. P. Denisov[38], H. Denizli[22a,m], L. D'Eramo[41], D. Derendarz[88], F. Derue[130], P. Dervan[94,*], K. Desch[25], F. A. Di Bello[57b,57a], A. Di Ciaccio[76a,76b], L. Di Ciaccio[4], A. Di Domenico[75a,75b], C. Di Donato[72a,72b], A. Di Girolamo[37], G. Di Gregorio[37], A. Di Luca[78a,78b], B. Di Micco[77a,77b], R. Di Nardo[77a,77b], K. F. Di Petrillo[40], M. Diamantopoulou[35], F. A. Dias[117], M. A. Diaz[140a,140b], A. R. Didenko[39], M. Didenko[169], S. D. Diefenbacher[18a], E. B. Diehl[108], S. Díez Cornell[48], C. Diez Pardos[147], C. Dimitriadi[150], A. Dimitrievska[21], A. Dimri[151], J. Dingfelder[25], T. Dingley[129], I- M. Dinu[28b], S. J. Dittmeier[63b], F. Dittus[37], M. Divisek[136], B. Dixit[94], F. Djama[104], T. Djobava[155b], C. Doglioni[103,100],

A. Dohnalova[29a], Z. Dolezal[136], K. Domijan[87a], K. M. Dona[40], M. Donadelli[83d], B. Dong[109], J. Donini[41], A. D'Onofrio[72a,72b], M. D'Onofrio[94], J. Dopke[137], A. Doria[72a], N. Dos Santos Fernandes[133a], P. Dougan[103], M. T. Dova[92], A. T. Doyle[59], M. A. Draguet[129], M. P. Drescher[55], E. Dreyer[175], I. Drivas-koulouris[10], M. Drnevich[120], M. Drozdova[56], D. Du[62], T. A. du Pree[117], Z. Duan[114a], F. Dubinin[39], M. Dubovsky[29a], E. Duchovni[175], G. Duckeck[111], P. K. Duckett[98], O. A. Ducu[28b], D. Duda[52], A. Dudarev[37], E. R. Duden[27], M. D'uffizi[103], L. Duflot[66], M. Dührssen[37], I. Duminica[28g], A. E. Dumitriu[28b], M. Dunford[63a], S. Dungs[49], K. Dunne[47a,47b], A. Duperrin[104], H. Duran Yildiz[3a], M. Düren[58], A. Durglishvili[155b], D. Duvnjak[35], B. L. Dwyer[118], G. I. Dyckes[18a], M. Dyndal[87a], B. S. Dziedzic[37], Z. O. Earnshaw[152], G. H. Eberwein[129], B. Eckerova[29a], S. Eggebrecht[55], E. Egidio Purcino De Souza[83e], G. Eigen[17], K. Einsweiler[18a], T. Ekelof[167], P. A. Ekman[100], S. El Farkh[36b], Y. El Ghazali[62], H. El Jarrari[37], A. El Moussaouy[36a], V. Ellajosyula[167], M. Ellert[167], F. Ellinghaus[177], N. Ellis[37], J. Elmsheuser[30], M. Elsawy[119a], M. Elsing[37], D. Emeliyanov[137], Y. Enari[84], I. Ene[18a], S. Epari[110], D. Ernani Martins Neto[88], F. Ernst[37], M. Errenst[177], M. Escalier[66], C. Escobar[169], E. Etzion[157], G. Evans[133a,133b], H. Evans[68], L. S. Evans[97], A. Ezhilov[38], S. Ezzarqtouni[36a], F. Fabbri[24b,24a], L. Fabbri[24b,24a], G. Facini[98], V. Fadeyev[139], R. M. Fakhrutdinov[38], D. Fakoudis[102], S. Falciano[75a], L. F. Falda Ulhoa Coelho[133a], F. Fallavollita[112], G. Falsetti[44b,44a], J. Faltova[136], C. Fan[168], K. Y. Fan[64b], Y. Fan[14], Y. Fang[14,114c], M. Fanti[71a,71b], M. Faraj[69a,69b], Z. Farazpay[99], A. Farbin[8], A. Farilla[77a], T. Farooque[109], J. N. Farr[178], S. M. Farrington[137,52], F. Fassi[36e], D. Fassouliotis[9], L. Fayard[66], P. Federic[136], P. Federicova[134], O. L. Fedin[38,a], M. Feickert[176], L. Feligioni[104], D. E. Fellers[18a], C. Feng[143a], Z. Feng[117], M. J. Fenton[165], L. Ferencz[48], B. Fernandez Barbadillo[93], P. Fernandez Martinez[67], M. J. V. Fernoux[104], J. Ferrando[93], A. Ferrari[167], P. Ferrari[117,116], R. Ferrari[73a], D. Ferrere[56], C. Ferretti[108], M. P. Fewell[1], D. Fiacco[75a,75b], F. Fiedler[102], P. Fiedler[135], S. Filimonov[39], M. S. Filip[28b,u], A. Filipčič[95], E. K. Filmer[162a], F. Filthaut[116], M. C. N. Fiolhais[133a,133c,c], L. Fiorini[169], W. C. Fisher[109], T. Fitschen[103], P. M. Fitzhugh[138], I. Fleck[147], P. Fleischmann[108], T. Flick[177], M. Flores[34d,ag], L. R. Flores Castillo[64a], L. Flores Sanz De Acedo[37], F. M. Follega[78a,78b], N. Fomin[33], J. H. Foo[161], A. Formica[138], A. C. Forti[103], E. Fortin[37], A. W. Fortman[18a], L. Foster[18a], L. Fountas[9,j], D. Fournier[66], H. Fox[93], P. Francavilla[74a,74b], S. Francescato[61], S. Franchellucci[56], M. Franchini[24b,24a], S. Franchino[63a], D. Francis[37], L. Franco[116], V. Franco Lima[37], L. Franconi[48], M. Franklin[61], G. Frattari[27], Y. Y. Frid[157], J. Friend[59], N. Fritzsche[37], A. Froch[56], D. Froidevaux[37], J. A. Frost[129], Y. Fu[109], S. Fuenzalida Garrido[140f], M. Fujimoto[104], K. Y. Fung[64a], E. Furtado De Simas Filho[83e], M. Furukawa[159], J. Fuster[169], A. Gaa[55], A. Gabrielli[24b,24a], A. Gabrielli[161], P. Gadow[37], G. Gagliardi[57b,57a], L. G. Gagnon[18a], S. Gaid[85b], S. Galantzan[157], J. Gallagher[1], E. J. Gallas[129], A. L. Gallen[167], B. J. Gallop[137], K. K. Gan[122], S. Ganguly[159], Y. Gao[52], A. Garabaglu[142], F. M. Garay Walls[140a,140b], C. García[169], A. Garcia Alonso[117], A. G. Garcia Caffaro[178], J. E. García Navarro[169], M. Garcia-Sciveres[18a], G. L. Gardner[131], R. W. Gardner[40], N. Garelli[164], R. B. Garg[149], J. M. Gargan[52], C. A. Garner[161], C. M. Garvey[34a], V. K. Gassmann[164], G. Gaudio[73a], V. Gautam[13], P. Gauzzi[75a,75b], J. Gavranovic[95], I. L. Gavrilenko[133a], A. Gavrilyuk[38], C. Gay[170], G. Gaycken[126], E. N. Gazis[10], A. Gekow[122], C. Gemme[57b], M. H. Genest[60], A.D. Gentry[115], S. George[97], T. Geralis[46], A. A. Gerwin[123], P. Gessinger-Befurt[37], M. E. Geyik[177], M. Ghani[173], K. Ghorbanian[96], A. Ghosal[147], A. Ghosh[165], A. Ghosh[7], B. Giacobbe[24b], S. Giagu[75a,75b], T. Giani[117], A. Giannini[62], S. M. Gibson[97], M. Gignac[139], D. T. Gil[87b], A. K. Gilbert[87a], B. J. Gilbert[42], D. Gillberg[35], G. Gilles[117], D. M. Gingrich[2,ai], M. P. Giordani[69a,69c], P. F. Giraud[138], G. Giugliarelli[69a,69c], D. Giugni[71a], F. Giuli[76a,76b], I. Gkialas[9,j], L. K. Gladilin[38], C. Glasman[101], M. Glazewska[20], R. M. Gleason[165], G. Glemža[48], M. Glisic[126], I. Gnesi[44b], Y. Go[30], M. Goblirsch-Kolb[37], B. Gocke[49], D. Godin[110], B. Gokturk[22a], S. Goldfarb[107], T. Golling[56], M. G. D. Gololo[34c], D. Golubkov[38], J. P. Gombas[109], A. Gomes[133a,133b], G. Gomes Da Silva[147], A. J. Gomez Delegido[169], R. Gonçalo[133a], L. Gonella[21], A. Gongadze[155c], F. Gonnella[21], J. L. Gonski[149], R. Y. González Andana[52], S. González de la Hoz[169], M. V. Gonzalez Rodrigues[48], R. Gonzalez Suarez[167], S. Gonzalez-Sevilla[56], L. Goossens[37], B. Gorini[37], E. Gorini[70a,70b], A. Gorišek[95], T. C. Gosart[131], A. T. Goshaw[51], M. I. Gostkin[39], S. Goswami[124], C. A. Gottardo[37], S. A. Gotz[111], M. Gouighri[36b], A. G. Goussiou[142], N. Govender[34c], R. P. Grabarczyk[129], I. Grabowska-Bold[87a], K. Graham[35], E. Gramstad[128], S. Grancagnolo[70a,70b], C. M. Grant[1], P. M. Gravila[28f], F. G. Gravili[70a,70b], H. M. Gray[18a], M. Greco[112], M. J. Green[1], C. Grefe[25], A. S. Grefsrud[17], I. M. Gregor[48], K. T. Greif[165], P. Grenier[149], S. G. Grewe[112], A. A. Grillo[139], K. Grimm[32], S. Grinstein[13,y], J. -F. Grivaz[66], E. Gross[175], J. Grosse-Knetter[55], L. Guan[108], G. Guerrieri[37], R. Guevara[128], R. Gugel[102], J. A. M. Guhit[108], A. Guida[19], E. Guilloton[173], S. Guindon[37], F. Guo[14,114c], J. Guo[144a], L. Guo[48], L. Guo[114b,w], Y. Guo[108], A. Gupta[49], R. Gupta[132],

S. Gupta[27], S. Gurbuz[25], S. S. Gurdasani[48], G. Gustavino[75a,75b], P. Gutierrez[123], L. F. Gutierrez Zagazeta[131], M. Gutsche[50], C. Gutschow[98], C. Gwenlan[129], C. B. Gwilliam[94], E. S. Haaland[128], A. Haas[120], M. Habedank[59], C. Haber[18a], H. K. Hadavand[8], A. Haddad[41], A. Hadef[50], A. I. Hagan[93], J. J. Hahn[147], E. H. Haines[98], M. Haleem[172], J. Haley[124], G. D. Hallewell[104], L. Halser[20], K. Hamano[171], M. Hamer[25], S. E. D. Hammoud[66], E. J. Hampshire[97], J. Han[143a], L. Han[114a], L. Han[62], S. Han[18a], K. Hanagaki[84], M. Hance[139], D. A. Hangal[42], H. Hanif[148], M. D. Hank[131], J. B. Hansen[43], P. H. Hansen[43], D. Harada[56], T. Harenberg[177], S. Harkusha[179], M. L. Harris[105], Y. T. Harris[25], J. Harrison[13], N. M. Harrison[122], P. F. Harrison[173], M. L. E. Hart[98], N. M. Hartman[112], N. M. Hartmann[111], R. Z. Hasan[97,137], Y. Hasegawa[146], F. Haslbeck[129], S. Hassan[17], R. Hauser[109], M. Haviernik[136], C. M. Hawkes[21], R. J. Hawkings[37], Y. Hayashi[159], D. Hayden[109], C. Hayes[108], R. L. Hayes[117], C. P. Hays[129], J. M. Hays[96], H. S. Hayward[94], M. He[14,114c], Y. He[48], Y. He[98], N. B. Heatley[96], V. Hedberg[100], C. Heidegger[54], K. K. Heidegger[54], J. Heilman[35], S. Heim[48], T. Heim[18a], J. G. Heinlein[131], J. J. Heinrich[126], L. Heinrich[112], J. Hejbal[134], M. Helbig[50], A. Held[176], S. Hellesund[17], C. M. Helling[170], S. Hellman[47a,47b], L. Henkelmann[33], A. M. Henriques Correia[37], H. Herde[100], Y. Hernández Jiménez[151], L. M. Herrmann[25], T. Herrmann[50], G. Herten[54], R. Hertenberger[111], L. Hervas[37], M. E. Hesping[102], N. P. Hessey[162a], J. Hessler[112], M. Hidaoui[36b], N. Hidic[136], E. Hill[161], T. S. Hillersoy[17], S. J. Hillier[21], J. R. Hinds[109], F. Hinterkeuser[25], M. Hirose[127], S. Hirose[163], D. Hirschbuehl[177], T. G. Hitchings[103], B. Hiti[95], J. Hobbs[151], R. Hobincu[28e], N. Hod[175], A. M. Hodges[168], M. C. Hodgkinson[145], B. H. Hodkinson[129], A. Hoecker[37], D. D. Hofer[108], J. Hofer[169], M. Holzbock[37], L. B. A. H. Hommels[33], V. Homsak[129], B. P. Honan[103], J. J. Hong[68], T. M. Hong[132], B. H. Hooberman[168], W. H. Hopkins[6], M. C. Hoppesch[168], Y. Horii[113], M. E. Horstmann[112], S. Hou[154], M. R. Housenga[168], A. S. Howard[95], J. Howarth[59], J. Hoya[6], M. Hrabovsky[125], T. Hryn'ova[4], P. J. Hsu[65], S. -C. Hsu[142], T. Hsu[66], M. Hu[18a], Q. Hu[62], S. Huang[33], X. Huang[14,114c], Y. Huang[136], Y. Huang[114b], Y. Huang[102], Y. Huang[14], Z. Huang[66], Z. Hubacek[135], M. Huebner[25], F. Huegging[25], T. B. Huffman[129], M. Hufnagel Maranha De Faria[83a], C. A. Hugli[48], M. Huhtinen[37], S. K. Huiberts[17], R. Hulsken[106], C. E. Hultquist[18a], N. Huseynov[12,g], J. Huston[109], J. Huth[61], R. Hyneman[7], G. Iacobucci[56], G. Iakovidis[30], L. Iconomidou-Fayard[66], J. P. Iddon[37], P. Iengo[72a,72b], R. Iguchi[159], Y. Iiyama[159], T. Iizawa[159], Y. Ikegami[84], D. Iliadis[158], N. Ilic[161], H. Imam[36a], G. Inacio Goncalves[83d], S. A. Infante Cabanas[140c], T. Ingebretsen Carlson[47a,47b], J. M. Inglis[96], G. Introzzi[73a,73b], M. Iodice[77a], V. Ippolito[75a,75b], R. K. Irwin[94], M. Ishino[159], W. Islam[176], C. Issever[19], S. Istin[22a,an], K. Itabashi[84], H. Ito[174], R. Iuppa[78a,78b], A. Ivina[175], V. Izzo[72a], P. Jacka[134], P. Jackson[1], P. Jain[48], K. Jakobs[54], T. Jakoubek[175], J. Jamieson[59], W. Jang[159], S. Jankovych[136], M. Javurkova[105], P. Jawahar[103], L. Jeanty[126], J. Jejelava[155a,af], P. Jenni[54,f], C. E. Jessiman[35], C. Jia[143a], H. Jia[170], J. Jia[151], X. Jia[14,114c], Z. Jia[114a], C. Jiang[52], Q. Jiang[64b], S. Jiggins[48], M. Jimenez Ortega[169], J. Jimenez Pena[13], S. Jin[114a], A. Jinaru[28b], O. Jinnouchi[141], P. Johansson[145], K. A. Johns[7], J. W. Johnson[139], F. A. Jolly[48], D. M. Jones[152], E. Jones[48], K. S. Jones[8], P. Jones[33], R. W. L. Jones[93], T. J. Jones[94], H. L. Joos[55,37], R. Joshi[122], J. Jovicevic[16], X. Ju[18a], J. J. Junggeburth[37], T. Junkermann[63a], A. Juste Rozas[13,y], M. K. Juzek[88], S. Kabana[140e], A. Kaczmarska[88], M. Kado[112], H. Kagan[122], M. Kagan[149], A. Kahn[131], C. Kahra[102], T. Kaji[159], E. Kajomovitz[156], N. Kakati[175], N. Kakoty[13], I. Kalaitzidou[54], S. Kandel[8], N. J. Kang[139], D. Kar[34g], K. Karava[129], E. Karentzos[25], O. Karkout[117], S. N. Karpov[39], Z. M. Karpova[39], V. Kartvelishvili[93], A. N. Karyukhin[38], E. Kasimi[158], J. Katzy[48], S. Kaur[35], K. Kawade[146], M. P. Kawale[123], C. Kawamoto[89], T. Kawamoto[62], E. F. Kay[37], F. I. Kaya[164], S. Kazakos[109], V. F. Kazanin[38], J. M. Keaveney[34a], R. Keeler[171], G. V. Kehris[61], J. S. Keller[35], J. J. Kempster[152], O. Kepka[134], J. Kerr[162b], B. P. Kerridge[137], B. P. Kerševan[95], L. Keszeghova[29a], R. A. Khan[132], A. Khanov[124], A. G. Kharlamov[38], T. Kharlamova[38], E. E. Khoda[142], M. Kholodenko[133a], T. J. Khoo[19], G. Khoriauli[172], Y. Khoulaki[36a], J. Khubua[155b,*], Y. A. R. Khwaira[130], B. Kibirige[34g], D. Kim[6], D. W. Kim[47a,47b], Y. K. Kim[40], N. Kimura[98], M. K. Kingston[55], A. Kirchhoff[55], C. Kirfel[25], F. Kirfel[25], J. Kirk[137], A. E. Kiryunin[112], S. Kita[163], O. Kivernyk[25], M. Klassen[164], C. Klein[35], L. Klein[172], M. H. Klein[45], S. B. Klein[56], U. Klein[94], A. Klimentov[30], T. Klioutchnikova[37], P. Kluit[117], S. Kluth[112], E. Kneringer[79], T. M. Knight[161], A. Knue[49], M. Kobel[50], D. Kobylianskii[175], S. F. Koch[129], M. Kocian[149], P. Kodyš[136], D. M. Koeck[126], T. Koffas[35], O. Kolay[50], I. Koletsou[4], T. Komarek[88], K. Köneke[55], A. X. Y. Kong[1], T. Kono[121], N. Konstantinidis[98], P. Kontaxakis[56], B. Konya[100], R. Kopeliansky[42], S. Koperny[87a], K. Korcyl[88], K. Kordas[158,d], A. Korn[98], S. Korn[55], I. Korolkov[13], N. Korotkova[38], B. Kortman[117], O. Kortner[112], S. Kortner[112], W. H. Kostecka[118], M. Kostov[29a], V. V. Kostyukhin[147], A. Kotsokechagia[37], A. Kotwal[51], A. Koulouris[37], A. Kourkoumeli-Charalampidi[73a,73b],

C. Kourkoumelis[9], E. Kourlitis[112], O. Kovanda[126], R. Kowalewski[171], W. Kozanecki[126], A. S. Kozhin[38], V. A. Kramarenko[38], G. Kramberger[95], P. Kramer[25], M. W. Krasny[130], A. Krasznahorkay[105], A. C. Kraus[118], J. W. Kraus[177], J. A. Kremer[48], N. B. Krengel[147], T. Kresse[50], L. Kretschmann[177], J. Kretzschmar[94], K. Kreul[19], P. Krieger[161], K. Krizka[21], K. Kroeninger[49], H. Kroha[112], J. Kroll[134], J. Kroll[131], K. S. Krowpman[109], U. Kruchonak[39], H. Krüger[25], N. Krumnack[81], M. C. Kruse[51], O. Kuchinskaia[39], S. Kuday[3a], S. Kuehn[37], R. Kuesters[54], T. Kuhl[48], V. Kukhtin[39], Y. Kulchitsky[39], S. Kuleshov[140d,140b], J. Kull[1], M. Kumar[34g], N. Kumari[48], P. Kumari[162b], A. Kupco[134], T. Kupfer[49], A. Kupich[38], O. Kuprash[54], H. Kurashige[86], L. L. Kurchaninov[162a], O. Kurdysh[4], Y. A. Kurochkin[38], A. Kurova[38], M. Kuze[141], A. K. Kvam[105], J. Kvita[125], N. G. Kyriacou[108], C. Lacasta[169], F. Lacava[75a,75b], H. Lacker[19], D. Lacour[130], N. N. Lad[98], E. Ladygin[39], A. Lafarge[41], B. Laforge[130], T. Lagouri[178], F. Z. Lahbabi[36a], S. Lai[55], J. E. Lambert[171], S. Lammers[68], W. Lampl[7], C. Lampoudis[158,d], G. Lamprinoudis[102], A. N. Lancaster[118], E. Lançon[30], U. Landgraf[54], M. P. J. Landon[96], V. S. Lang[54], O. K. B. Langrekken[128], A. J. Lankford[165], F. Lanni[37], K. Lantzsch[25], A. Lanza[73a], M. Lanzac Berrocal[169], J. F. Laporte[138], T. Lari[71a], D. Larsen[17], L. Larson[11], F. Lasagni Manghi[24b], M. Lassnig[37], S. D. Lawlor[145], R. Lazaridou[173], M. Lazzaroni[71a,71b], H. D. M. Le[109], E. M. Le Boulicaut[178], L. T. Le Pottier[18a], B. Leban[24b,24a], F. Ledroit-Guillon[60], T. F. Lee[162b], L. L. Leeuw[34c], M. Lefebvre[171], C. Leggett[18a], G. Lehmann Miotto[37], M. Leigh[56], W. A. Leight[105], W. Leinonen[116], A. Leisos[158,v], M. A. L. Leite[83c], C. E. Leitgeb[19], R. Leitner[136], K. J. C. Leney[45], T. Lenz[25], S. Leone[74a], C. Leonidopoulos[52], A. Leopold[150], J. H. Lepage Bourbonnais[35], R. Les[109], C. G. Lester[33], M. Levchenko[38], J. Levêque[4], L. J. Levinson[175], G. Levrini[24b,24a], M. P. Lewicki[88], C. Lewis[142], D. J. Lewis[4], L. Lewitt[145], A. Li[30], B. Li[143a], C. Li[108], C- Q. Li[112], H. Li[143a], H. Li[103], H. Li[15], H. Li[62], H. Li[143a], J. Li[144a], K. Li[14], L. Li[144a], R. Li[178], S. Li[14,114c], S. Li[144b,144a], T. Li[5], X. Li[106], Z. Li[159], Z. Li[14,114c], Z. Li[62], S. Liang[14,114c], Z. Liang[14], M. Liberatore[138], B. Liberti[76a], K. Lie[64c], J. Lieber Marin[83e], H. Lien[68], H. Lin[108], S. F. Lin[151], L. Linden[111], R. E. Lindley[7], J. H. Lindon[37], J. Ling[61], E. Lipeles[131], A. Lipniacka[17], A. Lister[170], J. D. Little[68], B. Liu[14], B. X. Liu[114b], D. Liu[144b,144a], D. Liu[139], E. H. L. Liu[21], J. K. K. Liu[120], K. Liu[144b], K. Liu[144b,144a], M. Liu[62], M. Y. Liu[62], P. Liu[14], Q. Liu[144b,142,144a], X. Liu[62], X. Liu[143a], Y. Liu[114b,114c], Y. L. Liu[143a], Y. W. Liu[62], Z. Liu[66,l], S. L. Lloyd[96], E. M. Lobodzinska[48], P. Loch[7], E. Lodhi[161], T. Lohse[19], K. Lohwasser[145], E. Loiacono[48], J. D. Lomas[21], J. D. Long[42], I. Longarini[165], R. Longo[168], A. Lopez Solis[13], N. A. Lopez-canelas[7], N. Lorenzo Martinez[4], A. M. Lory[111], M. Losada[119a], G. Löschcke Centeno[152], X. Lou[47a,47b], X. Lou[14,114c], A. Lounis[66], P. A. Love[93], M. Lu[66], S. Lu[131], Y. J. Lu[154], H. J. Lubatti[142], C. Luci[75a,75b], F. L. Lucio Alves[114a], F. Luehring[68], B. S. Lunday[131], O. Lundberg[150], J. Lunde[37], N. A. Luongo[6], M. S. Lutz[37], A. B. Lux[26], D. Lynn[30], R. Lysak[134], V. Lysenko[135], E. Lytken[100], V. Lyubushkin[39], T. Lyubushkina[39], M. M. Lyukova[151], H. Ma[30], K. Ma[62], L. L. Ma[143a], W. Ma[62], Y. Ma[124], J. C. MacDonald[102], P. C. Machado De Abreu Farias[83e], R. Madar[41], T. Madula[98], J. Maeda[86], T. Maeno[30], P. T. Mafa[34c,k], H. Maguire[145], V. Maiboroda[66], A. Maio[133a,133b,133d], K. Maj[87a], O. Majersky[48], S. Majewski[126], R. Makhmanazarov[38], N. Makovec[66], V. Maksimovic[16], B. Malaescu[130], J. Malamant[128], Pa. Malecki[88], V. P. Maleev[38], F. Malek[60,p], M. Mali[95], D. Malito[97], U. Mallik[80,*], A. Maloizel[5], S. Maltezos[10], A. Malvezzi Lopes[83d], S. Malyukov[39], J. Mamuzic[13], G. Mancini[53], M. N. Mancini[27], G. Manco[73a,73b], J. P. Mandalia[96], S. S. Mandarry[152], I. Mandić[95], L. Manhaes de Andrade Filho[83a], I. M. Maniatis[175], J. Manjarres Ramos[91], D. C. Mankad[175], A. Mann[111], T. Manoussos[37], M. N. Mantinan[40], S. Manzoni[37], L. Mao[144a], X. Mapekula[34c], A. Marantis[158], R. R. Marcelo Gregorio[96], G. Marchiori[5], M. Marcisovsky[134], C. Marcon[71a], E. Maricic[16], M. Marinescu[48], S. Marium[48], M. Marjanovic[123], A. Markhoos[54], M. Markovitch[66], M. K. Maroun[105], G. T. Marsden[103], E. J. Marshall[93], Z. Marshall[18a], S. Marti-Garcia[169], J. Martin[98], T. A. Martin[137], V. J. Martin[52], B. Martin dit Latour[17], L. Martinelli[75a,75b], M. Martinez[13,y], P. Martinez Agullo[169], V. I. Martinez Outschoorn[105], P. Martinez Suarez[13], S. Martin-Haugh[137], G. Martinovicova[136], V. S. Martoiu[28b], A. C. Martyniuk[98], A. Marzin[37], D. Mascione[78a,78b], L. Masetti[102], J. Masik[103], A. L. Maslennikov[39], S. L. Mason[42], P. Massarotti[72a,72b], P. Mastrandrea[74a,74b], A. Mastroberardino[44b,44a], T. Masubuchi[127], T. T. Mathew[126], J. Matousek[136], D. M. Mattern[49], J. Maurer[28b], T. Maurin[59], A. J. Maury[66], B. Maček[95], C. Mavungu Tsava[104], D. A. Maximov[38], A. E. May[103], E. Mayer[41], R. Mazini[34g], I. Maznas[118], S. M. Mazza[139], E. Mazzeo[37], J. P. Mc Gowan[171], S. P. Mc Kee[108], C. A. Mc Lean[6], C. C. McCracken[170], E. F. McDonald[107], A. E. McDougall[117], L. F. Mcelhinney[93], J. A. Mcfayden[152], R. P. McGovern[131], R. P. Mckenzie[34g], T. C. Mclachlan[48], D. J. Mclaughlin[98], S. J. McMahon[137], C. M. Mcpartland[94],

R. A. McPherson[171,ac], S. Mehlhase[111], A. Mehta[94], D. Melini[169], B. R. Mellado Garcia[34g], A. H. Melo[55], F. Meloni[48], A. M. Mendes Jacques Da Costa[103], L. Meng[93], S. Menke[112], M. Mentink[37], E. Meoni[44b,44a], G. Mercado[118], S. Merianos[158], C. Merlassino[69a,69c], C. Meroni[71a,71b], J. Metcalfe[6], A. S. Mete[6], E. Meuser[102], C. Meyer[68], J- P. Meyer[138], Y. Miao[114a], R. P. Middleton[137], M. Mihovilovic[66], L. Mijović[52], G. Mikenberg[175], M. Mikestikova[134], M. Mikuž[95], H. Mildner[102], A. Milic[37], D. W. Miller[40], E. H. Miller[149], L. S. Miller[35], A. Milov[175], D. A. Milstead[47a,47b], T. Min[114a], A. A. Minaenko[38], I. A. Minashvili[155b], A. I. Mincer[120], B. Mindur[87a], M. Mineev[39], Y. Mino[89], L. M. Mir[13], M. Miralles Lopez[59], M. Mironova[18a], M. Missio[116], A. Mitra[173], V. A. Mitsou[169], Y. Mitsumori[113], O. Miu[161], P. S. Miyagawa[96], T. Mkrtchyan[63a], M. Mlinarevic[98], T. Mlinarevic[98], M. Mlynarikova[37], S. Mobius[20], M. H. Mohamed Farook[115], S. Mohapatra[42], M.F. Mohd Soberi[52], S. Mohiuddin[124], G. Mokgatitswane[34g], L. Moleri[175], U. Molinatti[129], L. G. Mollier[20], B. Mondal[134], S. Mondal[135], K. Mönig[48], E. Monnier[104], L. Monsonis Romero[169], J. Montejo Berlingen[13], A. Montella[47a,47b], M. Montella[122], F. Montereali[77a,77b], F. Monticelli[92], S. Monzani[69a,69c], A. Morancho Tarda[43], N. Morange[66], A. L. Moreira De Carvalho[48], M. Moreno Llácer[169], C. Moreno Martinez[56], J. M. Moreno Perez[23b], P. Morettini[57b], S. Morgenstern[37], M. Morii[61], M. Morinaga[159], M. Moritsu[90], F. Morodei[75a,75b], P. Moschovakos[37], B. Moser[54], M. Mosidze[155b], T. Moskalets[45], P. Moskvitina[116], J. Moss[32], P. Moszkowicz[87a], A. Moussa[36d], Y. Moyal[175], H. Moyano Gomez[13], E. J. W. Moyse[105], O. Mtintsilana[34g], S. Muanza[104], M. Mucha[25], J. Mueller[132], R. Müller[37], G. A. Mullier[167], A. J. Mullin[33], J. J. Mullin[51], A. C. Mullins[45], A. E. Mulski[61], D. P. Mungo[161], D. Munoz Perez[169], F. J. Munoz Sanchez[103], W. J. Murray[173,137], M. Muškinja[95], C. Mwewa[48], A. G. Myagkov[38,a], A. J. Myers[8], G. Myers[108], M. Myska[135], B. P. Nachman[18a], K. Nagai[129], K. Nagano[84], R. Nagasaka[159], J. L. Nagle[30,ak], E. Nagy[104], A. M. Nairz[37], Y. Nakahama[84], K. Nakamura[84], K. Nakkalil[5], A. Nandi[63b], H. Nanjo[127], E. A. Narayanan[45], Y. Narukawa[159], I. Naryshkin[38], L. Nasella[71a,71b], S. Nasri[119b], C. Nass[25], G. Navarro[23a], J. Navarro-Gonzalez[169], A. Nayaz[19], P. Y. Nechaeva[38], S. Nechaeva[24b,24a], F. Nechansky[134], L. Nedic[129], T. J. Neep[21], A. Negri[73a,73b], M. Negrini[24b], C. Nellist[117], C. Nelson[106], K. Nelson[108], S. Nemecek[134], M. Nessi[37,h], M. S. Neubauer[168], J. Newell[94], P. R. Newman[21], Y. W. Y. Ng[168], B. Ngair[119a], H. D. N. Nguyen[110], J. D. Nichols[123], R. B. Nickerson[129], R. Nicolaidou[138], J. Nielsen[139], M. Niemeyer[55], J. Niermann[37], N. Nikiforou[37], V. Nikolaenko[38,a], I. Nikolic-Audit[130], P. Nilsson[30], I. Ninca[48], G. Ninio[157], A. Nisati[75a], N. Nishu[2], R. Nisius[112], N. Nitika[69a,69c], J- E. Nitschke[50], E. K. Nkadimeng[34b], T. Nobe[159], T. Nommensen[153], M. B. Norfolk[145], B. J. Norman[35], M. Noury[36a], J. Novak[95], T. Novak[95], R. Novotny[135], L. Nozka[125], K. Ntekas[165], N. M. J. Nunes De Moura Junior[83b], J. Ocariz[130], A. Ochi[86], I. Ochoa[133a], S. Oerdek[48,z], J. T. Offermann[40], A. Ogrodnik[136], A. Oh[103], C. C. Ohm[150], H. Oide[84], M. L. Ojeda[37], Y. Okumura[159], L. F. Oleiro Seabra[133a], I. Oleksiyuk[56], G. Oliveira Correa[13], D. Oliveira Damazio[30], J. L. Oliver[165], Ö. O. Öncel[54], A. P. O'Neill[20], A. Onofre[133a,133e,e], P. U. E. Onyisi[11], M. J. Oreglia[40], D. Orestano[77a,77b], R. Orlandini[77a,77b], R. S. Orr[161], L. M. Osojnak[131], Y. Osumi[113], G. Otero y Garzon[31], H. Otono[90], G. J. Ottino[18a], M. Ouchrif[36d], F. Ould-Saada[128], T. Ovsiannikova[142], M. Owen[59], R. E. Owen[137], V. E. Ozcan[22a], F. Ozturk[88], N. Ozturk[8], S. Ozturk[82], H. A. Pacey[129], K. Pachal[162a], A. Pacheco Pages[13], C. Padilla Aranda[13], G. Padovano[75a,75b], S. Pagan Griso[18a], G. Palacino[68], A. Palazzo[70a,70b], J. Pampel[25], J. Pan[178], T. Pan[64a], D. K. Panchal[11], C. E. Pandini[60], J. G. Panduro Vazquez[137], H. D. Pandya[1], H. Pang[138], P. Pani[48], G. Panizzo[69a,69c], L. Panwar[130], L. Paolozzi[56], S. Parajuli[168], A. Paramonov[6], C. Paraskevopoulos[53], D. Paredes Hernandez[64b], A. Pareti[73a,73b], K. R. Park[42], T. H. Park[112], F. Parodi[57b,57a], J. A. Parsons[42], U. Parzefall[54], B. Pascual Dias[41], L. Pascual Dominguez[101], E. Pasqualucci[75a], S. Passaggio[57b], F. Pastore[97], P. Patel[88], U. M. Patel[51], J. R. Pater[103], T. Pauly[37], F. Pauwels[136], C. I. Pazos[164], M. Pedersen[128], R. Pedro[133a], S. V. Peleganchuk[38], O. Penc[37], E. A. Pender[52], S. Peng[15], G. D. Penn[178], K. E. Penski[111], M. Penzin[38], B. S. Peralva[83d], A. P. Pereira Peixoto[142], L. Pereira Sanchez[149], D. V. Perepelitsa[30,ak], G. Perera[105], E. Perez Codina[37], M. Perganti[10], H. Pernegger[37], S. Perrella[75a,75b], O. Perrin[41], K. Peters[48], R. F. Y. Peters[103], B. A. Petersen[37], T. C. Petersen[43], E. Petit[104], V. Petousis[135], A. R. Petri[71a,71b], C. Petridou[158,d], T. Petru[136], A. Petrukhin[147], M. Pettee[18a], A. Petukhov[82], K. Petukhova[37], R. Pezoa[140f], L. Pezzotti[24b,24a], G. Pezzullo[178], L. Pfaffenbichler[37], A. J. Pfleger[37], T. M. Pham[176], T. Pham[107], P. W. Phillips[137], G. Piacquadio[151], E. Pianori[18a], F. Piazza[126], R. Piegaia[31], D. Pietreanu[28b], A. D. Pilkington[103], M. Pinamonti[69a,69c], J. L. Pinfold[2], B.C. Pinheiro Pereira[133a], J. Pinol Bel[13], A. E. Pinto Pinoargote[130], L. Pintucci[69a,69c], K. M. Piper[152], A. Pirttikoski[56], D. A. Pizzi[35],

L. Pizzimento[64b], A. Plebani[33], M. -A. Pleier[30], V. Pleskot[136], E. Plotnikova[39], G. Poddar[96], R. Poettgen[100], L. Poggioli[130], S. Polacek[136], G. Polesello[73a], A. Poley[148], A. Polini[24b], C. S. Pollard[173], Z. B. Pollock[122], E. Pompa Pacchi[123], N. I. Pond[98], D. Ponomarenko[68], L. Pontecorvo[37], S. Popa[28a], G. A. Popeneciu[28d], A. Poreba[37], D. M. Portillo Quintero[162a], S. Pospisil[135], M. A. Postill[145], P. Postolache[28c], K. Potamianos[173], P. A. Potepa[87a], I. N. Potrap[39], C. J. Potter[33], H. Potti[153], J. Poveda[169], M. E. Pozo Astigarraga[37], R. Pozzi[37], A. Prades Ibanez[76a,76b], J. Pretel[171], D. Price[103], M. Primavera[70a], L. Primomo[69a,69c], M. A. Principe Martin[101], R. Privara[125], T. Procter[87b], M. L. Proffitt[142], N. Proklova[131], K. Prokofiev[64c], G. Proto[112], J. Proudfoot[6], M. Przybycien[87a], W. W. Przygoda[87b], A. Psallidas[46], J. E. Puddefoot[145], D. Pudzha[53], D. Pyatiizbyantseva[116], J. Qian[108], R. Qian[109], D. Qichen[103], Y. Qin[13], T. Qiu[52], A. Quadt[55], M. Queitsch-Maitland[103], G. Quetant[56], R. P. Quinn[170], G. Rabanal Bolanos[61], D. Rafanoharana[112], F. Raffaeli[76a,76b], F. Ragusa[71a,71b], J. L. Rainbolt[40], J. A. Raine[56], S. Rajagopalan[30], E. Ramakoti[39], L. Rambelli[57b,57a], I. A. Ramirez-Berend[35], K. Ran[48,114c], D. S. Rankin[131], N. P. Rapheeha[34g], H. Rasheed[28b], D. F. Rassloff[63a], A. Rastogi[18a], S. Rave[102], S. Ravera[57b,57a], B. Ravina[37], I. Ravinovich[175], M. Raymond[37], A. L. Read[128], N. P. Readioff[145], D. M. Rebuzzi[73a,73b], A. S. Reed[112], K. Reeves[27], J. A. Reidelsturz[177], D. Reikher[126], A. Rej[49], C. Rembser[37], H. Ren[62], M. Renda[28b], F. Renner[48], A. G. Rennie[59], A. L. Rescia[48], S. Resconi[71a], M. Ressegotti[57b,57a], S. Rettie[37], W. F. Rettie[35], E. Reynolds[18a], O. L. Rezanova[39], P. Reznicek[136], H. Riani[36d], N. Ribaric[51], E. Ricci[78a,78b], R. Richter[112], S. Richter[47a,47b], E. Richter-Was[87b], M. Ridel[130], S. Ridouani[36d], P. Rieck[120], P. Riedler[37], E. M. Riefel[47a,47b], J. O. Rieger[117], M. Rijssenbeek[151], M. Rimoldi[37], L. Rinaldi[24b,24a], P. Rincke[167,55], G. Ripellino[167], I. Riu[13], J. C. Rivera Vergara[171], F. Rizatdinova[124], E. Rizvi[96], B. R. Roberts[18a], S. S. Roberts[139], D. Robinson[33], M. Robles Manzano[102], A. Robson[59], A. Rocchi[76a,76b], C. Roda[74a,74b], S. Rodriguez Bosca[37], Y. Rodriguez Garcia[23a], A. M. Rodríguez Vera[118], S. Roe[37], J. T. Roemer[37], O. Røhne[128], R. A. Rojas[37], C. P. A. Roland[130], A. Romaniouk[79], E. Romano[73a,73b], M. Romano[24b], A. C. Romero Hernandez[168], N. Rompotis[94], L. Roos[130], S. Rosati[75a], B. J. Rosser[40], E. Rossi[129], E. Rossi[72a,72b], L. P. Rossi[61], L. Rossini[54], R. Rosten[122], M. Rotaru[28b], B. Rottler[54], D. Rousseau[66], D. Rousso[48], S. Roy-Garand[161], A. Rozanov[104], Z. M. A. Rozario[59], Y. Rozen[156], A. Rubio Jimenez[169], V. H. Ruelas Rivera[19], T. A. Ruggeri[1], A. Ruggiero[129], A. Ruiz-Martinez[169], A. Rummler[37], Z. Rurikova[54], N. A. Rusakovich[39], H. L. Russell[171], G. Russo[75a,75b], J. P. Rutherfoord[7], S. Rutherford Colmenares[33], M. Rybar[136], P. Rybczynski[87a], A. Ryzhov[45], J. A. Sabater Iglesias[56], H. F-W. Sadrozinski[139], F. Safai Tehrani[75a], S. Saha[1], M. Sahinsoy[82], B. Sahoo[175], A. Saibel[169], B. T. Saifuddin[123], M. Saimpert[138], G. T. Saito[83c], M. Saito[159], T. Saito[159], A. Sala[71a,71b], A. Salnikov[149], J. Salt[169], A. Salvador Salas[157], F. Salvatore[152], A. Salzburger[37], D. Sammel[54], E. Sampson[93], D. Sampsonidis[158,d], D. Sampsonidou[126], J. Sánchez[169], V. Sanchez Sebastian[169], H. Sandaker[128], C. O. Sander[48], J. A. Sandesara[176], M. Sandhoff[177], C. Sandoval[23b], L. Sanfilippo[63a], D. P. C. Sankey[137], T. Sano[89], A. Sansoni[53], L. Santi[37], C. Santoni[41], H. Santos[133a,133b], A. Santra[175], E. Sanzani[24b,24a], K. A. Saoucha[85b], J. G. Saraiva[133a,133d], J. Sardain[7], O. Sasaki[84], K. Sato[163], C. Sauer[37], E. Sauvan[4], P. Savard[161,ai], R. Sawada[159], C. Sawyer[137], L. Sawyer[99], C. Sbarra[24b], A. Sbrizzi[24b,24a], T. Scanlon[98], J. Schaarschmidt[142], U. Schäfer[102], A. C. Schaffer[66,45], D. Schaile[111], R. D. Schamberger[151], C. Scharf[19], M. M. Schefer[20], V. A. Schegelsky[38], D. Scheirich[136], M. Schernau[140e], C. Scheulen[56], C. Schiavi[57b,57a], M. Schioppa[44b,44a], B. Schlag[149], S. Schlenker[37], J. Schmeing[177], E. Schmidt[112], M. A. Schmidt[177], K. Schmieden[102], C. Schmitt[102], N. Schmitt[102], S. Schmitt[48], L. Schoeffel[138], A. Schoening[63b], P. G. Scholer[35], E. Schopf[147], M. Schott[25], S. Schramm[56], T. Schroer[56], H-C. Schultz-Coulon[63a], M. Schumacher[54], B. A. Schumm[139], Ph. Schune[138], H. R. Schwartz[139], A. Schwartzman[149], T. A. Schwarz[108], Ph. Schwemling[138], R. Schwienhorst[109], F. G. Sciacca[20], A. Sciandra[30], G. Sciolla[27], F. Scuri[74a], C. D. Sebastiani[37], K. Sedlaczek[118], S.C. Seidel[115], A. Seiden[139], B. D. Seidlitz[42], C. Seitz[48], J. M. Seixas[83b], G. Sekhniaidze[72a], L. Selem[60], N. Semprini-Cesari[24b,24a], A. Semushin[179], D. Sengupta[56], V. Senthilkumar[169], L. Serin[66], M. Sessa[76a,76b], H. Severini[123], F. Sforza[57b,57a], A. Sfyrla[56], Q. Sha[14], E. Shabalina[55], H. Shaddix[118], A. H. Shah[33], R. Shaheen[150], J. D. Shahinian[131], M. Shamim[37], L. Y. Shan[14], M. Shapiro[18a], A. Sharma[37], A. S. Sharma[170], P. Sharma[30], P. B. Shatalov[38], K. Shaw[152], S. M. Shaw[103], Q. Shen[14], D. J. Sheppard[148], P. Sherwood[98], L. Shi[98], X. Shi[14], S. Shimizu[84], C. O. Shimmin[178], I. P. J. Shipsey[129,*], S. Shirabe[90], M. Shiyakova[39,aa], M. J. Shochet[40], D. R. Shope[128], B. Shrestha[123], S. Shrestha[122,am], I. Shreyber[39], M. J. Shroff[171], P. Sicho[134], A. M. Sickles[168], E. Sideras Haddad[34g,166], A. C. Sidley[117], A. Sidoti[24b], F. Siegert[50], Dj. Sijacki[16], F. Sili[92], J. M. Silva[52], I. Silva Ferreira[83b], M. V. Silva Oliveira[30], S. B. Silverstein[47a],

S. Simion[66], R. Simoniello[37], E. L. Simpson[103], H. Simpson[152], L. R. Simpson[6], S. Simsek[82], S. Sindhu[55], P. Sinervo[161], S. N. Singh[27], S. Singh[30], S. Sinha[48], S. Sinha[103], M. Sioli[24b,24a], K. Sioulas[9], I. Siral[37], E. Sitnikova[48], J. Sjölin[47a,47b], A. Skaf[55], E. Skorda[21], P. Skubic[123], M. Slawinska[88], I. Slazyk[17], I. Sliusar[128], V. Smakhtin[175], B. H. Smart[137], S. Yu. Smirnov[140b], Y. Smirnov[82], L. N. Smirnova[38,a], O. Smirnova[100], A. C. Smith[42], D. R. Smith[165], J. L. Smith[103], M. B. Smith[35], R. Smith[149], H. Smitmanns[102], M. Smizanska[93], K. Smolek[135], P. Smolyanskiy[135], A. A. Snesarev[39], H. L. Snoek[117], S. Snyder[30], R. Sobie[171,ac], A. Soffer[157], C. A. Solans Sanchez[37], E. Yu. Soldatov[39], U. Soldevila[169], A. A. Solodkov[34g], S. Solomon[27], A. Soloshenko[39], K. Solovieva[54], O. V. Solovyanov[41], P. Sommer[50], A. Sonay[13], A. Sopczak[135], A. L. Sopio[52], F. Sopkova[29b], J.D. Sorenson[115], I.R. Sotarriva Alvarez[141], V. Sothilingam[63a], O. J. Soto Sandoval[140c,140b], S. Sottocornola[68], R. Soualah[85a], Z. Soumaimi[36e], D. South[48], N. Soybelman[175], S. Spagnolo[70a,70b], M. Spalla[112], D. Sperlich[54], B. Spisso[72a,72b], D. P. Spiteri[59], L. Splendori[104], M. Spousta[136], E. J. Staats[35], R. Stamen[63a], E. Stanecka[88], W. Stanek-Maslouska[48], M. V. Stange[50], B. Stanislaus[18a], M. M. Stanitzki[48], B. Stapf[48], E. A. Starchenko[38], G. H. Stark[139], J. Stark[91], P. Staroba[134], P. Starovoitov[85b], R. Staszewski[88], G. Stavropoulos[46], A. Stefl[37], P. Steinberg[30], B. Stelzer[148,162a], H. J. Stelzer[132], O. Stelzer[162a], H. Stenzel[58], T. J. Stevenson[152], G. A. Stewart[37], J. R. Stewart[124], M. C. Stockton[37], G. Stoicea[28b], M. Stolarski[133a], S. Stonjek[112], A. Straessner[50], J. Strandberg[150], S. Strandberg[47a,47b], M. Stratmann[177], M. Strauss[123], T. Strebler[104], P. Strizenec[29b], R. Ströhmer[172], D. M. Strom[126], R. Stroynowski[45], A. Strubig[47a,47b], S. A. Stucci[30], B. Stugu[17], J. Stupak[123], N. A. Styles[48], D. Su[149], S. Su[62], X. Su[62], D. Suchy[29a], K. Sugizaki[131], V. V. Sulin[38], M. J. Sullivan[94], D. M. S. Sultan[129], L. Sultanaliyeva[38], S. Sultansoy[3b], S. Sun[176], W. Sun[14], O. Sunneborn Gudnadottir[167], N. Sur[100], M. R. Sutton[152], H. Suzuki[163], M. Svatos[134], P. N. Swallow[33], M. Swiatlowski[162a], T. Swirski[172], I. Sykora[29a], M. Sykora[136], T. Sykora[136], D. Ta[102], K. Tackmann[48,z], A. Taffard[165], R. Tafirout[162a], Y. Takubo[84], M. Talby[104], A. A. Talyshev[38], K. C. Tam[64b], N. M. Tamir[157], A. Tanaka[159], J. Tanaka[159], R. Tanaka[66], M. Tanasini[151], Z. Tao[170], S. Tapia Araya[140f], S. Tapprogge[102], A. Tarek Abouelfadl Mohamed[109], S. Tarem[156], K. Tariq[14], G. Tarna[28b], G. F. Tartarelli[71a], M. J. Tartarin[91], P. Tas[136], M. Tasevsky[134], E. Tassi[44b,44a], A. C. Tate[168], G. Tateno[159], Y. Tayalati[36e,ab], G. N. Taylor[107], W. Taylor[162b], A. S. Tegetmeier[91], P. Teixeira-Dias[97], J. J. Teoh[161], K. Terashi[159], J. Terron[101], S. Terzo[13], M. Testa[53], R. J. Teuscher[161,ac], A. Thaler[79], O. Theiner[56], T. Theveneaux-Pelzer[104], D. W. Thomas[97], J. P. Thomas[21], E. A. Thompson[18a], P. D. Thompson[21], E. Thomson[131], R. E. Thornberry[45], C. Tian[62], Y. Tian[56], V. Tikhomirov[82], Yu. A. Tikhonov[39], S. Timoshenko[38], D. Timoshyn[136], E. X. L. Ting[1], P. Tipton[178], A. Tishelman-Charny[30], K. Todome[141], S. Todorova-Nova[136], S. Todt[50], L. Toffolin[69a,69c], M. Togawa[84], J. Tojo[90], S. Tokár[29a], O. Toldaiev[68], G. Tolkachev[104], M. Tomoto[84,113], L. Tompkins[149,o], E. Torrence[126], H. Torres[91], E. Torró Pastor[169], M. Toscani[31], C. Tosciri[40], M. Tost[11], D. R. Tovey[145], T. Trefzger[172], P. M. Tricarico[13], A. Tricoli[30], I. M. Trigger[162a], S. Trincaz-Duvoid[130], D. A. Trischuk[27], A. Tropina[39], L. Truong[34c], M. Trzebinski[88], A. Trzupek[88], F. Tsai[151], M. Tsai[108], A. Tsiamis[158], P. V. Tsiareshka[39], S. Tsigaridas[162a], A. Tsirigotis[158,v], V. Tsiskaridze[161], E. G. Tskhadadze[155a], M. Tsopoulou[158], Y. Tsujikawa[89], I. I. Tsukerman[38], V. Tsulaia[18a], S. Tsuno[84], K. Tsuri[121], D. Tsybychev[151], Y. Tu[64b], A. Tudorache[28b], V. Tudorache[28b], S. Turchikhin[57b,57a], I. Turk Cakir[3a], R. Turra[71a], T. Turtuvshin[39,ad], P. M. Tuts[42], S. Tzamarias[158,d], E. Tzovara[102], Y. Uematsu[84], F. Ukegawa[163], P. A. Ulloa Poblete[140c,140b], E. N. Umaka[30], G. Unal[37], A. Undrus[30], G. Unel[165], J. Urban[29b], P. Urrejola[140a], G. Usai[8], R. Ushioda[160], M. Usman[110], F. Ustuner[52], Z. Uysal[82], V. Vacek[135], B. Vachon[106], T. Vafeiadis[37], A. Vaitkus[98], C. Valderanis[111], E. Valdes Santurio[47a,47b], M. Valente[37], S. Valentinetti[24b,24a], A. Valero[169], E. Valiente Moreno[169], A. Vallier[91], J. A. Valls Ferrer[169], D. R. Van Arneman[117], T. R. Van Daalen[142], A. Van Der Graaf[49], H. Z. Van Der Schyf[34g], P. Van Gemmeren[6], M. Van Rijnbach[37], S. Van Stroud[98], I. Van Vulpen[117], P. Vana[136], M. Vanadia[76a,76b], U. M. Vande Voorde[150], W. Vandelli[37], E. R. Vandewall[124], D. Vannicola[157], L. Vannoli[53], R. Vari[75a], M. Varma[178], E. W. Varnes[7], C. Varni[18b], D. Varouchas[66], L. Varriale[169], K. E. Varvell[153], M. E. Vasile[28b], L. Vaslin[84], M. D. Vassilev[149], A. Vasyukov[39], L. M. Vaughan[124], R. Vavricka[136], T. Vazquez Schroeder[13], J. Veatch[32], V. Vecchio[103], M. J. Veen[105], I. Veliscek[30], I. Velkovska[95], L. M. Veloce[161], F. Veloso[133a,133c], S. Veneziano[75a], A. Ventura[70a,70b], S. Ventura Gonzalez[138], A. Verbytskyi[112], M. Verducci[74a,74b], C. Vergis[96], M. Verissimo De Araujo[83b], W. Verkerke[117], J. C. Vermeulen[117], C. Vernieri[149], M. Vessella[165], M. C. Vetterli[148,ai], A. Vgenopoulos[102], N. Viaux Maira[140f], T. Vickey[145], O. E. Vickey Boeriu[145], G. H. A. Viehhauser[129], L. Vigani[63b], M. Vigl[112], M. Villa[24b,24a], M. Villaplana Perez[169], E. M. Villhauer[40],

E. Vilucchi[53], M. G. Vincter[35], A. Visibile[117], C. Vittori[37], I. Vivarelli[24b,24a], E. Voevodina[112], F. Vogel[111], J. C. Voigt[50], P. Vokac[135], Yu. Volkotrub[87b], E. Von Toerne[25], B. Vormwald[37], K. Vorobev[51], M. Vos[169], K. Voss[147], M. Vozak[37], L. Vozdecky[123], N. Vranjes[16], M. Vranjes Milosavljevic[16], M. Vreeswijk[117], N. K. Vu[144b,144a], R. Vuillermet[37], O. Vujinovic[102], I. Vukotic[40], I. K. Vyas[35], J. F. Wack[33], S. Wada[163], C. Wagner[149], J. M. Wagner[18a], W. Wagner[177], S. Wahdan[177], H. Wahlberg[92], C. H. Waits[123], J. Walder[137], R. Walker[111], K. Walkingshaw Pass[59], W. Walkowiak[147], A. Wall[131], E. J. Wallin[100], T. Wamorkar[18a], A. Z. Wang[139], C. Wang[102], C. Wang[11], H. Wang[18a], J. Wang[64c], P. Wang[103], P. Wang[98], R. Wang[61], R. Wang[6], S. M. Wang[154], S. Wang[14], T. Wang[62], T. Wang[62], W. T. Wang[80], W. Wang[14], X. Wang[168], X. Wang[144a], X. Wang[48], Y. Wang[114a], Y. Wang[62], Z. Wang[108], Z. Wang[144b], Z. Wang[108], C. Wanotayaroj[84], A. Warburton[106], A. L. Warnerbring[147], N. Warrack[59], S. Waterhouse[97], A. T. Watson[21], H. Watson[52], M. F. Watson[21], E. Watton[59], G. Watts[142], B. M. Waugh[98], J. M. Webb[54], C. Weber[30], H. A. Weber[19], M. S. Weber[20], S. M. Weber[63a], C. Wei[62], Y. Wei[54], A. R. Weidberg[129], E. J. Weik[120], J. Weingarten[49], C. Weiser[54], C. J. Wells[48], T. Wenaus[30], B. Wendland[49], T. Wengler[37], N. S. Wenke[112], N. Wermes[25], M. Wessels[63a], A. M. Wharton[93], A. S. White[61], A. White[8], M. J. White[1], D. Whiteson[165], L. Wickremasinghe[127], W. Wiedenmann[176], M. Wielers[137], R. Wierda[150], C. Wiglesworth[43], H. G. Wilkens[37], J. J. H. Wilkinson[33], D. M. Williams[42], H. H. Williams[131], S. Williams[33], S. Willocq[105], B. J. Wilson[103], D. J. Wilson[103], P. J. Windischhofer[40], F. I. Winkel[31], F. Winklmeier[126], B. T. Winter[54], M. Wittgen[149], M. Wobisch[99], T. Wojtkowski[60], Z. Wolffs[117], J. Wollrath[37], M. W. Wolter[88], H. Wolters[133a,133c], M. C. Wong[139], E. L. Woodward[42], S. D. Worm[48], B. K. Wosiek[88], K. W. Woźniak[88], S. Wozniewski[55], K. Wraight[59], C. Wu[161], C. Wu[21], J. Wu[159], M. Wu[114b], M. Wu[116], S.L. Wu[176], S. Wu[14], X. Wu[62], Y. Wu[62], Z. Wu[4], J. Wuerzinger[112], T. R. Wyatt[103], B. M. Wynne[52], S. Xella[43], L. Xia[114a], M. Xia[15], M. Xie[62], A. Xiong[126], J. Xiong[18a], D. Xu[14], H. Xu[62], L. Xu[62], R. Xu[131], T. Xu[108], Y. Xu[142], Z. Xu[52], Z. Xu[114a], B. Yabsley[153], S. Yacoob[34a], Y. Yamaguchi[84], E. Yamashita[159], H. Yamauchi[163], T. Yamazaki[18a], Y. Yamazaki[86], S. Yan[59], Z. Yan[105], H. J. Yang[144a,144b], H. T. Yang[62], S. Yang[62], T. Yang[64c], X. Yang[37], X. Yang[14], Y. Yang[159], Y. Yang[62], W-M. Yao[18a], C.L. Yardley[152], J. Ye[14], S. Ye[30], X. Ye[62], Y. Yeh[98], I. Yeletskikh[39], B. Yeo[18b], M. R. Yexley[98], T. P. Yildirim[129], P. Yin[42], K. Yorita[174], C. J. S. Young[37], C. Young[149], N. D. Young[126], Y. Yu[62], J. Yuan[14,114c], M. Yuan[108], R. Yuan[144b,144a], L. Yue[98], M. Zaazoua[62], B. Zabinski[88], I. Zahir[36a], A. Zaio[57b,57a], Z. K. Zak[88], T. Zakareishvili[169], S. Zambito[56], J. A. Zamora Saa[140d], J. Zang[159], R. Zanzottera[71a,71b], O. Zaplatilek[135], C. Zeitnitz[177], H. Zeng[14], J. C. Zeng[168], D. T. Zenger Jr[27], O. Zenin[38], T. Ženiš[29a], S. Zenz[96], D. Zerwas[66], M. Zhai[14,114c], D. F. Zhang[145], G. Zhang[14], J. Zhang[143a], J. Zhang[6], K. Zhang[14,114c], L. Zhang[62], L. Zhang[114a], P. Zhang[14,114c], R. Zhang[114a], S. Zhang[91], T. Zhang[159], Y. Zhang[142], Y. Zhang[98], Y. Zhang[62], Y. Zhang[114a], Z. Zhang[143a], Z. Zhang[66], H. Zhao[142], T. Zhao[143a], Y. Zhao[35], Z. Zhao[62], Z. Zhao[62], A. Zhemchugov[39], J. Zheng[114a], K. Zheng[168], X. Zheng[62], Z. Zheng[149], D. Zhong[168], B. Zhou[108], H. Zhou[7], N. Zhou[144a], Y. Zhou[15], Y. Zhou[114a], Y. Zhou[7], C. G. Zhu[143a], J. Zhu[108], X. Zhu[144b], Y. Zhu[144a], Y. Zhu[62], X. Zhuang[14], K. Zhukov[68], N.I. Zimine[39], J. Zinsser[63b], M. Ziolkowski[147], L. Živković[16], A. Zoccoli[24b,24a], K. Zoch[61], A. Zografos[37], T. G. Zorbas[145], O. Zormpa[46], L. Zwalinski[37]

[1] Department of Physics, University of Adelaide, Adelaide, Australia
[2] Department of Physics, University of Alberta, Edmonton, AB, Canada
[3] [(a)]Department of Physics, Ankara University, Ankara, Türkey; [(b)]Division of Physics, TOBB University of Economics and Technology, Ankara, Türkey
[4] LAPP, Université Savoie Mont Blanc, CNRS/IN2P3, Annecy, France
[5] APC, Université Paris Cité, CNRS/IN2P3, Paris, France
[6] High Energy Physics Division, Argonne National Laboratory, Argonne, IL, USA
[7] , University of Arizona, Tucson, AZ, USA
[8] Department of Physics, University of Texas at Arlington, Arlington, TX, USA
[9] Physics Department, National and Kapodistrian University of Athens, Athens, Greece
[10] Physics Department, National Technical University of Athens, Zografou, Greece
[11] Department of Physics, University of Texas at Austin, Austin, TX, USA
[12] Institute of Physics, Azerbaijan Academy of Sciences, Baku, Azerbaijan
[13] Institut de Física d'Altes Energies (IFAE), Barcelona Institute of Science and Technology, Barcelona, Spain
[14] Institute of High Energy Physics, Chinese Academy of Sciences, Beijing, China

[15] Physics Department, Tsinghua University, Beijing, China
[16] Institute of Physics, University of Belgrade, Belgrade, Serbia
[17] Department for Physics and Technology, University of Bergen, Bergen, Norway
[18] [(a)]Physics Division, Lawrence Berkeley National Laboratory, Berkeley, CA, USA; [(b)]University of California, Berkeley, CA, USA
[19] Institut für Physik, Humboldt Universität zu Berlin, Berlin, Germany
[20] Albert Einstein Center for Fundamental Physics and Laboratory for High Energy Physics, University of Bern, Bern, Switzerland
[21] School of Physics and Astronomy, University of Birmingham, Birmingham, UK
[22] [(a)]Department of Physics, Bogazici University, Istanbul, Türkey; [(b)]Department of Physics Engineering, Gaziantep University, Gaziantep, Türkey; [(c)]Department of Physics, Istanbul University, Istanbul, Türkey
[23] [(a)]Facultad de Ciencias y Centro de Investigaciónes, Universidad Antonio Nariño, Bogotá, Colombia; [(b)]Departamento de Física, Universidad Nacional de Colombia, Bogotá, Colombia
[24] [(a)]Dipartimento di Fisica e Astronomia A. Righi, Università di Bologna, Bologna, Italy; [(b)]INFN Sezione di Bologna, Bologna, Italy
[25] Physikalisches Institut, Universität Bonn, Bonn, Germany
[26] Department of Physics, Boston University, Boston, MA, USA
[27] Department of Physics, Brandeis University, Waltham, MA, USA
[28] [(a)]Transilvania University of Brasov, Brasov, Romania; [(b)]Horia Hulubei National Institute of Physics and Nuclear Engineering, Bucharest, Romania; [(c)]Department of Physics, Alexandru Ioan Cuza University of Iasi, Iasi, Romania; [(d)]National Institute for Research and Development of Isotopic and Molecular Technologies, Physics Department, Cluj-Napoca, Romania; [(e)]National University of Science and Technology Politechnica, Bucharest, Romania; [(f)]West University in Timisoara, Timisoara, Romania; [(g)]Faculty of Physics, University of Bucharest, Bucharest, Romania
[29] [(a)]Faculty of Mathematics, Physics and Informatics, Comenius University, Bratislava, Slovakia; [(b)]Department of Subnuclear Physics, Institute of Experimental Physics of the Slovak Academy of Sciences, Kosice, Slovak Republic
[30] Physics Department, Brookhaven National Laboratory, Upton, NY, USA
[31] Universidad de Buenos Aires, Facultad de Ciencias Exactas y Naturales, Departamento de Física, y CONICET, Instituto de Física de Buenos Aires (IFIBA), Buenos Aires, Argentina
[32] California State University, Long Beach, CA, USA
[33] Cavendish Laboratory, University of Cambridge, Cambridge, UK
[34] [(a)]Department of Physics, University of Cape Town, Cape Town, South Africa; [(b)]iThemba Labs, Western Cape, South Africa; [(c)]Department of Mechanical Engineering Science, University of Johannesburg, Johannesburg, South Africa; [(d)]National Institute of Physics, University of the Philippines Diliman (Philippines), Quezon City, Philippines; [(e)]Department of Physics, University of South Africa, Pretoria, South Africa; [(f)]University of Zululand, KwaDlangezwa, South Africa; [(g)]School of Physics, University of the Witwatersrand, Johannesburg, South Africa
[35] Department of Physics, Carleton University, Ottawa, ON, Canada
[36] [(a)]Faculté des Sciences Ain Chock, Université Hassan II de Casablanca, Casablanca, Morocco; [(b)]Faculté des Sciences, Université Ibn-Tofail, Kénitra, Morocco; [(c)]Faculté des Sciences Semlalia, Université Cadi Ayyad, LPHEA-Marrakech, Marrakech, Morocco; [(d)]LPMR, Faculté des Sciences, Université Mohamed Premier, Oujda, Morocco; [(e)]Faculté des sciences, Université Mohammed V, Rabat, Morocco; [(f)]Institute of Applied Physics, Mohammed VI Polytechnic University, Ben Guerir, Morocco
[37] CERN, Geneva, Switzerland
[38] Affiliated with an institute formerly covered by a cooperation agreement with CERN, Geneva, Switzerland
[39] Affiliated with an international laboratory covered by a cooperation agreement with CERN, Geneva, Switzerland
[40] Enrico Fermi Institute, University of Chicago, Chicago, IL, USA
[41] LPC, Université Clermont Auvergne, CNRS/IN2P3, Clermont-Ferrand, France
[42] Nevis Laboratory, Columbia University, Irvington, NY, USA
[43] Niels Bohr Institute, University of Copenhagen, Copenhagen, Denmark
[44] [(a)]Dipartimento di Fisica, Università della Calabria, Rende, Italy; [(b)]INFN Gruppo Collegato di Cosenza, Laboratori Nazionali di Frascati, Frascati, Italy
[45] Physics Department, Southern Methodist University, Dallas, TX, USA
[46] National Centre for Scientific Research “Demokritos”, Agia Paraskevi, Greece

[47] [(a)]Department of Physics, Stockholm University, Stockholm, Sweden; [(b)]Oskar Klein Centre, Stockholm, Sweden
[48] Deutsches Elektronen-Synchrotron DESY, Hamburg and Zeuthen, Germany
[49] Fakultät Physik , Technische Universität Dortmund, Dortmund, Germany
[50] Institut für Kern- und Teilchenphysik, Technische Universität Dresden, Dresden, Germany
[51] Department of Physics, Duke University, Durham, NC, USA
[52] SUPA-School of Physics and Astronomy, University of Edinburgh, Edinburgh, UK
[53] INFN e Laboratori Nazionali di Frascati, Frascati, Italy
[54] Physikalisches Institut, Albert-Ludwigs-Universität Freiburg, Freiburg, Germany
[55] II. Physikalisches Institut, Georg-August-Universität Göttingen, Göttingen, Germany
[56] Département de Physique Nucléaire et Corpusculaire, Université de Genève, Geneva, Switzerland
[57] [(a)]Dipartimento di Fisica, Università di Genova, Genoa, Italy; [(b)]INFN Sezione di Genova, Genoa, Italy
[58] II. Physikalisches Institut, Justus-Liebig-Universität Giessen, Giessen, Germany
[59] SUPA-School of Physics and Astronomy, University of Glasgow, Glasgow, UK
[60] LPSC, Université Grenoble Alpes, CNRS/IN2P3, Grenoble INP, Grenoble, France
[61] Laboratory for Particle Physics and Cosmology, Harvard University, Cambridge, MA, USA
[62] Department of Modern Physics and State Key Laboratory of Particle Detection and Electronics, University of Science and Technology of China, Hefei, China
[63] [(a)]Kirchhoff-Institut für Physik, Ruprecht-Karls-Universität Heidelberg, Heidelberg, Germany; [(b)]Physikalisches Institut, Ruprecht-Karls-Universität Heidelberg, Heidelberg, Germany
[64] [(a)]Department of Physics, Chinese University of Hong Kong, Shatin, N.T., Hong Kong; [(b)]Department of Physics, University of Hong Kong, Hong Kong, China; [(c)]Department of Physics and Institute for Advanced Study, Hong Kong University of Science and Technology, Clear Water Bay, Kowloon, Hong Kong, China
[65] Department of Physics, National Tsing Hua University, Hsinchu, Taiwan
[66] IJCLab, Université Paris-Saclay, CNRS/IN2P3, 91405 Orsay, France
[67] Centro Nacional de Microelectrónica (IMB-CNM-CSIC), Barcelona, Spain
[68] Department of Physics, Indiana University, Bloomington, IN, USA
[69] [(a)]INFN Gruppo Collegato di Udine, Sezione di Trieste, Udine, Italy; [(b)]ICTP, Trieste, Italy; [(c)]Dipartimento Politecnico di Ingegneria e Architettura, Università di Udine, Udine, Italy
[70] [(a)]INFN Sezione di Lecce, Lecce, Italy; [(b)]Dipartimento di Matematica e Fisica, Università del Salento, Lecce, Italy
[71] [(a)]INFN Sezione di Milano, Milan, Italy; [(b)]Dipartimento di Fisica, Università di Milano, Milan, Italy
[72] [(a)]INFN Sezione di Napoli, Naples, Italy; [(b)]Dipartimento di Fisica, Università di Napoli, Naples, Italy
[73] [(a)]INFN Sezione di Pavia, Pavia, Italy; [(b)]Dipartimento di Fisica, Università di Pavia, Pavia, Italy
[74] [(a)]INFN Sezione di Pisa, Pisa, Italy; [(b)]Dipartimento di Fisica E. Fermi, Università di Pisa, Pisa, Italy
[75] [(a)]INFN Sezione di Roma, Rome, Italy; [(b)]Dipartimento di Fisica, Sapienza Università di Roma, Rome, Italy
[76] [(a)]INFN Sezione di Roma Tor Vergata, Rome, Italy; [(b)]Dipartimento di Fisica, Università di Roma Tor Vergata, Rome, Italy
[77] [(a)]INFN Sezione di Roma Tre, Rome, Italy; [(b)]Dipartimento di Matematica e Fisica, Università Roma Tre, Rome, Italy
[78] [(a)]INFN-TIFPA, Povo, Italy; [(b)]Università degli Studi di Trento, Trento, Italy
[79] Universität Innsbruck, Department of Astro and Particle Physics, Innsbruck, Austria
[80] University of Iowa, Iowa City, IA, USA
[81] Department of Physics and Astronomy, Iowa State University, Ames, IA, USA
[82] Istinye University, Sariyer, Istanbul, Türkey
[83] [(a)]Departamento de Engenharia Elétrica, Universidade Federal de Juiz de Fora (UFJF), Juiz de Fora, Brazil; [(b)]Universidade Federal do Rio De Janeiro COPPE/EE/IF, Rio de Janeiro, Brazil; [(c)]Instituto de Física, Universidade de São Paulo, São Paulo, Brazil; [(d)]Rio de Janeiro State University, Rio de Janeiro, Brazil; [(e)]Federal University of Bahia, Bahia, Brazil
[84] KEK, High Energy Accelerator Research Organization, Tsukuba, Japan
[85] [(a)]Khalifa University of Science and Technology, Abu Dhabi, United Arab Emirates; [(b)]University of Sharjah, Sharjah, United Arab Emirates
[86] Graduate School of Science, Kobe University, Kobe, Japan
[87] [(a)]AGH University of Krakow, Faculty of Physics and Applied Computer Science, Krakow, Poland; [(b)]Marian Smoluchowski Institute of Physics, Jagiellonian University, Krakow, Poland
[88] Institute of Nuclear Physics Polish Academy of Sciences, Krakow, Poland

[89] Faculty of Science, Kyoto University, Kyoto, Japan
[90] Research Center for Advanced Particle Physics and Department of Physics, Kyushu University, Fukuoka, Japan
[91] L2IT, Université de Toulouse, CNRS/IN2P3, UPS, Toulouse, France
[92] Instituto de Física La Plata, Universidad Nacional de La Plata and CONICET, La Plata, Argentina
[93] Physics Department, Lancaster University, Lancaster, UK
[94] Oliver Lodge Laboratory, University of Liverpool, Liverpool, UK
[95] Department of Experimental Particle Physics, Jožef Stefan Institute and Department of Physics, University of Ljubljana, Ljubljana, Slovenia
[96] Department of Physics and Astronomy, Queen Mary University of London, London, UK
[97] Department of Physics, Royal Holloway University of London, Egham, UK
[98] Department of Physics and Astronomy, University College London, London, UK
[99] Louisiana Tech University, Ruston, LA, USA
[100] Fysiska institutionen, Lunds universitet, Lund, Sweden
[101] Departamento de Física Teorica C-15 and CIAFF, Universidad Autónoma de Madrid, Madrid, Spain
[102] Institut für Physik, Universität Mainz, Mainz, Germany
[103] School of Physics and Astronomy, University of Manchester, Manchester, UK
[104] CPPM, Aix-Marseille Université, CNRS/IN2P3, Marseille, France
[105] Department of Physics, University of Massachusetts, Amherst, MA, USA
[106] Department of Physics, McGill University, Montreal, QC, Canada
[107] School of Physics, University of Melbourne, Victoria, Australia
[108] Department of Physics, University of Michigan, Ann Arbor, MI, USA
[109] Department of Physics and Astronomy, Michigan State University, East Lansing, MI, USA
[110] Group of Particle Physics, University of Montreal, Montreal, QC, Canada
[111] Fakultät für Physik, Ludwig-Maximilians-Universität München, München, Germany
[112] Max-Planck-Institut für Physik (Werner-Heisenberg-Institut), München, Germany
[113] Graduate School of Science and Kobayashi-Maskawa Institute, Nagoya University, Nagoya, Japan
[114] [(a)]Department of Physics, Nanjing University, Nanjing, China; [(b)]School of Science, Shenzhen Campus of Sun Yat-sen University, Shenzhen, China; [(c)]University of Chinese Academy of Science (UCAS), Beijing, China
[115] Department of Physics and Astronomy, University of New Mexico, Albuquerque, NM, USA
[116] Institute for Mathematics, Astrophysics and Particle Physics, Radboud University/Nikhef, Nijmegen, Netherlands
[117] Nikhef National Institute for Subatomic Physics and University of Amsterdam, Amsterdam, Netherlands
[118] Department of Physics, Northern Illinois University, DeKalb, IL, USA
[119] [(a)]New York University Abu Dhabi, Abu Dhabi, United Arab Emirates; [(b)]United Arab Emirates University, Al Ain, United Arab Emirates
[120] Department of Physics, New York University, New York, NY, USA
[121] Ochanomizu University, Otsuka, Bunkyo-ku, Tokyo, Japan
[122] Ohio State University, Columbus, OH, USA
[123] Homer L. Dodge Department of Physics and Astronomy, University of Oklahoma, Norman, OK, USA
[124] Department of Physics, Oklahoma State University, Stillwater, OK, USA
[125] Palacký University, Joint Laboratory of Optics, Olomouc, Czech Republic
[126] Institute for Fundamental Science, University of Oregon, Eugene, OR, USA
[127] Graduate School of Science, University of Osaka, Osaka, Japan
[128] Department of Physics, University of Oslo, Oslo, Norway
[129] Department of Physics, Oxford University, Oxford, UK
[130] LPNHE, Sorbonne Université, Université Paris Cité, CNRS/IN2P3, Paris, France
[131] Department of Physics, University of Pennsylvania, Philadelphia, PA, USA
[132] Department of Physics and Astronomy, University of Pittsburgh, Pittsburgh, PA, USA
[133] [(a)]Laboratório de Instrumentação e Física Experimental de Partículas - LIP, Lisbon, Portugal; [(b)]Departamento de Física, Faculdade de Ciências, Universidade de Lisboa, Lisbon, Portugal; [(c)]Departamento de Física, Universidade de Coimbra, Coimbra, Portugal; [(d)]Centro de Física Nuclear da Universidade de Lisboa, Lisbon, Portugal; [(e)]Departamento de Física, Escola de Ciências, Universidade do Minho, Braga, Portugal; [(f)]Departamento de Física Teórica y del Cosmos, Universidad de Granada, Granada, Spain; [(g)]Departamento de Física, Instituto Superior Técnico, Universidade de Lisboa, Lisbon, Portugal

[134] Institute of Physics of the Czech Academy of Sciences, Prague, Czech Republic
[135] Czech Technical University in Prague, Prague, Czech Republic
[136] Charles University, Faculty of Mathematics and Physics, Prague, Czech Republic
[137] Particle Physics Department, Rutherford Appleton Laboratory, Didcot, UK
[138] IRFU, CEA, Université Paris-Saclay, Gif-sur-Yvette, France
[139] Santa Cruz Institute for Particle Physics, University of California Santa Cruz, Santa Cruz, CA, USA
[140] [(a)]Departamento de Física, Pontificia Universidad Católica de Chile, Santiago, Chile; [(b)]Millennium Institute for Subatomic Physics at High Energy Frontier (SAPHIR), Santiago, Chile; [(c)]Instituto de Investigación Multidisciplinario en Ciencia y Tecnología, y Departamento de Física, Universidad de La Serena, La Serena, Chile; [(d)]Department of Physics, Universidad Andres Bello, Santiago, Chile; [(e)]Instituto de Alta Investigación, Universidad de Tarapacá, Arica, Chile; [(f)]Departamento de Física, Universidad Técnica Federico Santa María, Valparaíso, Chile
[141] Department of Physics, Institute of Science, Tokyo, Japan
[142] Department of Physics, University of Washington, Seattle, WA, USA
[143] [(a)]Institute of Frontier and Interdisciplinary Science and Key Laboratory of Particle Physics and Particle Irradiation (MOE), Shandong University, Qingdao, China; [(b)]School of Physics, Zhengzhou University, China
[144] [(a)]State Key Laboratory of Dark Matter Physics, School of Physics and Astronomy, Shanghai Jiao Tong University, Key Laboratory for Particle Astrophysics and Cosmology (MOE), SKLPPC, Shanghai, China; [(b)]State Key Laboratory of Dark Matter Physics, Tsung-Dao Lee Institute, Shanghai Jiao Tong University, Shanghai, China
[145] Department of Physics and Astronomy, University of Sheffield, Sheffield, UK
[146] Department of Physics, Shinshu University, Nagano, Japan
[147] Department Physik, Universität Siegen, Siegen, Germany
[148] Department of Physics, Simon Fraser University, Burnaby, BC, Canada
[149] SLAC National Accelerator Laboratory, Stanford, CA, USA
[150] Department of Physics, Royal Institute of Technology, Stockholm, Sweden
[151] Departments of Physics and Astronomy, Stony Brook University, Stony Brook, NY, USA
[152] Department of Physics and Astronomy, University of Sussex, Brighton, UK
[153] School of Physics, University of Sydney, Sydney, Australia
[154] Institute of Physics, Academia Sinica, Taipei, Taiwan
[155] [(a)]E. Andronikashvili Institute of Physics, Iv. Javakhishvili Tbilisi State University, Tbilisi, Georgia; [(b)]High Energy Physics Institute, Tbilisi State University, Tbilisi, Georgia; [(c)]University of Georgia, Tbilisi, Georgia
[156] Department of Physics, Technion, Israel Institute of Technology, Haifa, Israel
[157] Raymond and Beverly Sackler School of Physics and Astronomy, Tel Aviv University, Tel Aviv, Israel
[158] Department of Physics, Aristotle University of Thessaloniki, Thessaloniki, Greece
[159] International Center for Elementary Particle Physics and Department of Physics, University of Tokyo, Tokyo, Japan
[160] Graduate School of Science and Technology, Tokyo Metropolitan University, Tokyo, Japan
[161] Department of Physics, University of Toronto, Toronto, ON, Canada
[162] [(a)]TRIUMF, Vancouver, BC, Canada; [(b)]Department of Physics and Astronomy, York University, Toronto, ON, Canada
[163] Division of Physics and Tomonaga Center for the History of the Universe, Faculty of Pure and Applied Sciences, University of Tsukuba, Tsukuba, Japan
[164] Department of Physics and Astronomy, Tufts University, Medford, MA, USA
[165] Department of Physics and Astronomy, University of California Irvine, Irvine, CA, USA
[166] University of West Attica, Athens, Greece
[167] Department of Physics and Astronomy, University of Uppsala, Uppsala, Sweden
[168] Department of Physics, University of Illinois, Urbana, IL, USA
[169] Instituto de Física Corpuscular (IFIC), Centro Mixto Universidad de Valencia - CSIC, Valencia, Spain
[170] Department of Physics, University of British Columbia, Vancouver, BC, Canada
[171] Department of Physics and Astronomy, University of Victoria, Victoria, BC, Canada
[172] Fakultät für Physik und Astronomie, Julius-Maximilians-Universität Würzburg, Würzburg, Germany
[173] Department of Physics, University of Warwick, Coventry, UK
[174] Waseda University, Tokyo, Japan
[175] Department of Particle Physics and Astrophysics, Weizmann Institute of Science, Rehovot, Israel
[176] Department of Physics, University of Wisconsin, Madison, WI, USA

[177] Fakultät für Mathematik und Naturwissenschaften, Fachgruppe Physik, Bergische Universität Wuppertal, Wuppertal, Germany
[178] Department of Physics, Yale University, New Haven, CT, USA
[179] Yerevan Physics Institute, Yerevan, Armenia

[a] Also at Affiliated with an institute formerly covered by a cooperation agreement with CERN, Geneva, Switzerland
[b] Also at An-Najah National University, Nablus, Palestine
[c] Also at Borough of Manhattan Community College, City University of New York, New York, NY, USA
[d] Also at Center for Interdisciplinary Research and Innovation (CIRI-AUTH), Thessaloniki, Greece
[e] Also at Centre of Physics of the Universities of Minho and Porto (CF-UM-UP), Porto, Portugal
[f] Also at CERN, Geneva, Switzerland
[g] Also at CMD-AC UNEC Research Center, Azerbaijan State University of Economics (UNEC), Azerbaijan
[h] Also at Département de Physique Nucléaire et Corpusculaire, Université de Genève, Genève, Switzerland
[i] Also at Departament de Fisica de la Universitat Autonoma de Barcelona, Barcelona, Spain
[j] Also at Department of Financial and Management Engineering, University of the Aegean, Chios, Greece
[k] Also at Department of Mathematical Sciences, University of South Africa, Johannesburg, South Africa
[l] Also at Department of Modern Physics and State Key Laboratory of Particle Detection and Electronics, University of Science and Technology of China, Hefei, China
[m] Also at Department of Physics, Bolu Abant Izzet Baysal University, Bolu, Türkey
[n] Also at Department of Physics, King's College London, London, UK
[o] Also at Department of Physics, Stanford University, Stanford, CA, USA
[p] Also at Department of Physics, Stellenbosch University, Stellenbosch, South Africa
[q] Also at Department of Physics, University of Fribourg, Fribourg, Switzerland
[r] Also at Department of Physics, University of Thessaly, Greece
[s] Also at Department of Physics, Westmont College, Santa Barbara, USA
[t] Also at Faculty of Physics, Sofia University 'St. Kliment Ohridski', Sofia, Bulgaria
[u] Also at Faculty of Physics, University of Bucharest, Bucharest, Romania
[v] Also at Hellenic Open University, Patras, Greece
[w] Also at Henan University, Kaifeng, China
[x] Also at Imam Mohammad Ibn Saud Islamic University, Riyadh, Saudi Arabia
[y] Also at Institucio Catalana de Recerca i Estudis Avancats, ICREA, Barcelona, Spain
[z] Also at Institut für Experimentalphysik, Universität Hamburg, Hamburg, Germany
[aa] Also at Institute for Nuclear Research and Nuclear Energy (INRNE) of the Bulgarian Academy of Sciences, Sofia, Bulgaria
[ab] Also at Institute of Applied Physics, Mohammed VI Polytechnic University, Ben Guerir, Morocco
[ac] Also at Institute of Particle Physics (IPP), Toronto, Canada
[ad] Also at Institute of Physics and Technology, Mongolian Academy of Sciences, Ulaanbaatar, Mongolia
[ae] Also at Institute of Physics, Azerbaijan Academy of Sciences, Baku, Azerbaijan
[af] Also at Institute of Theoretical Physics, Ilia State University, Tbilisi, Georgia
[ag] Also at National Institute of Physics, University of the Philippines Diliman (Philippines), Quezon City, Philippines
[ah] Also at The Collaborative Innovation Center of Quantum Matter (CICQM), Beijing, China
[ai] Also at TRIUMF, Vancouver, BC, Canada
[aj] Also at Università di Napoli Parthenope, Naples, Italy
[ak] Also at Department of Physics, University of Colorado Boulder, Colorado, USA
[al] Also at University of Sienna, Sienna, Italy
[am] Also at Washington College, Chestertown, MD, USA
[an] Also at Yeditepe University, Physics Department, Istanbul, Türkey
* Deceased